Master Thesis

On the attainable accuracy of multi-system GNSS positioning in high-multipath urban environments

vorgelegt

zur Erlangung des akademischen Grades eines Diplom-Ingenieurs
der Studienrichtung Geomatics Science

Alexander Ebner

Institut für Ingenieurgeodäsie und Messsysteme
der Technischen Universität Graz

Betreuer:
Univ.-Doz. DI Dr.Techn. Andreas Wieser
B.Sc., M.Sc. L.Ph., Dr.Techn., P.Eng. Gérard Lachapelle

Begutachter:
O.Univ.-Prof. DI Dr.Techn. Fritz Karl Brunner

Graz, April 2008

Acknowledgments

Abstract

Positioning using Global Navigation Satellite Systems (GNSS) is especially challenging in urban environments where a variety of natural and man-made objects may impair the line-of-sight signal propagation from the satellites to the user. An insufficient number of satellites or "bad geometry" (i.e. bad distribution of the available satellite signals over the sky) typically results from signal obstruction, and limits the availability and precision of position solutions. In an urban environment, the situation is aggravated by the fact that the available signals do not only reach the user's receiver along the line-of-sight (LOS) but may result from indirect propagation (reflection and diffraction), LOS propagation, or a mix of both. This may significantly deteriorate the attainable positioning accuracy as compared to environments with mainly LOS propagation. A multi-system GNSS receiver (e.g. GPS+Galileo) will usually provide more observations than a single-system receiver and thus allow higher positioning precision. Dilution of precision (DOP) and satellite availability studies carried out by different research groups have demonstrated this. However, in an urban environment also the additional observations provided by a second GNSS will be affected by non-LOS propagation. Thus, the attainable accuracy may not increase by the same amount as the precision.

In this thesis, an urban canyon situation is simulated using MATLAB and a geometrical model of reflectors/obstacles. Based on generic satellite orbit information and on models of the receiver tracking loops, satellite availability and multipath effects on measured pseudoranges are investigated. The impact of multipath errors is also studied and visualized in the coordinate domain. This analysis is then used to assess the attainable positioning accuracy and compare it to the predicted precision as expressed through the DOP values.

Kurzfassung

Die satellitengestützte Positionierung in dicht besiedelten Gebieten ist stark beeinträchtigt aufgrund von nahe liegenden Objekten wie zum Beispiel Bauwerken. Schlechte Sichtbarkeit der Satelliten am Horizont, die ungünstige Geometrie und zusätzlich vermehrt auftretende Mehrwegeffekte sind die Ursachen für eine wahrscheinliche Verschlechterung der Positionsgenauigkeit. Durch die Nutzung von mehreren Satellitensystemen und dadurch einer steigenden Anzahl an Satelliten, ist es möglich die ersten beiden Effekte auszuschließen bzw. zu reduzieren. Die Sicherheit, dass das Signal direkt zum Empfänger gelangt ist jedoch nicht gegeben und die Positionslösung ist noch immer stark von Mehrwegeffekten abhängig.

Diese Diplomarbeit befasst sich mit den Auswirkungen von genau diesen Mehrwegeffekten. Mit Hilfe eines einfachen geometrischen Modells für Straßenschluchten und eines einfachen Modells für die Empfänger Tracking loop werden die Auswirkungen von Mehrwegeffekten auf die Pseudostrecke erarbeitet. Diese Auswirkung der Mehrwegeffekte werden auch fü die Positionslösungen des Empfängers berechnet und die Ergebnisse werden dargestellt. Diese Analyse wird für die Bestimmung der Erreichbaren Positionsgenauigkeit herangezogen und zugleich verglichen mit erwarteten Genauigkeiten die aus DOP Analysen gerechnet werden können.

Contents

List of Figures

5 Field Test and Analysis

List of Tables

Abbreviations

AUR	Average User Reception
BPSK	Binary Phase Shift Keying
BOC	Binary Offset Carrier
CCIT	Calgary Center for Innovative Technology
C/A	Coarse/Acquisition
C/N_0	Carrier to Noise ratio
C^3NAVG^2	Combined Code and Carrier for NAVigation with GPS and GLONASS
DLL	Delay Lock Loop
DOP	Dilution of Precision
EM	Electromagnetic
EML	Early Minus Late
EPA	Estimated Position Accuracy
ES	Earth-Science
E-W	East-West
FUR	Favorable User Reception
GDOP	Geometry Dilution of Precision
GNSS	Global Navigation Satellite System
GPS	Global Positioning System
HDOP	Horizontal Dilution of Precision
HS	High Sensitivity
ICT	Information and Communications Technology
IF	Intermediate Frequency
IGS	International GNSS Service

IP	In-Phase
LC	Low Cost
LHCP	left-handed circular polarized
LOS	Line of Sight
LS	Least-Squares
MDR	Multipath to Direct Ratio
MP	Multipath
N-S	North-South
OP	Out-of-Phase
PDOP	Position Dilution of Precision
PPS	Precise Positioning Service
PRN	Pseudo Random Noise
RAIM	Receiver Autonomous Integrity Monitoring
RF	Radio Frequency
RHCP	right-handed circular polarized
RMS	Root Mean Square
SIS	Signal in Space
SMR	Signal to Multipath Ratio
SPS	Standard Positioning Service
SA	Selective Availability
TDOP	Time Dilution of Precision
TEM	Transversal electromagnetic wave
UCM	Urban Canyon Model
UERE	User Equivalent Range Error
URA	User Range Accuracy
URE	User Range Error
USCG	United States Coast Guard
UofC	University of Calgary
VDOP	Vertical Dilution of Precision
WCUR	Worst Case User Reception
WGS-84	World Geodetic System 1984

Introduction

1.1 Motivation

With today's modern GNSS, the question "What time, what position, and what velocity is it?" can be answered at any time and for any position around the globe. Since the beginning of satellite-based systems, the demand for increased accuracy occupies scientists and researchers. Today's position accuracies are obtainable because many of the problems, which have limited the accuracy of time and position estimation, are now well understood and can be adequately solved (Wieser, 2002). These improvements have significantly reduced the systematic errors effects on the U.S. Global Positioning System (GPS) measurements and multipath is now one of the most significant, if not the dominant error source for many applications. Especially for position and navigation problems in degraded signal environments, such as in urban canyons, the effect of multipath is a serious problem.

The use of multiple systems (e.g. GPS and Galileo) will provide more observations than the use of a single system. Better satellite availability and higher positioning precision are the main advantages for the user, obtained in environments where the satellites are not obstructed. However, in an urban environment, obstructions from close buildings and indirect signal propagation have an influence on the measurements. In an urban canyon more satellites do not necessarily lead to better accuracies because most of the signals within such degraded environments are affected by multipath. The degradation of pseudoranges and finally the position error due to multipath effects shall be investigated in this thesis. The actual position errors are also compared to accuracy estimations using DOP analysis.

1.2 Related research

Even before GPS was born, the effect of multipath on Pseudo Random Noise (PRN) ranging receiver was studied by Hagerman (1973). Later investigations of multipath effects on a delay lock loop (DLL) were made by researchers like Braasch (1992), van

---

Direndonck et al. (1992), and van Nee (1995), just to mention a few. Braasch (1992) presented detailed models for multipath errors, including error envelopes for various front-end and code tracking configurations. Van Direndonck et al. (1992) analyzed the theory and the performance of narrow correlator spacing in a GPS receiver. The first multipath models were implemented by van Nee (1995) where a planar reflector caused reflections. With a detailed tracking loop model the simulation carried out similar results as obtained from experimental data collections.

In the recent past, several multipath models have been published, with the following being of special interest for this thesis: Winkel (2000), Hannah (2001), Weiss (2007). Winkel (2000) focuses on the signal and signal propagation model for GNSS. A receiver model, combining antenna reception, down conversion, discriminator output, tracking performance and finally position estimation, are discussed and strengths and limitations are listed. Simulations for different receiver models and scenarios in suburban and urban areas have been evaluated extensively in this work.

Hannah (2001) developed and implemented an electromagnetic propagation model specifically for GPS multipath propagation. A thorough analysis of terrestrial multipath propagation, including reflection, diffraction and rough surface effects, for the GPS L1 signal has been made. With the combination of a receiver model, also developed within that work, simulations of simple scenarios are made and validated against experimental data. Comparisons between real and simulated carrier to noise (C/N_0) measurements show excellent agreement.

Weiss (2007) uses the advanced GNSS multipath model developed at the University of Colorado since 2004 in his thesis. The model integrates a reflector environment geometry, satellite motion, and antenna/receiver models to simulate multipath errors. The surrounding structures and material properties are defined accurately and a ray-tracing algorithm determines signal paths from the GNSS satellite to the receiving antenna. With the antenna/receiver module the effect of these path delays can be calculated and the error on the pseudorange can be estimated. Comparisons of real and simulated error statistics show that the simulation typically matches the experiment within 5-15 cm.

1.3   Thesis outline

Within this thesis an urban canyon situation is simulated. The accuracy of the implemented models developed for this thesis cannot compete against that of more sophisticated models described above. The urban canyon model in this work is used to investigate on multipath effects, affecting the pseudoranges and the estimated user positions.

The theory in this thesis starts from the estimation of the position solution. A mathematical model describes the calculation of the user position using an epoch-by-epoch least-squares (LS) adjustment in chapter 2. Since the observations for the

LS adjustment are biased, the error range of the pseudoranges have to be determined, to later derive the accuracy of the position solution. The combined navigation errors on the ranging signals is known as user equivalent range error (UERE).An estimated position accuracy (EPA) can be obtained by multiplication of the UERE with simulated DOP factors. Outliers in the observations can degrade the position solution and statistical tests may help to detect and exclude these outliers. An overview of statistical tests is also given in chapter 2.

The UERE is described as the standard positioning service (SPS) signal in space (SIS) performance for all the satellites. It does not cover severe effects like multipath, which can highly affect the pseudoranges in degraded signal environments, for example urban canyons. In chapter 3 the theory of indirect signal propagation and the effect of multipath signals on the measured pseudoranges is described. An overview of the main indirect signal effects in an urban canyon is given and the process of reflection is discussed in detail. All the signals are received by the antenna and processed by the receiver to estimate the pseudoranges. The effect of the antenna on indirect signal propagation and how antennas are typically designed to mitigate multipath effects are described. A general receiver design is explained as well and the estimation of the pseudorange is shown (i) just for direct signals and (ii) if the direct signal and at least one indirect signal, and (iii) if only indirect signals reach the antenna. Future GNSS signals are designed among others to increase the pseudorange estimation performance and some comments are made for future GPS and Galileo signals.

While chapters 3 and 2 describe the behaviour of multipath, the estimation of the pseudorange and the calculation of the user position, chapter 4 uses this theory to create a theoretical model. This model simulates the effect of multipath on pseudoranges and is especially implemented for urban canyon analysis. With the implemented model several scenarios are tested: different antenna performances and receiver designs, or various signal strengths are simulated and the results are compared. Finally the estimation of the user position in an urban environment is evaluated.

The simulations with the urban canyon model are supplemented by experimental results. An evaluation of the UERE and the attainable position accuracy for a state of the art GPS solution is made for a free environment and the results are discussed. Real data is collected in benign and high multipath environments and the positions are calculated with a software provided by the PLAN Group of the University of Calgary (UofC). These results are compared to simulation results of the same environments. Possible multipath effects are shown and finally the effects of multipath on the position solutions are estimated.

Chapter 6 summarizes the results obtained from the simulations and the real data analysis. Conclusions from the results are drawn and recommendations for further work are presented.

Chapter 2

GNSS Navigation Solution

2.1 Introduction

To obtain a position solution using GNSS, the navigation algorithm has to combine the raw measurements from all the satellites in view and the satellites orbit data (Axelrad and Brown, 1994). The satellite orbit data are broadcast with the satellite signal via the navigation message and can be decoded by the receiver. The raw measurements are provided by the GNSS receiver. There are three types of measurements, code range, carrier phase and Doppler shift measurements, where in this thesis only code ranges are considered. The raw code measurements are estimates of apparent transit time of a signal (Misra and Enge, 2006) and so estimates of the instantaneous satellite-to-user range. These estimates are biased and therefore called pseudoranges.

With these measurements the user position can be calculated. The attainable accuracy of the position depends on two factors: the accuracy of the pseudorange measurements and the geometry of the satellite constellation. Both contributions are explained in this chapter. The pseudorange errors can be categorized and with different methods this contribution to the estimated position can be mitigated. The bias on the pseudorange is called user equivalent range error (UERE) and is a factor needed to determine the position accuracy. The standard positioning service performance standard (SPS-PS, U.S. Department of Defense, 2001; this notation will be used for the rest of the thesis) defines levels of performance that can be used to derive standard UERE values. The second factor is the distribution of the satellites in the sky. The DOP describes the satellite configuration and is a quality factor for the user-satellite geometry.

The position solution is relevant, if all outliers are removed from the observation domain. A way to detect such outliers in the observations is based on statistical reliability. In section 2.4 an overview of reliability control for the parameter estimation is given.

The UERE multiplied by the DOP factor yields an estimated accuracy of the user position, denoted as EPA. This quality description is a theoretical approach and describes the position accuracy with a global defined standards of the UERE and the local calculated DOP values. The theory behind this method is described and a theoretical example of the EPA is summarized in a table at the end of this chapter.

2.2 Mathematical model for the user position

In the literature we can find several algorithms to obtain a position solution for GNSS systems, e.g. Axelrad and Brown (1994), Leick (2004), and Kaplan and Hegarty (2006). Kalman filtering and the epoch-by-epoch LS technique are the most common used algorithms to calculate the user position. The benefit of a Kalman filter is that the estimation of the user position is not only based on data at a single epoch (Kaplan and Hegarty, 2006). The filter provides additional information on the dynamic model of the trajectory to improve the estimation. The least-squares (LS) technique first linearizes the basic equation for GNSS positioning about an approximate user position (Taylor approximation). After linearization, an iterative adjustment leads to better approximation to the true position until the difference between two consecutive solutions at the same epoch is below a certain threshold. The estimation of the user position with this method is based on an epoch-by-epoch adjustment.The approach for the LS adjustment can be found in many GPS textbooks (Kaplan and Hegarty, 2006; Misra and Enge, 2006; Hofmann-Wellenhof et al., 2001; Axelrad and Brown, 1994) and is not explained in detail here. Only the most important formulas that will be used herein are listed below.

The general vector-matrix notation for a LS adjustment is

$$\mathbf{y} = \mathbf{A} \cdot \boldsymbol{\xi} + \mathbf{e} \tag{2.1}$$

where $\mathbf{y}$ is the observation vector in the linearized model, $\mathbf{A}$ is the design matrix, $\boldsymbol{\xi}$ are the unknown parameter and $\mathbf{e}$ is the vector of the residuals. Each measurement is now related linearly to the parameters of interest. This equation describes the functional model of the least-squares adjustment.

The parameter vector $\boldsymbol{\xi}$ contains the three unknowns in the position domain and the clock bias. The numbers of observations must be at least equal to the number of parameters, so for a position solution we need at least four satellites. The observation vector $\mathbf{y}$ contains the pseudoranges to all the satellites in view. The code pseudorange ρ^k to the k-th satellite at epoch t (GPS time) can be modeled as

$$\rho^k(t) = r^k(t) + c \cdot \delta t_u + e_\rho^k \tag{2.2}$$

where $r^k = \left\| \mathbf{x}^k - \mathbf{x}_u \right\|$ is the geometric distance between the satellite $\mathbf{x}^k$ and the user position $\mathbf{x}_u$ for $k = 1, 2, \ldots, k$, where k is the number of satellites. The receiver clock bias is denoted as δt_u and c is the speed of light.

All the pseudoranges errors are combined in the term e_ρ^k. The main errors are ephemeris and satellite clock errors, ionospheric and tropospheric delays, multipath and receiver errors. All of them are described later in section 2.3.1. The user can correct some of the errors using parameter values in the satellite navigation message, additional models and extended measurement techniques (Misra and Enge, 2006). After correcting the measurements for these known errors we can rewrite the corrected pseudorange ρ_c^k as

$$\rho_c^k = r^k + c \cdot \delta t_u + e \tag{2.3}$$

where the error term e is the combined effect of the residual errors. This vector of residuals is unknown and therefore it is impossible to get the true values of the parameters. However, it is possible to estimate the parameters by using certain criteria (Caspary, 2000).

The residual errors are assumed to be normally distributed with an expectation of zero. Therefore the LS approach implies that the sum of the squares of the residuals is minimized:

$$\mathbf{e^T P e} = \Omega = minimum \tag{2.4}$$

where $\mathbf{P}$ is the positive-definite weight matrix of the observations. The solution to the minimum problem is

$$\hat{\boldsymbol{\xi}} = \left(\mathbf{A}^T\mathbf{P}\mathbf{A}\right)^{-1}\mathbf{A}^T\mathbf{P}\mathbf{y} \tag{2.5}$$

The LS result is the best linear unbiased estimator, if the weight matrix is the inverse of the cofactor matrix $\mathbf{V}$ of the observations $\mathbf{P} = \mathbf{V}^{-1}$, because it has minimum mean-square-error in this case. The estimation for the individual residuals $\hat{\mathbf{e}}$, related to the observations, and the cofactor matrix $V_{\hat{e}}$ for the residuals are

$$\hat{\mathbf{e}} = \left(\mathbf{A}\left(\mathbf{A}^T\mathbf{P}\mathbf{A}\right)^{-1}\mathbf{A}^T\mathbf{P} - \mathbf{I}\right) \cdot \mathbf{y} \tag{2.6}$$

$$\mathbf{V}_{\hat{e}} = \mathbf{V} - \mathbf{A}\left(\mathbf{A}^T\mathbf{P}\mathbf{A}\right)^{-1}\mathbf{A}^T \tag{2.7}$$

The variance-covariance matrix of the estimated parameters can be written as

$$\mathbf{D}\{\hat{\boldsymbol{\xi}}\} = \sigma^2\mathbf{V}_{\hat{\xi}}, \qquad \mathbf{V}_{\hat{\xi}} = \left(\mathbf{A}^T\mathbf{P}\mathbf{A}\right)^{-1} \tag{2.8}$$

2.3 Assessment of precision

The precision with which a GNSS receiver can determine its position depends mainly on two factors: the errors of the range measurement and the constellation of the satellites in view.

A GNSS receiver measures the pseudorange, which is a raw, noisy and erroneous one-way range measurement, corrupted by a user clock bias. Part of the errors, which Martin (1980) allocates to the various system segment contributors, can be

corrected with various models and methods. The remaining error is called UERE and is still part of the pseudorange measurement. Subsection 2.3.1 gives an overview of the six main pseudorange errors and a description of the possibilities to mitigate or eliminate them. The magnitude of the remaining parts of these errors on the pseudorange is summarized in table 2.1. Here only single point positioning with coarse acquisition (C/A) code measurements is considered. A step-by-step implementation of these corrections for GPS is given in the GPS Interface Specification (ICD-200, 2004; this notation will be used for the rest of the thesis, if the interface specification document is referenced).

The satellite constellation ("geometry") is an important factor for a good position accuracy and the computation results can be seriously degraded by a bad satellite constellation. The concept of the satellite geometry and the calculation for the DOP factors is explained in subsection 2.3.2.

2.3.1 User equivalent range error (UERE)

The pseudorange errors can be grouped into the six following classes (Parkinson, 1994):

1. Ephemeris error
2. Satellite clock error
3. Ionospheric error
4. Tropospheric error
5. Multipath
6. Receiver errors

The basic pseudorange measurement equation with the errors listed above can be written as follows:

$$\rho_u = r_u + \delta_{SV} + c\left(\delta t_{RX} - \delta t_{SV}\right) + \delta_{ION} + \delta_{TROP} + \varepsilon_{noise} + \delta_{MP} \tag{2.9}$$

where, ρ_u is the pseudorange measurement (m),
         r_u is the true geometric range between satellite and user (m),
      δ_{SV} is the orbital error (m),
         c is the speed of light (m/s),
    δt_{RX} is the receiver clock error (s),
    δt_{SV} is the satellite clock error (s),
    δ_{ION} is the delay due to the ionosphere (m),
  δ_{TROP} is the delay due to the troposphere (m),
   ε_{noise} is the pseudorange measurement noise (m) and
    δ_{MP} is the multipath error.

The error sources and the expected values for these errors are discussed briefly within the next pages, following the description by Kaplan and Hegarty (2006).

Ephemeris Error

The ephemeris of the satellites are predicted and uploaded from the control segment to the satellites to be rebroadcast to the user. This prediction of the satellite position for four hours can be erroneous and the error grows with the age of the data. The ephemeris errors are generally smallest in the radial direction (direction toward the earth centre), but contribute most to the pseudorange measurement (Kaplan and Hegarty, 2006). The effective pseudorange error due to ephemeris prediction is in the order of 0.8 m (1σ, Taylor and Barnes, 2005). Precise GPS orbits for post-mission applications can be downloaded from the International GNSS Service (IGS, www.igscb.jpl.nasa.gov) web site and the expected accuracy for the orbit data is about 5 cm (IGS, 2008).

Satellite clock Error

Although highly stable clocks are used in the satellites, these clocks still have biases and drifts. The satellite clock error is predicted by the control segment monitoring, and the correction parameters are transmitted to the satellite. These parameters are included in the navigation data and the user can use them to correct the satellite clock error. Range errors due to residual clock errors are between 0.8 m and 4 m, the nominal 1σ value for the constellation in 2004 averaged over the age of data is 1.1 m (Taylor and Barnes, 2005).

Ionospheric Error

The free electrons in the ionosphere influence the electromagnetic wave propagation of the GPS signal. In particular, the pseudorange signal is delayed with the delay being a fraction on electron density. The approximate delay can be modeled, and the navigation message contains parameters of an empirical model developed by Klobuchar (1987). The model is updated every week and removes about 50% of the ionospheric delay at mid-latitude. A better estimation of the ionospheric delay can be derived with a dual-frequency receiver (L1/L2) or it can be reduced by receiver single differences, if the distance between the two receivers is small. For a signal arriving from the zenith, the delay is about 3 m at night and 10 m during the day. The delay of low elevation satellites can be 3 times higher than zenith delay measurements due to a longer signal path through the ionosphere. A typical 1σ value for ionospheric delays is 7 m (Kaplan and Hegarty, 2006), averaged over the globe and over all elevation angles.

Tropospheric Error

The tropospheric delay of the GPS signal is a function of the refractive index along the signal propagation path, which depends on the respective temperature, pressure and relative humidity. The longer the signal propagates through the troposphere, the larger is the delay. So the effect of the troposphere on low elevation satellites is much higher than for high elevation satellites. There exists several models to determine the path delay within an accuracy of 0.2 m (Cannon and Lachapelle, 2006). The

Saastamoinen model and the Hopfield model are the most commonly used models to determine the tropospheric delay in GPS. The error, left uncompensated, can vary from 2.4 m at the zenith to about 25 m for a low elevation (5°) satellite. In general the tropospheric delay can be corrected by 80-90% through modeling at the user position (Cannon and Lachapelle, 2006).

Multipath Error

Multipath is one of the most significant error sources for GPS. It affects both pseudorange and carrier phase measurement and is caused by non-LOS signals entering the receiver front and distorting the correlation peak of the direct signal. A more detailed description is given in chapter 3. The multipath effect can vary significantly depending exclusively on the receiver environment. This effect can be mitigated by the antenna gain pattern and the receiver design. Typical multipath error in pseudorange measurement varies from 1 m in a benign environment to more than 5 m in highly reflective environment (Misra and Enge, 2006). Kaplan and Hegarty (2006) use a value of 0.2 m for the the typical 1σ multipath level in a relatively multipath free environment.

Receiver Errors

The receiver errors include receiver noise, resolution, and user equipment biases. These errors are relatively small in comparison to other error sources. The dominant receiver error sources are thermal noise and interference in the tracking loops. The receiver errors are in the order of about 0.1 m for typical modern receivers (1σ) on the code measurement for typical modern receivers (Kaplan and Hegarty, 2006).

Combined UERE

The combined effect of all these remaining error sources on the pseudorange measurement is referred to as the UERE. The error components are considered independent, but the combined UERE for a satellite is assumed to be Gaussian distributed. So it can be obtained by taking the root-sum-square of the single error components or the segment components (Misra and Enge, 2006). The equation is as follows:

$$\sigma_{UERE} = \sqrt{\sigma_{SV}^2 + \sigma_{clock-SV}^2 + \sigma_{ION}^2 + \sigma_{TROP}^2 + \sigma_{MP}^2 + e_{noise}^2} \qquad (2.10)$$

Table 2.1 shows estimates of typical UERE errors based on the previous discussion. Because of the different interpretation of the errors on the pseudorange measurement, in this table two error assessments given in well established textbooks are shown: (i) the pseudorange error budget by Kaplan and Hegarty (2006, p. 322), which are 1-sigma estimates of the typical contemporary UERE budgets and (ii) the one by Misra and Enge (2006, p. 179), which are RMS values based on empirical data. The error budget is presented for a single-frequency (L1) receiver.

Segment source	Error source	1σ Error (Kaplan, Hegarty)	1σ Error (Misra, Enge)
Space segment	broadcast ephemeris	0.8 m	3 m
	satellite clock	1.1 m	
Propagation Link	Ionospheric delay	7.0 m	5 m
	Tropospheric delay	0.2 m	
User segment	Multipath	0.2 m	1 m
	Receiver errors	0.1 m	
UERE		7.1 m	6 m

Table 2.1: *Typical UERE Budget for GPS Standard Positioning Service*

The UERE in table 2.1 are defined for the SPS assuming that selective availability (SA) is not operating. The dominant error is the ionosphere because of the inexact models for estimation of the ionospheric delay. The accuracy standard declared by the SPS-PS are similar to those described above. Within this document only the user range error (URE) has been described, which means the error components of the SIS performance are considered only, namely space segment errors and propagation errors. The user equipment errors (receiver errors and multipath) are not used for an estimation of the URE. The SPS-PS declares a root mean square (RMS) less than 6 m for the SIS SPS URE. The value is an average value of a 24-hour period for any point on the earth surface. Since the receiver and multipath errors in favorable environments are relatively small compared to other error sources, the URE and UERE are considered as the same values herein. The Precise Positioning Service (PPS) performances are similar to those of the SPS less the effect of the ionosphere and also available in the SPS-document. The main difference is the ionospheric delay, which can be estimated by a dual-frequency measurement. The effect of the ionosphere is reduced from 7 m (SPS ionospheric error) to 0.1 m. The obtained UERE for the PPS is about 1.4 m.

2.3.2 Dilution of precision (DOP)

The concept of DOP is based on the relative geometry from the satellites in view. It is an important factor to achieve good position accuracy and it changes with time due to the relative motion of the satellite and the user.

Geometrically the DOP can be interpreted as the possible error for the position estimation due to the errors of the user-satellite vectors. A simple 2D example from Misra and Enge (2006, p. 207) is shown in figure 2.1. The true ranges between the user and the satellites, shown as S_1 and S_2 in the figure, describe circles in the two-dimensional space. If these range measurements would not have any errors, the user position could be determined exactly as lying at the intersection between the true satellite-to-user vectors. If the range measurements are erroneous, the true ranges cannot be determined exactly. The observations might vary within a certain range;

the possible values with this range are displayed as the inner and outer circles in figure 2.1. The shaded area is the region of uncertainty in the position estimate, and it is smaller with good satellite geometry in figure 2.1(a). Here the intersection angle of the satellite-to-user ranges (seen from the user) is about 90°. In figure 2.1(b) this angle is acute, which leads to a larger area of uncertainty, a high DOP and a low accuracy for the calculation of the position.
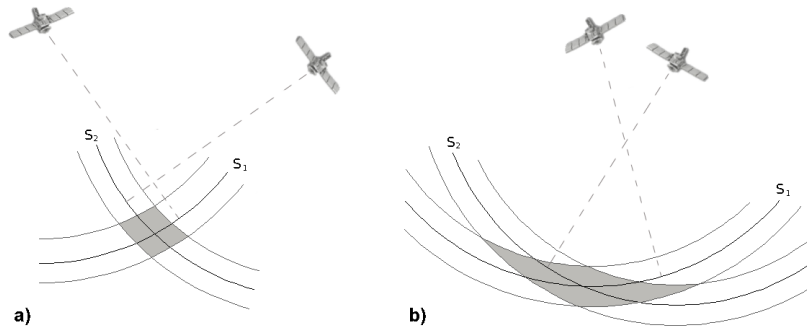
Figure 2.1: *Relative geometry and dilution of precision concept: (a) geometry with low DOP, and (b) geometry with high DOP. The shaded area is the region of uncertainty (after Misra and Enge, 2006)*

The DOP values can be obtained from the cofactor matrix, which is the inverse of the normal equation matrix of the solution (Hofmann-Wellenhof, 2001). The cofactor matrix $V_{\hat{\xi}}$ follows from 2.8

$$\mathbf{V}_{\hat{\xi}} = \left(\mathbf{A}^T \mathbf{P} \mathbf{A}\right)^{-1} = \begin{bmatrix} v_{xx} & v_{xy} & v_{xz} & v_{xt} \\ v_{yx} & v_{yy} & v_{yz} & v_{yt} \\ v_{zx} & v_{zy} & v_{zz} & v_{zt} \\ v_{tx} & v_{ty} & v_{tz} & v_{tt} \end{bmatrix} \tag{2.11}$$

where $\mathbf{A}$ is the design matrix. The cofactor matrix is a $4 \cdot 4$ matrix and contains the components of the user site position x, y, z and the receiver clock t. The commonly used DOP parameters are GDOP (Geometry DOP), PDOP (Position DOP), and TDOP (Time DOP) which can be derived from the diagonal elements of the cofactor matrix as follows:

$$\begin{aligned} GDOP &= \sqrt{v_{xx} + v_{yy} + v_{zz} + v_{tt}} \\ PDOP &= \sqrt{v_{xx} + v_{yy} + v_{zz}} \\ TDOP &= \sqrt{v_{tt}} \end{aligned} \tag{2.12}$$

The DOPs in equation 2.12 are expressed in the equatorial system. To determine the horizontal and the vertical dilution of precision the cofactor matrix has to be transformed into a local cofactor matrix (Hofmann-Wellenhof, 2001). If the time-correlated components of the cofactor matrix are not considered, the transformation

can be written as

$$\mathbf{V}_{\hat{\xi}}^{LL} = \mathbf{R}\mathbf{V}_{\hat{\xi}}\mathbf{R}^T = \begin{bmatrix} v_{nn} & v_{ne} & v_{nu} \\ v_{en} & v_{ee} & v_{eu} \\ v_{un} & v_{ue} & v_{uu} \end{bmatrix} \tag{2.13}$$

where the Rotation matrix $\mathbf{R} = [\mathbf{n}\ \mathbf{e}\ \mathbf{u}]^T$ contains the axes of the local coordinate system. By knowing the user position in latitude φ and longitude λ the three axes north $\mathbf{n}$, east $\mathbf{e}$ and up $\mathbf{u}$ can be described as:

$$\mathbf{n} = \begin{bmatrix} -\sin(\varphi)\cos(\lambda) \\ -\sin(\varphi)\sin(\lambda) \\ \cos(\varphi) \end{bmatrix}, \quad \mathbf{e} = \begin{bmatrix} -\sin(\lambda) \\ \cos(\lambda) \\ 0 \end{bmatrix}, \quad \mathbf{u} = \begin{bmatrix} \cos(\varphi)\cos(\lambda) \\ \cos(\varphi)\sin(\lambda) \\ \sin(\varphi) \end{bmatrix} \tag{2.14}$$

The elements of the transformed cofactor matrix $\mathbf{V}_{\hat{\xi}}^{LL}$ yield the HDOP (Horizontal DOP) and VDOP (Vertical DOP) values:

$$\begin{aligned} HDOP &= \sqrt{v_{nn} + v_{ee}} \\ VDOP &= \sqrt{v_{uu}} \end{aligned} \tag{2.15}$$

According to the SPS-PS, the PDOP for GPS constellation worldwide does not exceed the DOP value of 6 in 98% of the cases. A more representative median for day-to-day GPS data collections ($50th$ percentile) is a PDOP of about 2.5, a HDOP (1σ) about 2.0 and a VDOP (1σ) of again 2.5, found in Parkinson (1994, p. 477 and p. 481). Due to bad geometry factors the results for the position accuracy can be adversely affected by a large factor.

2.4 Assessment of Reliability

The accuracy of the position solution is relevant only if the data have been cleared from gross errors. For real data environments the detection of blunders may not occur with certainty. A way to detect outliers is the use of statistical reliability theory.

The relation between the measurements and unknown parameters is comprised in the functional model, stated in equation 2.1. The uncertainty of the constellation is described in the stochastic model, see equation 2.8. Random errors and noise can be described by a statistical distribution and do not affect the functional or the stochastic model (Tiberius, 1998). Outliers can be captured neither by the functional nor by the stochastic model. The goal of reliability testing is to detect these blunders, otherwise these biased observations would have an impact on the position solution and they would invalidate the quality description.

One of the results from the LS adjustment, considering a single epoch only, is the residual vector for the observations, see equation 2.6. The aim of the LS adjustment

is to minimize these residuals and so to reduce their impact on the final solution. But it also means, that a single outlier spreads its effect over all the other observations. Using the global model test, the sum of the squares of the residuals (see equation 2.4) is used to identify if the solution is internally consistent. If not, statistical tests with the individual residuals are used to identify possible erroneous observations.

To detect and to exclude one or more outliers, we need to follow an iterative process. To obtain plausible results, the functional and the statistical model have to be correct. The data is adjusted by a epoch-by-epoch LS and the so-called global model test detects potential model errors. If the global test fails, the data contains one or more biased observations. These errors can now be detected with the local model test, where every single observation is tested separately. Each individual residual, normalized with its standard deviation, is compared to a globally defined threshold. If a standardized residual exceeds this threshold, the observation is flagged as erroneous. Not every flagged observation has to be biased and need to be excluded for the LS adjustment. Traditional Receiver Autonomous Integrity Monitoring (RAIM) algorithms assume that there is only one blunder in the current time instance. The highest residual is treated as the biased observation and is eliminated (Baarda, 1968; Kuusniemi, 2004). After eliminating the most likely outlier, the position solution has to be recalculated and again the solution is tested for potential outliers. This iterative process is finished after the global test has been accepted, which means all errors are eliminated. The global and the local model test can be found in many textbooks and papers (Baarda, 1968; Caspary, 2000; Kuusniemi, 2004), where the process of statistical tests is described more in detail.

This method of detecting and eliminating blunders works well for large datasets with a small amount of erroneous observations. An example for satellite positioning is a satellite constellation of eight satellite vehicles, where one of the observations is affected by multipath. The erroneous pseudorange is affected by a few metres and so is the position solution. With the statistical tests it is possible to detect this outlier and to eliminate it, so that the calculation of the position solution is not affected by gross errors.

In urban canyons, which are considered high multipath environments, we already have a poor satellite visibility due to obstructions from close buildings. In addition, many signals that we receive at the antenna may be affected by multipath. So it can happen that the number of biased observations in urban canyons is higher than the number of unbiased observations. In this case an identification of the true outliers is not always possible and may cause the exclusion of unaffected observations due to the distribution of the residuals as result from the LS adjustment.

Standard procedures as described above try to eliminate potential outliers by an iterative rejection of individual observations. Ryan (2002) deals with the case of simultaneous multiple blunders. Simulations show that multiple blunders were effectively detected by the described blunder detection scenario.

For both outliers detection methods described above a LS approached is used. LS algorithms take into account only a single epoch and only the current measurements to estimate the user position and velocity. Kalman filtering combines the knowledge of the statistical nature of system errors with informations of system dynamics data, to estimate the current state of the system (Kaplan and Hegarty, 2006). The advantage of a Kalman filter is the ability to take past measurements and aid the current epoch, which makes the algorithm as the preferred algorithm in navigation applications. However, in degraded environments we may have low accuracy levels and poor knowledge of user dynamics, which may cause suboptimal results using a Kalman filter (Kuusniemi, 2005).

2.5 Assessment of Accuracy

As we have seen in the previous sections, the absolute accuracy of GPS point positioning depends on the accuracy of the measured pseudoranges as well as on the satellite geometry. The accuracy of GPS positioning is described in the SPS-PS. The document defines standards based on SIS performance and defines a UERE of 6 m RMS and a PDOP lower than 6. The standards are globally defined values, averaged over a 24-hour period at any place on the earth surface. Severe contributions of the ionosphere (for example during ionospheric storms), unexpected receiver errors, multipath, or interference are not included.

The UERE is different from satellite to satellite. However, for certain situations the UERE can be assumed identical for all the satellites in view (Kaplan and Hegarty, 2006). An example is position estimation with GPS satellites only. Here the components of the UERE can be assumed to be correlated among the satellites. So the UERE can be combined among all the satellites and is used to describe the standard accuracy of the range measurements to all the satellites.

The attainable accuracy of the position/time solution for GPS is a function of the overall range errors and the geometrical distribution of the satellites and can be approximated by the following formula (Misra and Enge, 2006; Kaplan and Hegarty, 2006):

$$\text{(error in GPS solution)} = \text{(DOP)} \cdot \text{(UERE)} \tag{2.16}$$

For the specific values of the position accuracy, the UERE has to be multiplied by the appropriate DOP factor. The equations can be rewritten as:

$$\text{3D RMS error} = \text{PDOP} \cdot \sigma_{UERE} \tag{2.17}$$

$$\text{2D RMS error} = \text{HDOP} \cdot \sigma_{UERE} \tag{2.18}$$

$$\text{vertical RMS error} = \text{VDOP} \cdot \sigma_{UERE} \tag{2.19}$$

With the above formulas, the EPA can be calculated. According to the SPS-PS

the global average positioning accuracy standard (for 95% of the results) are 13 m and 22 m for horizontal and vertical positioning, respectively. These standards are based on a measurement period of 24 hours averaged over all points within the service area of GPS. The 50% percentile accuracies, found in textbooks and documents (e.g. Parkinson, 1994; Misra and Enge, 2006; SPS-PS, 2001), are summarized in Table 2.2 and the RMS error on the position solution are calculated with equations 2.17-2.19.

	DOP (1σ)		**UERE** (1σ)	**Position error** (1σ)	
SPS	PDOP	3.2	6.0 m	3D RMS	19.2 m
	HDOP	2.0		2D RMS	12.0 m
	VDOP	2.5		vertical RMS	15.0 m
PPS	PDOP	3.2	1.4 m	3D RMS	4.5 m
	HDOP	2.0		2D RMS	2.8 m
	VDOP	2.5		vertical RMS	3.5 m

Table 2.2: *Attainable position accuracies with 50% percentile values for UERE and DOP factors*

These accuracies are representative only for a LOS environment, which means that the user has clear visibility to all satellites. No severe errors on the pseudorange (for example ionospheric errors due to ionospheric storms, severe multipath etc.) are accounted in these EPA estimates. In a urban environment the criteria for the positioning standards are not fulfilled and do not match the requirements described above. The satellites are not visible at every instant because obstacles like buildings can block the satellite signal. In addition, some of the pseudoranges might be affected by multipath and so the UERE exceeds the performance standards. The consequence is that the EPA estimates are not representative values. The impact on position estimation is much higher due to the large errors on pseudoranges, especially the multipath effect can cause severe errors. The effect of multipath on the pseudorange and finally on the estimated position is the main goal of this work and will be described in the next chapters.

Chapter 3

Multipath Theory and its Effects

3.1 From the satellite signal to the pseudorange

The GPS signal has to travel approximately 20000 km from the satellite to the user. On its way the signal is affected by many different perturbing sources, which have different degrees of impact on the estimated pseudorange. One of the major error sources is multipath, a phenomenon whereby a signal arrives at the receiver via multiple paths (Braasch, 1995). In this chapter the theory of multipath and its impact on the pseudorange is described.

Starting from the satellite the signal travels 20000 km through the atmosphere to reach the antenna at the earth surface. The signal must first pass the ionosphere, where due to the electromagnetic wave properties the electron density cause signal delays. The troposphere effects the GNSS signal mainly because of dryness of the neutral atmosphere and is responsible for additional signal delays. Reaching the Earth surface, the direct path to the antenna may be blocked by objects like buildings or trees. In such cases, the signal could be reflected, bent or even completely blocked from the reception at the antenna. Different types of non-LOS propagation have different impacts on the signal, which is explained in detail in section 3.3. The signal is received by the antenna and therefore the antenna has to provide best possible reception performance for the incoming signal. The antenna design should consider a specific gain pattern as well as multipath rejection or mitigation. These properties can already help to reduce possible errors. The receiver, or more precisely the receiver tracking loop, converts the incoming signal into the pseudorange. The code tracking loop as a part of the receiver design is described, to give a brief overview of the GPS C/A-code tracking algorithm. The effect of multipath on the tracking loop is covered theoretically and an example demonstrates the impact on the GPS pseudorange.

With the developments of new GNSS technologies, better positioning is expected. These developments include among others two new satellite systems, Galileo and Compass, and the modernization of two already existing systems, GPS and GLONASS.

In section 3.5.3 a brief overview of the new GNSS signals for Galileo and the modernized GPS and its improvements on the receiver tracking loop are provided.

3.2 The GPS signal propagation

3.2.1 The electromagnetic wave

Electromagnetic (EM) waves are formed when an electrical field is coupled with a magnetic field. The electric field (E) and the magnetic field (H) are perpendicular to each other at any time, while propagating through space. The GPS signal is a transverse electromagnetic (TEM) wave, which means perpendicular to the direction of the propagation, denoted by the propagation vector k in figure 3.1 (after Ray, 2000). Through vacuum the EM-wave propagates with the speed of light. The propagation can be described with Maxwell's laws and the derivations can be found in several textbooks, e.g. Griffiths (1999).
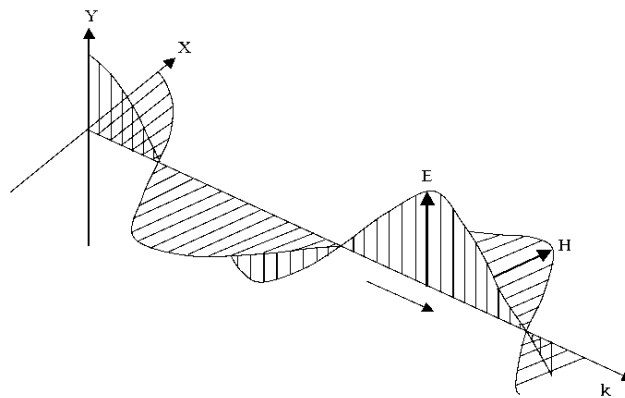
Figure 3.1: *Electromagnetic wave propagation (after Ray, 2000)*

The tip of the electric field vector describes a line in space while travelling in the direction of the wave. The shape of this line defines the polarization of the wave. If the direction of the electric field does not change over time, the wave is linearly polarized. If the electric field vector rotates as a function of time, the tip of the E-field vector describes a circle or an ellipsoid. This means that the wave is either circularly or elliptically polarized. Different polarizations are shown in figure 3.2 after Ray (2007). The GPS signal is a right-handed circular polarized (RHCP) TEM wave. Right-handed means, "that the rotation from E to H is in the direction of a right-hand-threaded screw if seen along the direction of propagation" (Kraus and Carver, 1973).

The signal has to travel through 20000 km of free space, ionosphere and troposphere from the satellite to the antenna. The major concerns for satellite communication in
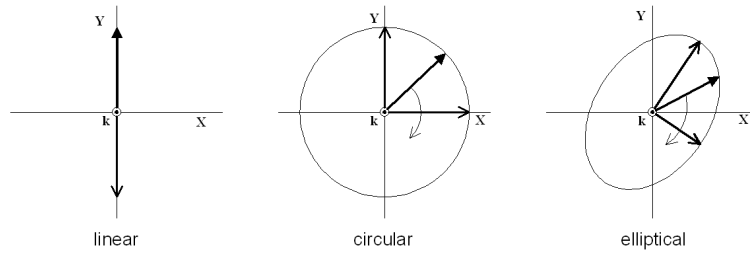
Figure 3.2: *Linear, circular and elliptical polarization (after Ray, 2007)*

the ionosphere are scintillation effects and changes in polarization, known as Faraday Rotation (see Collin,1985). The troposphere affects the GPS signal, it changes the path of the direct signal and introduces small path delays. A more detailed description of the ionospheric effects on the signal can be found in Klobuchar (1996), while the effect of the troposphere is described more detailed in Spilker (1994 a).

An accurate simulation of the electromagnetic wave propagation from the satellite to the user would be too extensive. An often used simplification for EM wave propagation can be described with geometrical optics, where the signal is described as a single ray. This method has also been used in Ray (2000), Hannah (2001), Ryan (2002) and Weiss (2007).

3.2.2   Representation of the signal

In an ideal case the GNSS receiver input consists only of the direct signal $S_d(t)$ from the satellite. Neglecting the navigation message and assuming that the signal carries the C/A code only, the input signal at a certain epoch t can be simplified according to Ray (2007) as:

$$S_d(t) = A \cdot C \left(t - \tau_0\right) \cdot \cos\left(\omega_0 t + \gamma_0\right) \tag{3.1}$$

where, A is the signal amplitude (Volt),
C is the C/A code,
τ_0 is the code delay (sec),
ω_0 is the signal centre frequency (rad/s), and
γ_0 is the signal carrier phase (rad).

In an urban environment, objects close to the antenna can affect the direct (line-of-sight, LOS) signals and produce multipath effects. In this case, the input signal consists of the direct signal $S_d(t)$ and one or more multipath signals $S_i(t)$ at a time t. The received signal in the presence of one direct and one or more indirect signals is represented as:

$$
\begin{aligned}
S(t) =& S_d(t) + \sum_{i=1}^{n} S_i(t) \\
=& A \cdot C\left(t - \tau_0\right) \cdot \cos\left(\omega_0 t + \gamma_0\right) \\
& + \sum_{i=1}^{n} \alpha_i \cdot A \cdot C\left(t - \tau_0 + \tau_i\right) \cdot \cos\left(\omega_0 t + \gamma_0 + \gamma_i\right)
\end{aligned}
\tag{3.2}
$$

where, n is the number of multipath signals,
α_i is the multipath to direct ratio (MDR) of amplitudes,
τ_i is the additional travel time of the reflected signal (sec), and
γ_i is the received carrier phase difference of the direct
and indirect signal (rad)

According to equation 3.2, the impact of a multipath signal depends on the path delay, the MDR and the carrier phase difference. The path delay is the additional path length from the multipath signal divided by the speed of light and it depends on the user environment. The relative amplitude expresses the power of a multipath signal, where a multipath signal with an MDR of one has the same power as the direct signal. The amplitude is a function of the properties of the reflector, the polarization of the incoming signal and the antenna gain pattern. The phase difference between direct and indirect signal describes the effective impact of the multipath signal on the pseudorange and is described in section 3.5.1.

3.3 GPS signal reflection

3.3.1 Reflection, diffraction and shadowing

In an urban canyon where the antenna is surrounded by objects like buildings, the direct signal reception is highly affected. The obstacles in the LOS between the antenna and the satellites can either completely block, attenuate, or also bend the direct signals. The consequences are a lower satellite visibility if the signals are blocked, shadowing effects if the signal has to travel through objects, or diffraction if the direct signal is bend from edges of the objects. Another large effect in urban canyons are reflections of the direct signal from the surrounding surfaces, well known as multipath. These effects on the signals in an urban environment are visualized in figure 3.3.

Shadowing is excess attenuation of the direct signal when it propagates through objects (Kaplan and Hegarty, 2006). The signal reception in forests is a typical environment where shadowing effects can occur. Diffraction is caused by edges of close objects. The diffracted signal will have an error in time-of-travel estimation and a loss of signal power. According to Hannah (2001), the so-called knife-edge diffraction can be described by the Fresnel diffraction parameter, which depends on the geometrical parameters of the receiver-object constellation. Neither shadowing
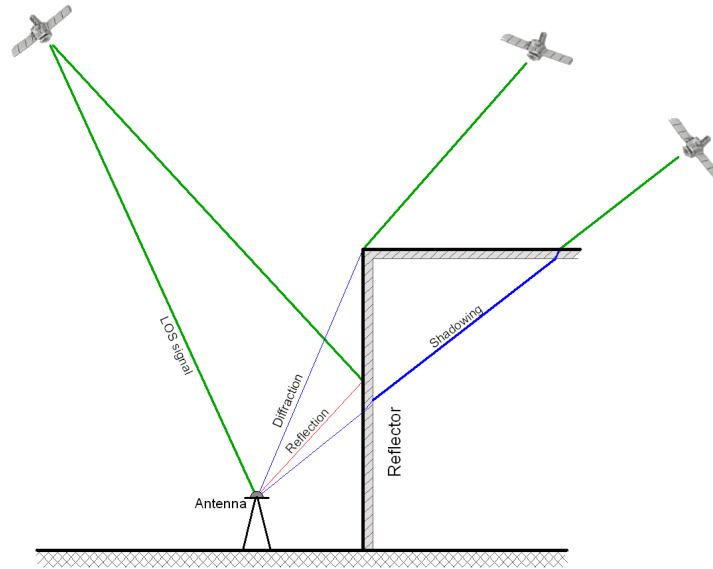
Figure 3.3: *Signal propagation effects in an urban environment*

nor diffraction will be considered in this work.

The important effect for this thesis is multipath, which is indirect signal reception. The indirect signal can be received (i) as a secondary signal, additional to the direct signal, or (ii) as the only received signal, if the direct signal is blocked by objects. An indirect signal can reach the antenna being reflected from close surfaces or the ground. These reflections are replicas of the direct signal with a certain time delay and usually weaker than the LOS signal. The secondary paths affect the receiver tracking loops through distortion of the correlation peak.

The reflection can be distinguished as two types, namely diffuse and specular. Diffuse scattering occurs on rough surfaces, is irregular and hard to estimate. Within this thesis this irregular multipath is not considered and is not therefore explained in detail. An overview of diffuse reflection theory and its effect on the GPS signals can be found in Braasch (1995) and Hannah (2001). Specular reflection occurs on smooth surfaces, is regular and deterministic. This reflection depends on the reflection coefficient of the surface and is discussed in subsection 3.3.2. For this thesis, only specular reflection on smooth surfaces is considered.

The irregularities on the surface determine if the reflector can be considered as smooth or rough. The Rayleigh criterion, described in Beckmann and Spizzichino (1963) or Warren (1983), quantifies the roughness of a surface, depending on the wavelength and the incident angle of the signal. The result is the critical height h of the irregularities on the surface, which is visualized in figure 3.4. If the height of surface irregularities is smaller than the critical height, we can assume that the

surface is smooth. For example a building with irregularities up to 5 cm is a smooth reflector for GPS L1 signals with incident angles of 60° or less (with an incident angle of 0° means, the signal is exactly perpendicular to the surface).

(a) Critical height (h): definition

(b) Critical heights for GNSS
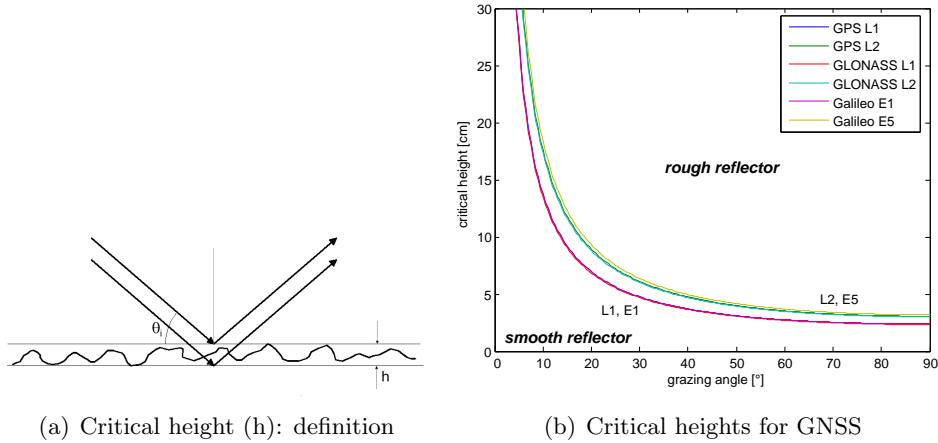
Figure 3.4: *Critical height h of a surfaces due to its irregularity*

3.3.2   The reflection on the surface

Reflection causes a change in direction, polarization, magnitude and phase of the signal. For a planar reflector, the signal reflection properties can be determined as follows. The change in the direction of travel follows Snell's law. It means that the angle of incident and the angle of reflection are equal for reflections on smooth surfaces. If a signal hits an object and is reflected, the electromagnetic properties of the signal change. This change in polarization, magnitude, and phase can be described by the reflection coefficients of the interfacing object, which depends on the signal wavelength (GPS L1: $\lambda =$ 19 cm), the incident angle of the signal, and the electrical properties of the reflector (conductivity, relative permittivity, and the dielectric constant). The formula to calculate the reflection coefficients are derived from the Fresnel equations and can be found in Collins (1985). Since the calculation of the reflection coefficients for certain materials is very complicated and not of a great help for this work, different coefficients are assumed and expressed in dB-loss of signal power due to reflection (described better in section 4.2.3).

The change in magnitude and the phase shift of the reflected signal depend mainly on the type of reflector. If the signal is highly absorbed from the surface, we can say that the reflecting surface is a weak reflector or bad conductor. A wall of concrete is a bad conductor, what means that the signal looses much power when it gets reflected. On the other hand we have good conductors where the reflected signal is almost as strong as the direct signal (e.g. glass). The GPS L1 signal, which carries

the C/A-code, is a RHCP signal (see also discussion in section 3.2.1), transmitted on a frequency of 1575.42 MHz. The maximum change of polarization is achieved when the signal is exactly perpendicular to the reflecting surface and so the polarization turns into left-handed circular polarized (LHCP). For simplicity we assume that a reflection from a surface causes a total change in polarization.

For a more detailed treatment of electromagnetic waves reflections, see Beckmann and Spizzichino (1963), Kraus and Carver (1973), Collin (1985), Balmain (1989), and Griffiths (1999).

3.4 The antenna gain pattern

A GPS antenna has to fulfill certain requirements to provide the best possible reception performance for the incoming signal. According to Dierendonck (1995, p. 332) the parameters that dedicate the antenna requirements are as follows: gain vs. azimuth and elevation, multipath rejection, interference rejection, phase stability and repeatability, profile, size, and environmental conditions. But not all of these parameters are necessarily important for this work and so the description is limited to the antenna gain pattern.

The gain requirements are a function of satellite visibility and closely related to partial mitigation of some elevation dependent errors (e.g. multipath). The goal is to have near uniform gain toward all satellites above a certain elevation, but at the same time reject multipath signals and interference, typically present at low elevation angles (Dierendonck, 1995, p. 332). Therefore, a typical GPS antenna has a high gain at angles toward the zenith and a low gain toward low elevation angles.

The GPS signal is RHCP and so the ideal antenna should be designed to receive only RHCP signals and reject LHCP signals. But this is possible only in theory. Even well-designed antennas will exhibit a small crosspolarized response (Kaplan and Hegarty, 2006). Therefore the antennas has to be designed in an optimal sense: maximum reception for RHCP signals and at the same time maximum attenuation of LHCP signals. Since a reflection in general cause a total change of polarization, the attenuation of LHCP signals is a great benefit to mitigate multipath effects. Nevertheless a signal reflected twice is again RHCP and so the problem of multipath is still present and has to be considered.

The antenna gain pattern for the NovAtel GG-702 antenna for the GPS L1 frequency is shown in figure 3.5 as an example. The gain difference for RHCP and LHCP signals varies from 15° to 30°, depending on the elevation angle. The higher the elevation, the higher the difference between co- and crosspolarization. The antenna gain pattern might not look the same for every type of antenna. Antenna designs vary, depending on the user requirements. The NovAtel GG-702 antenna is a geodetic antenna and is specially effective for static measurements. Low cost
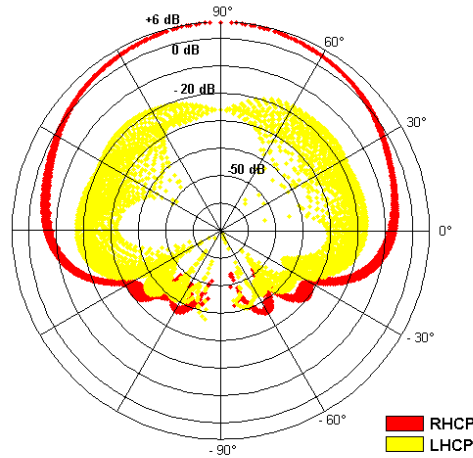
Figure 3.5: *GPS L1 antenna gain pattern from NovAtel GG-702 (courtesy of NovAtel Inc.)*

antennas are often used for navigation purposes and this research will also cover the theoretical performance of such low-cost (LC) antenna.

3.5 Impact on the receiver tracking loop

3.5.1 The receiver tracking loops

A typical GPS receiver is used to determine the user position, velocity, and time. It can be separated in a receiver part, which provides the measurements, and a navigation processor, which calculates the user position and velocity and the time. The receiver part consists of two general parts: the radio frequency (RF) front end module and the signal processing module (Dierendonck, 1995; Ray, 2007).

The main functions of the RF front end are the down conversion of the GPS frequency to an intermediate frequency (IF) and the transformation from an analog to a digital signal. After this point the digitized IF signals are ready to be processed by the signal processor. This module is the core of a receiver and performs the acquisition and tracking of the satellite signal. The results are the navigation data, the Doppler frequency, the C/N_0, the pseudorange, and the range-rate measurements of the received signal. The measurements are done for each visible satellite separately. The estimation of the pseudoranges with the C/A-code is provided from the code tracking algorithms. The algorithm measures the time shift required to align the C/A-code replica generated at the receiver with the incoming signal from the satellite (Misra and Enge, 2006, p. 148). This time shift multiplied with the speed of light result in the pseudorange.

The delay look loop (DLL) is used for pseudorange measurements. The DLL aligns the locally generated code with the incoming signal by using correlators. Figure

3.6, from Kaplan and Hegarty (2006, p. 177), shows a simple diagram of the receiver tracking algorithm. For this visualization three correlators have been used, with a correlator spacing between the early (E) and late (L) correlator of 1 chip (1 chip error in the code tracking loop corresponds to 293 m error on the C/A-code pseudorange for GPS). One single chip of the incoming signal is visualized in the upper part of the figure. Below the replica signal for the early, the prompt and the late correlators are shown for the exact same chip. Once the replica code is aligned
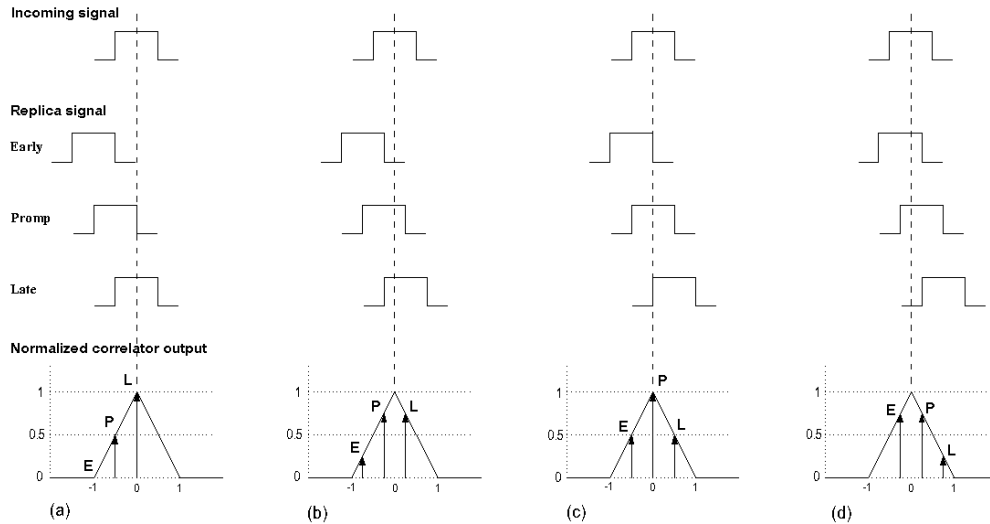
Figure 3.6: *Code correlation phases for a wide correlator: (a) replica code 0.5 chip early, (b) replica code 0.25 chip early, (c) replica code aligned, (d) replica code 0.25 chip late (from Kaplan and Hegarty, 2006, p. 177)*

with the incoming signal (figure 3.6 (c)), the prompt (P) correlator is exactly on the maximum. The early (E) and late (L) correlator are equal in amplitude and no error is generated by the discriminator. If the replica code is misaligned (figure 3.6 (a), (b) and (d)) the early and late correlator are unequal. This error is proportional to the code delay between the replica and the incoming signal.

There are several discriminator-based DLL algorithms which differ in terms of correlator spacing and the number of used correlators. The following description is based on a very simple tracking algorithm, which will be used for further simulations in this thesis. It is based on two correlators and the chip spacing corresponds to 1.0 chip for for wide and 0.1 chip for Narrow Correlator™ spacing. The discriminator algorithm is a coherent early minus late (EML) envelope, normalized by $E + L$ to remove the amplitude sensitivity. The code error τ_{DLL} can be described as follows (Ray, 2007):

$$\tau_{DLL} = \frac{T}{2} \frac{E - L}{E + L} \tag{3.3}$$

where T is the chip spacing between the early (E) and late (L) correlator outputs.

The performance of a DLL is well characterized by the so called S-curve. Here, the expected discriminator value of the error is shown as a function of the code tracking error. The S-curve is shown in figure 3.7.
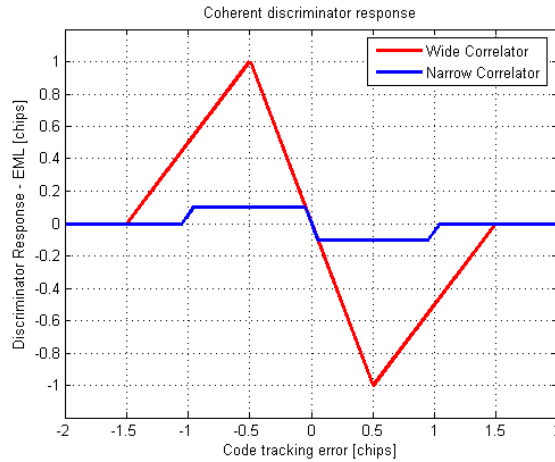
Figure 3.7: *Discriminator output for EML discriminator with wide and narrow correlator spacing*

3.5.2 Influence of multipath on the code tracking loop

In the presence of multipath, the autocorrelation triangle shown in figure 3.6 becomes distorted. Additional to the LOS signal, the input signal carries also a multipath signal, a copy of the direct signal with a certain delay, attenuation and phase shift (equation 3.2). Figure 3.8 shows the effect on the correlation function on the tracking loop in the presence of one multipath signal. The multipath signal is delayed by 0.5 chips or approximately 150 m, and attenuated by 70% or with a signal to multipath ratio (SMR) of 3 dB compared to the direct signal. The multipath signal is in-phase (IP) in figure 3.8 (a) and out-of-phase (OP, phase offset of 180°) in figure 3.8 (b), as compared to the direct signal.

In figure 3.8 only IP and OP results are shown. If the phase difference between the direct and multipath signal is between these two maximal values, the amplitude of the multipath signal can decrease. So for example if we have a phase difference of 45°, the hight of the correlation function for the multipath signal would be 0.35 instead of 0.7 in figure 3.8. If the indirect signal is shifted by 90°, the correlation function would even be zero. IP and OP values for the phase difference are the maximum possible effects on the correlation function.

The discriminator output of the receiver gives a value of the pseudorange error of 60 m and 10 m for in-phase and -76 m and -10 m for out-of-phase multipath for a

(a) In-phase correlation output (b) Out-of-phase correlation output
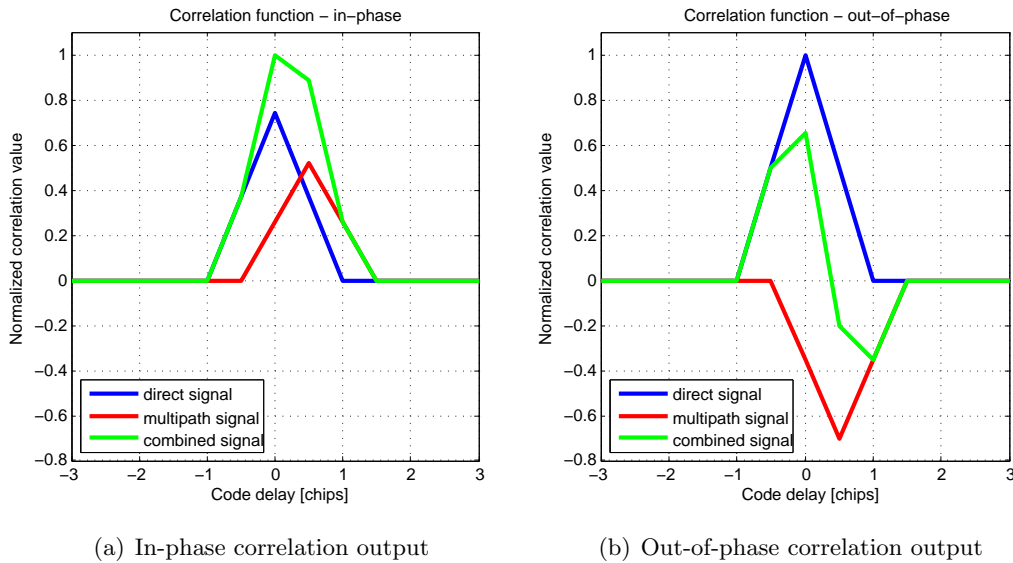
Figure 3.8: *Effect of multipath on the Code Tracking Loop: MP-delay = 0.5 chips, approx. 150 m, SMR = 3 dB, and MP-signal is (a) in-phase and (b) out-of-phase*

receiver with wide and narrow correlator chip spacing. The discriminator function EML is described in equation 3.3. If the SMR is kept constant but the path delay changes over time, starting from 0 m and ending at 450 m, the visualization of the calculated pseudorange error describes the form of an envelope. Therefore this presentation of the estimated pseudorange error is called the multipath envelope and is shown in figure 3.9.

In figure 3.7 to figure 3.9, an infinite front-end bandwidth of the incoming signal is assumed. That means the correlation triangle, the discriminator output and the envelope have sharp peaks and edges. Infinite bandwidth is only possible for theoretical analysis. In reality these peaks and edges are rounded-off due to a finite bandwidth limitation. While low-cost receivers usually perform with a bandwidth of 2 MHz, high performance C/A code receivers use bandwidth of 8 MHz and higher. The high bandwidth allows to detect side lobes of the C/A code correlation, which leads to a better performance of the tracking loop (Ray, 2000).

3.5.3 GNSS improvements

For the combination of code and carrier to form the GPS signal, the code has to be modulated upon the carrier. Binary phase shift keying (BPSK) is a simple digital signaling scheme, which is used for GPS code modulation (Kaplan and Hegarty, 2006, p. 113). For the new GPS signal, the M-code, the binary offset carrier (BOC) modulation will be used to combine code and carrier. The BOC modulation, developed by Betz (1999), is also planned for several Galileo signals. The explanation of
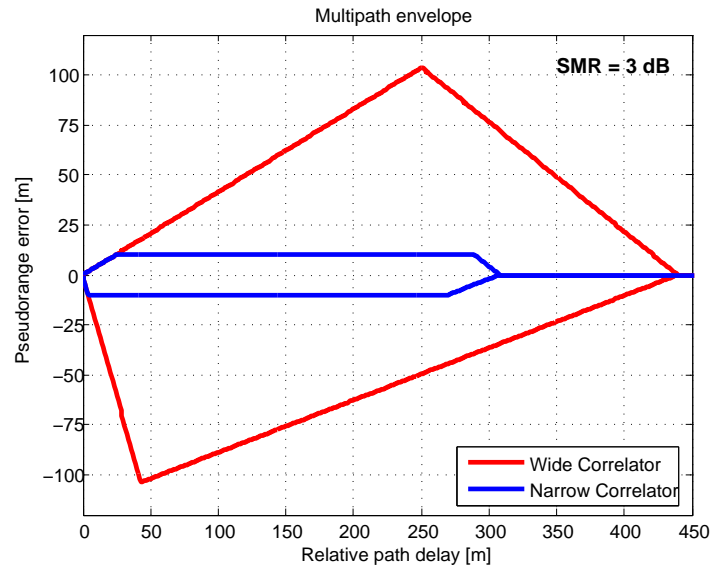
Figure 3.9: *Multipath envelope for wide and narrow correlator, SMR=3 dB*

the BPSK and the BOC modulation scheme can be found in Betz (1999), Kaplan and Hegarty (2006), and Misra and Enge (2006).

The use of BOC modulation for the new GNSS signals provides essential benefits (Betz, 2002). The modulation leads to novel shapes of spectra and correlation functions, including a much sharper peak in the correlation function, shown in figure 3.10 (a).

(a) Correlation function

(b) Discriminator output
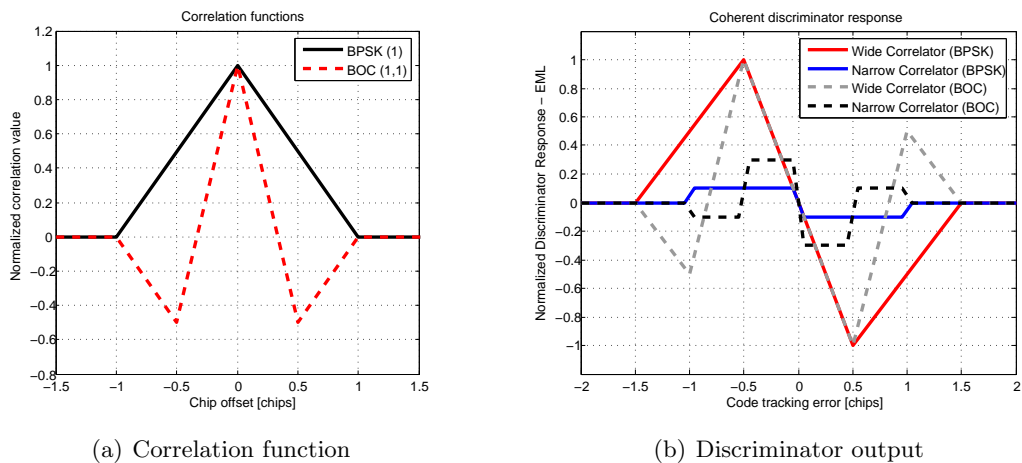
Figure 3.10: *Comparison of the BPSK and the BOC modulated signal on the (a) correlation function and the (b) discriminator output*

The EML discriminator function can be obtained using the autocorrelation function. The results for both BPSK and BOC modulation and a wide and narrow correlator are shown in figure 3.10 (b). The main difference is the secondary peaks on the discriminator response of the BOC signals, which are caused by the negative correlation if the signal is misaligned by half a chip.

To examine the multipath performance, the correlation of the direct signal and the indirect signal can be combined. If the amplitude and the phase are constant over time and only the path delay changes, the multipath envelope can be obtained. The EML discriminator used for this purpose is represented by equation 3.3.
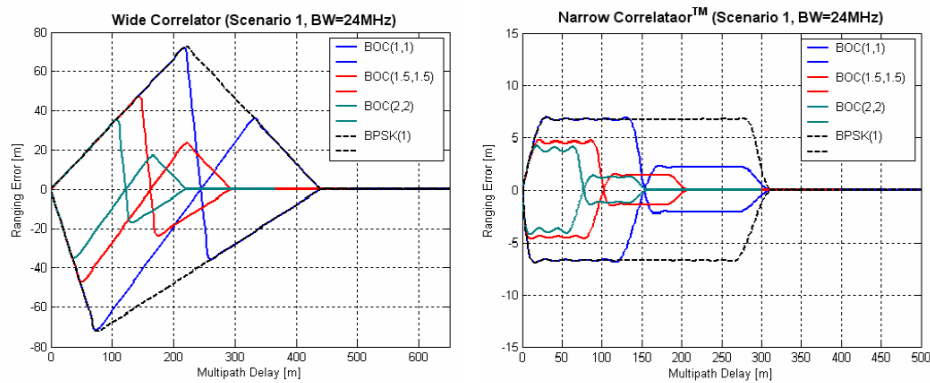
Figure 3.11: *Multipath envelope for wide and narrow correlator, SMR=6 dB (from Irsigler et al., 2004)*

Figure 3.11(a) and figure 3.11(b) shows the multipath performance for the BPSK and the BOC signal with a SMR of 6 dB. The main difference between the multipath performance of BPSK and BOC signals are the effects on the ranging error due to the secondary peaks, which causes the BOC signals to be less sensitive to medium delay multipath.

As we look at the performance with a wide correlator, the BOC(2,2) signal shows the best overall multipath performance, caused by the higher chipping rate. If we compare BOC(1,1) and BPSK (these two modulations have the same chipping rate), the maximum error for both signals is nearly the same. However the BOC signal shows a better performance for medium delay multipath for path delays of approximately 250 m. The results obtained with a narrow correlator are similar. Best overall multipath performance shows again the BOC(2,2) signal with the highest chipping rate. Comparison between signals with an identical chipping rate shows a better performance of the BOC(1,1) for medium and large multipath delays.

As in urban canyons the path delays for indirect signals are generally smaller than 100 m, the improvements are mainly achieved due to the higher chipping rate of

the BOC signals. Unfortunately the simulation of the multipath performance in an urban canyon with BOC signals and simulated Galileo satellites has not been evaluated. Therefore in chapter 4 (Simulation of Urban Canyon Effects) only the GPS system with the BPSK signal is considered for the analysis.

Simulation of Urban Canyon Effects

4.1 Introduction

With the knowledge of the previous chapters, an urban canyon model (UCM) can be developed to simulate different urban canyon situations. The purpose of the model is to assess the shading effects close to buildings and multipath effects on the pseudoranges. Both assessments can than be used to estimate the attainable accuracy of positions. The results can be compared to accuracy estimations using UERE and DOP factors.

Similar models have been proposed by Winkel (2000), Hannah (2001), and Weiss (2007), with different focus on the problem introduced by multipath. The model developed in this thesis (UCM) focuses on multipath in urban canyon environments and will be used to simulate the effect of multipath on the satellite-to-user range. The UCM consists of a satellite motion module, a user environment module, and an antenna-receiver reception module. All these three components are described in the first part of this chapter.

The obstacles in an urban canyon have an impact on the satellite visibility. The number of satellites may decrease and the DOP factors are affected by poor satellite geometry. Therefore we can expect that the position accuracy to be worse than in free environments. The difference for the satellite visibility and the DOP factors between both environments is shown in section 4.3.

Since the standard UERE does not contain the errors caused by multipath effects, these error sources have to be considered separately. To understand the overall behaviour of signal reception in urban canyons, analysis of the multipath and LOS reception and the expected path delays are presented. Due to the reflection and the antenna-receiver performance, these path delays have different impacts on the pseudorange. With the UCM these impacts can be estimated and the results are presented in section 4.4.

The position solution is calculated with a LS adjustment. Using the pseudoranges affected by multipath, the attainable position accuracy in certain urban canyon situations is calculated. These results are compared with EPA values and summarized at the end of this chapter. The calculations will cover the position estimation with and without reliability control.

4.2 Urban canyon simulation model

To calculate the path of the indirect signal, the satellite-to-user geometry and the user environment have to be known. The effect of indirect signals on the range measurements can be assessed with an antenna-receiver model.

The UCM has been implemented in MATLAB and comprises three modules. The satellite motion module uses almanac data to compute satellite positions with respect to the antenna location. The user environment module describes the user environment and is used to calculate possible obstructions and additional path lengths for the indirect signals. The user reception module combines the antenna model and the receiver tracking loop model and determines the multipath impact on the pseudorange measurement.

All three components are described more in detail in the following sections.

4.2.1 The satellite motion module

Due to the motion of the satellite vehicles and the earth rotation the satellite constellation changes continuously. For the calculation of the user position one needs to know the satellite position for each measurement epoch. The geometric distribution of the satellites also affects the position accuracy and can be described by the DOP factors (see section 2.3.2).

There are different sets of data available to calculate the satellite positions. Three of them are described in Hofmann-Wellenhof et al. (2001): almanac data, broadcast ephemeris, and precise orbit data. The main difference of the three datasets is the accuracy and the availability. The almanac data file contains parameters for the orbits and the clock corrections for all the satellites and is the least accurate dataset. The purpose of the almanac data is satellite selection and it also helps for signal acquisition. The ephemeris data are broadcast with the navigation message to the user in real time. With orbital parameters, clock correction, and general informations the user is able to compute the satellite position.The most accurate orbital information is provided by the IGS and consists of satellite positions and velocities. The orbital data has been obtained by post processing and is available in form of various data sets for precise ephemerids. The best accuracy is about 5 cm for the satellite positions. The products are offered by the IGS and are free of charge (IGS,

2008).

Within the UCM the almanac information is used to calculate the satellite positions for all the GPS satellites for a certain time period. The goal of the UCM is a qualitative analysis and so the accuracy of the computations for the satellites position using almanac data is enough. The almanacs can be downloaded from the homepage of the U.S. Coast Guard Navigation Center (USCG) and are available since 1980. The accuracies of the orbits calculated with almanac data (see table 4.1) depend on the age of data, but the almanac informations are generally usable for months (USCG).

Age of data	Almanac accuracy ($1\ \sigma$)
1 day	900 m
1 week	1200 m
2 weeks	3600 m

Table 4.1: *Accuracy of orbit calculation using almanac data (from Spilker, 1994, p. 140)*

4.2.2 User environment module

The user environment module consists of a geometric model of the urban canyon and a simple ray tracing algorithm. It has been implemented to find and evaluate possible indirect signal propagation paths. The algorithm is based on geometrical optics, where the signal is modeled as a single ray. The rays are treated as straight lines and so the implementation and calculation are based on simple geometry. The reflections on a smooth surface are modeled using Snell's law of reflection (angle of incidence is equal to the angle of reflection). The explanation of the model is given below, first for a single reflection and then for multiple reflections.

Single reflection

Since the satellites are moving in an orbit $20000\,\mathrm{km}$ above the earth, the signals on the earth surface are assumed to be parallel rays. In figure 4.1 only two rays are visualized as green lines: the direct and an indirect ray. The two rays are propagating with the same speed, so when the direct signal reaches the centre of the antenna, the indirect signal reaches an imaginary antenna, denoted as point B in figure 4.1. From point B the indirect signal has to follow an additional path to reach the antenna.

The additional path can be decomposed into two parts, denoted as d_1 and d_2. If we know the perpendicular distance D from the antenna to the reflector and the incident angle Φ (known from the azimuth and the elevation of the satellite and from the orientation of the reflector), the geometric relation between the path delays and the incident angle can be easily seen. The following equations are derived to calculate
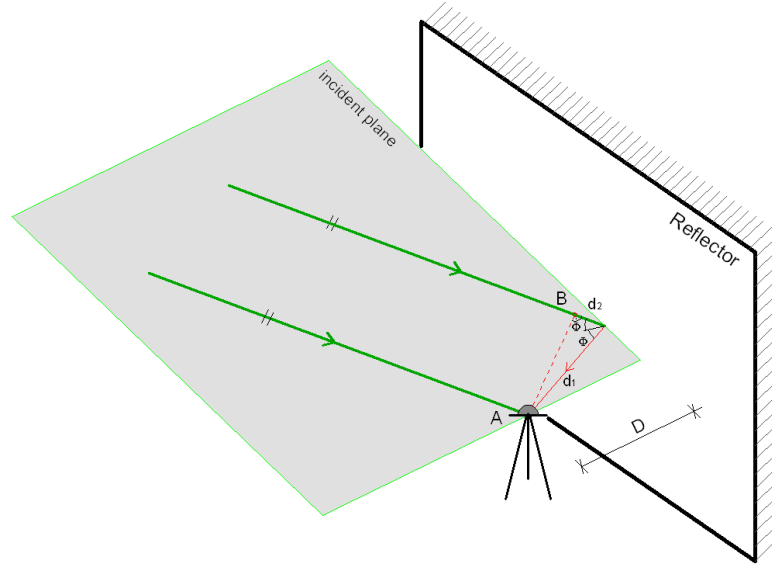
Figure 4.1: *Single reflection on a planar reflector*

d_1, d_2 and the path delay ℓ_{delay} for the indirect signal:

$$\ell_{delay} = d_1 + d_2 \tag{4.1}$$

$$d_1 = \frac{D}{\cos(\Phi)} \tag{4.2}$$

$$d_2 = d_1 \cdot \cos(\Phi + \Phi) = d_1 \cdot \cos(2\Phi) \tag{4.3}$$

where d_2 can also be negative, if the reflector is closer to the satellite as compared to the imaginary antenna (point B is behind the wall). By inserting equations 4.2 and 4.3 into equation 4.1, the total path delay can now be calculated as

$$\ell_{delay} = \frac{D}{\cos(\Phi)} + d_1 \cdot \cos(2\Phi) = 2D \cdot \cos(\Phi) \tag{4.4}$$

Multiple reflections

To simulate an urban canyon situation, we have to consider multiple reflecting surfaces. A frequent situation in an urban canyon is two opposite buildings and the street located in between these two buildings. For the UCM two planar walls are assumed, the antenna is placed in the middle of the street and between the two buildings. The height and the length of the obstacles can be varied to simulate different scenarios. The orientation of the street has to be known or assumed as well. Both reflectors are specular.

A possible multiple reflection scenario is shown in figure 4.2, where the signal is reflected three times before reaching the antenna. The principle is the same as for
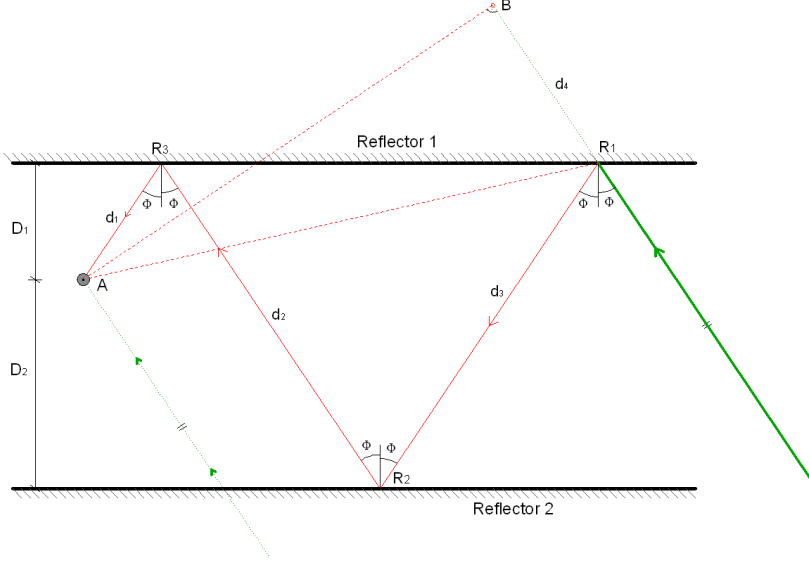
Figure 4.2: *Multiple reflection scenario (top view)*

single reflections. The total multipath delay is the sum of all the single path delays from d_1 to d_4

$$\ell_{delay} = d_1 + d_2 + d_3 + d_4 \tag{4.5}$$

where d_4 can be negative. Each single path can be calculated separately, if we know the perpendicular distance from the antenna to the reflector D_1 and D_2, and the incident angle Φ of the signal. The first three delays can be easily derived from the following geometric relations:

$$d_1 = \frac{D_1}{\cos(\Phi)}, \qquad d_2 = \frac{D_1 + D_2}{\cos(\Phi)}, \qquad d_3 = \frac{D_1 + D_2}{\cos(\Phi)} \tag{4.6}$$

With the relations of the right triangle A (antenna), B (imaginary antenna) and R_1 (first reflection point on the building) the remaining delay d_4 can be calculated using the Pythagorean theorem.

$$d_4 = \sqrt{\overline{AR_1}^2 - \overline{AB}^2} \tag{4.7}$$

where $\overline{AR_1}$ is the distance between the antenna A and the first reflection point R_1 and $\overline{AB}$ is the distance between the antenna A and the imaginary antenna B. The coordinates for the reflection points R_1, R_2, and R_3 in figure 4.2 can be calculated using the single path delays d_1 to d_3 from equation 4.6. The distance $\overline{AB}$ is the shortest distance from the antenna to the path of the incoming indirect signal and can be calculated as follows:

$$\overline{AB} = \frac{\|AX_{\mathbf{sat}} \times AR_{\mathbf{1}}\|}{\|AX_{\mathbf{sat}}\|} \tag{4.8}$$

The example described above is shown for a scenario where the signal is reflected

three times, but the calculation can be extended for scenarios of more than three reflections. Nevertheless the calculations for the analysis in this thesis only consider a maximum number of two reflections (see 4.2.3, multipath attenuation).

4.2.3 User reception module

The signal reaches the antenna and is processed by the receiver to provide the necessary GNSS measurements. Before and during this process, from the signal reflection on the surface, to the signal reception at the antenna and finally the correlation process in the receiver, several effects can have an impact on the accuracy of the measurements. The user reception module models these effects and the impact on the pseudorange measurement using various assumptions and simplifications. The implemented UCM considers only C/A-code measurements and the chip length is exactly 293 m. The effects, which are described in the following pages, are the polarization of the signal, the reflection coefficient, the multipath amplitude, the phase delay, the antenna gain, and the tracking loop design.

Polarization:

The reflection on the wall causes a change in polarization. In general the reflection from a surface causes a total reversal of polarization. This assumption has also been made for the UCM: the RHCP GPS signal is LHCP signal after one reflection, and after two reflections, it is again a RHCP signal.

Multipath amplitude:

The multipath amplitude is the combined effect of the attenuation of the signal due to reflection and the antenna gain pattern. Both of them are described below. The amplitude ratio α if often expressed as SMR and can be calculated as follows:

$$\text{SMR} = 20 \log(\alpha) \tag{4.9}$$

If the multipath amplitude α is very small and below 0.05 (SMR = 26 dB), the effect on the pseudorange can be neglected, because the related tracking errors are below the code tracking noise (Weiss, 2007).

Reflection coefficient/multipath attenuation:

A reflected signal is generally weaker than the direct signal. This attenuation depends on the surface's reflection coefficient and the angle of incidence. A list of reflection coefficients for different surfaces is given by Hannah (2001).

According to Jahn et al. (1996) indirect signals with small delays ($\leq 200\,\text{m}$) are generally attenuated by 10 to 30 dB. These results have been obtained from real data collections and this behaviour is common to rural and urban environments. So a signal, reflected three times would already be attenuated by a minimum of 30 dB.

As the antenna gain difference between co- and crosspolarization is considered, the LHCP signal obtained with a third reflection is attenuated further, and such signals would be very weak. Therefore the simulation uses indirect signals up to two reflections. Signals received by the antenna via three or more reflections are not considered.

Braasch (1996) mentions that, in reality, the attenuation of multipath signals is on the order of 10 dB. The situation is different if the direct signal were reflected from rough surfaces. Here typical values of only 3 dB of attenuation can be expected in reality. Even if specular reflection is considered for the UCM, we also use this worst case scenario as an example. Three different multipath magnitudes are simulated: strong multipath is here defined as having a magnitude of 0.7 (SMR = 3 dB), an average reflection is defined with a SMR of 7 dB, and the weak multipath reflection scenario is simulated with a magnitude of 0.2 (SMR = 12 dB).

Antenna gain:

The choice of the antenna type, used for the data collection, is based on the desired measurement performance. Within the UCM the most important antenna parameter is the antenna gain pattern. For the research three different types of antenna gain pattern are used and compared.

The performance of a geodetic antenna is represented by the NovAtel GG-702 antenna gain pattern (a courtesy of NovAtel Inc.) and is shown in figure 3.5 in section 3.4. For the model the most important feature of the antenna is the amplitude difference between co-polarized (RHCP) and cross-polarized (LHCP) signals. For the geodetic antenna the difference is highest at the zenith and becomes lower with decreasing elevation angle, but is always more than 15 dB for all the received signals from above the horizon. The second gain pattern is similar to the gain pattern of a
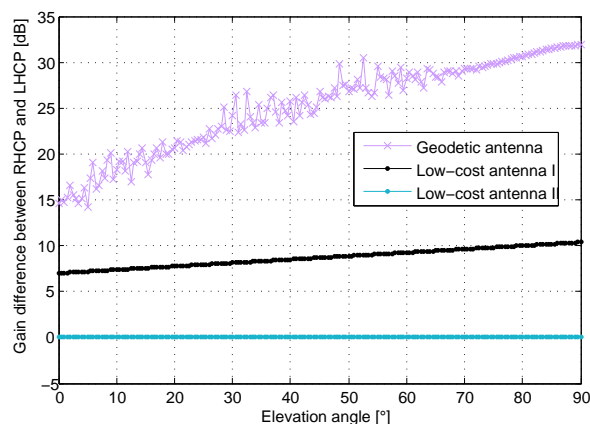
Figure 4.3: *Difference between RHCP and LHCP signal for the three antennas.*

Sarantel helix antenna (see http://www.sarantel.com). The attenuation for LHCP

signals is a function of the elevation angle, where the difference between the copolarization and the crosspolarization is 10 dB at an elevation of 80° and 7 dB at an elevation of 0°. This antenna performance is named low-cost antenna type I (LC I) herein. The last antenna gain does not have a difference between co- and crosspolarization. It means that RHCP and LHCP have the same gain for all the incoming signals. This antenna performance is named low-cost antenna type II (LC II) herein.

The gain difference due to different polarizations of the signal is shown in figure 4.3 for the three antenna models. The difference between RHCP and the LHCP signal is shown as a function of the elevation angle, where at 0° the signals are coming from the horizon and at +90°, from the zenith.

Phase shift:

The phase shift of the indirect signal compared to the direct signal determines how much the pseudorange is affected by multipath. As described in section 3.5.2, the effect has maximum magnitude (but different sign) if the indirect signal is exactly in-phase with the direct signal or exactly out-of-phase (180° shifted). If the phase shift is not exactly IP or OP, the pseudorange error is between these extreme values.

The following simulation provides two scenarios for the phase delays. One scenario considers the worst case, which means that the absolute maximum effect of the multipath signal on the pseudorange (IP or OP result) is shown. Since the error envelope of the pseudorange is not symmetric (see figure 3.9), IP and OP results are different for the same path delay. The second scenario is the average pseudorange error between in-phase and out-of-phase results.

Receiver tracking loop/correlator spacing:

The tracking loop structure used for the UCM is a DLL, described in section 3.5.1, which uses a coherent EML discriminator algorithm. The correlator spacing between the early and late correlator has an impact on the tracking performance of the C/A-code measurements. For the UCM two different correlator spacings are included in the simulation and compared.

The classical tracking structure uses a wide correlator spacing, where the early and late correlators are spaced at 1 chip apart from each other. The Narrow Correlator™ spacing was first proposed in 1992 by NovAtel and it reduced the correlator spacing from 1 chip to 0.1 chip. The advantages of narrow chip spacing are the reduction of tracking errors in the presence of noise and multipath. On the other hand a wider precorrelation bandwidth is required, coupled with higher sample rates and higher digital signal processing rates (van Dierendonck et al., 1992).

4.3   Simulation of the satellite constellation

The GPS system provides four or more satellites in view over any 24 hour period, averaged over the globe, with a probability of 99.9% (SPS-PS). PDOP values of 6 or less are also guaranteed under the same conditions with a probability of 98%. The values of PDOP and satellite visibility given in the SPS-PS are global averages. With simulations, values for a local solution can be computed and therefore a better representation of a day-to-day GPS measurements can be obtained.

Such simulations are computed with the satellite constellation of June 13th 2007, sampled every 5 minutes for 24 hours. Worldwide GPS coverage is evaluated for latitudes from 90°N to 90°S and longitudes between ±180°, with user positions spaced every 5° for both latitude and longitude. The satellite constellation consists of 29 healthy satellite, which is a favorable GPS constellation. According to the SPS-PS, the GPS space segment consists nominally of 24 operational satellites. The simulation results are shown in figure 4.4.
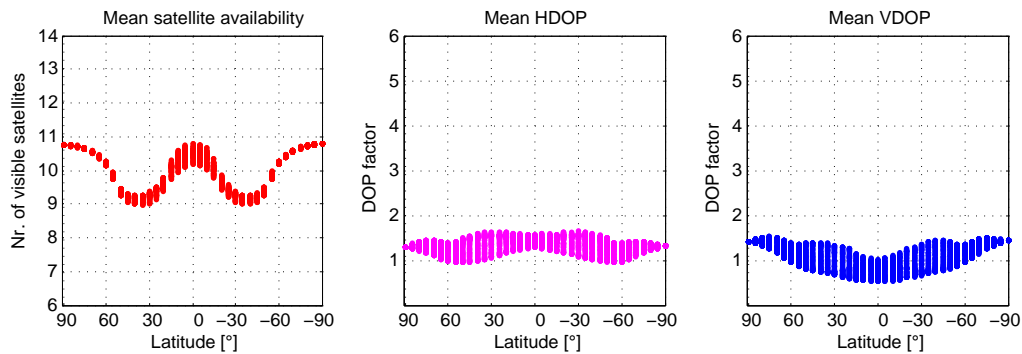
Figure 4.4: *Mean satellite visibility and DOPs for a global constellation in free environments*

The figure shows the average satellite visibility, HDOP, and VDOP obtained from the simulation (24-hour data simulation). The global constellation is plotted as a function of latitude, which means every latitude shows the values between ±180° longitude. The global average obtained with this constellation is 10 visible satellites. The lowest satellite visibility is for latitudes around ±45° with nine visible satellites. Maximum values for the mean satellite visibility for the 24-hour period of the simulations are obtained at the poles and around the equator. At these locations the user can see 11 satellites on average. The mean HDOP values vary between 0.9 and 1.7, VDOP values between 0.5 and 1.6, depending on the latitude and the longitude of the user position. The global averaged values are 1.3 and 1.1 for HDOP and VDOP, respectively. In an urban canyon the direct signals might not be received and clear visibility to the satellites is not always given. Obstructions block the signals and so the satellite visibility will decrease and the DOP factors will increase. The following analysis will give an idea how much these values are affected by the obstructions in

an urban canyon.

4.3.1 Satellite availability

The analysis is not made for a global constellation but only for a certain location. The WGS-84 ellipsoidal coordinates for the simulated user position are [51.08 °N 114.13 °W 1100 m], which are the coordinates of Calgary. The date and time of the simulation are the same as for the above example, and an elevation mask of 5° is assumed.

The assumed street canyon itself is 18 m in width, and the walls on both sides of the street are 100 m long. The height of the walls is 25 m, which can be compared to a six-floor building. A static GPS antenna is located in the middle of the street canyon. The simulation is made for different azimuths of the street canyon, North-South (N-S) and East-West (E-W).

The skyplots for the two simulations are shown in figure 4.5. The dots represent the satellite positions, the gray area shows the LOS obstructions. It means that the user cannot receive direct signals if the satellite is in the gray shaded area. Satellites from which the user can receive direct signals are denoted as "LOS satellites" for the rest of this thesis.

(a) North-South orientation   (b) East-West orientation
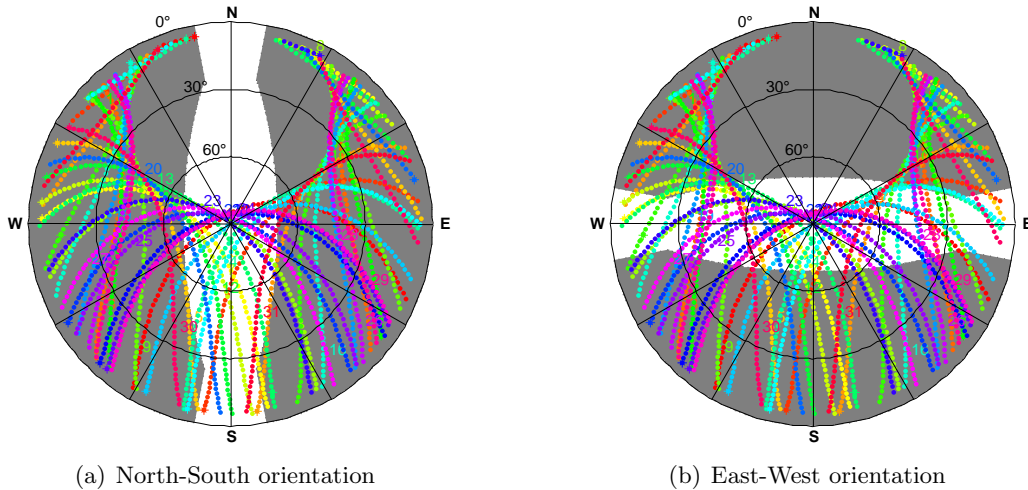
Figure 4.5: *Skyplot of the urban canyon simulation with different orientation of the canyon*

The lack of available satellites in the North can be explained with the GPS design and the antenna location. The inclination of the GPS satellites is 55°, and for positions in mid and high latitudes in the northern hemisphere, the user has very few available satellites in the North. The same scenario can be observed on the southern hemisphere for satellites toward South. Due to this geometrical constellation we can

expect a lower satellite visibility for N-S oriented canyons. This phenomenon is only observable for mid and high latitudes, while for user positions close to the equator the visibility is the same for both canyon orientations.

The satellite visibility for two urban canyons is shown in figure 4.6. The shaded area is the satellite visibility for a free environment. The blue dots are the total number of satellites, which signals can be received by the antenna in the urban canyon. This includes all direct and indirect signals, simulated for a maximum of two reflections. The red dots represent the number of LOS satellites.

(a) North-South orientation   (b) East-West orientation
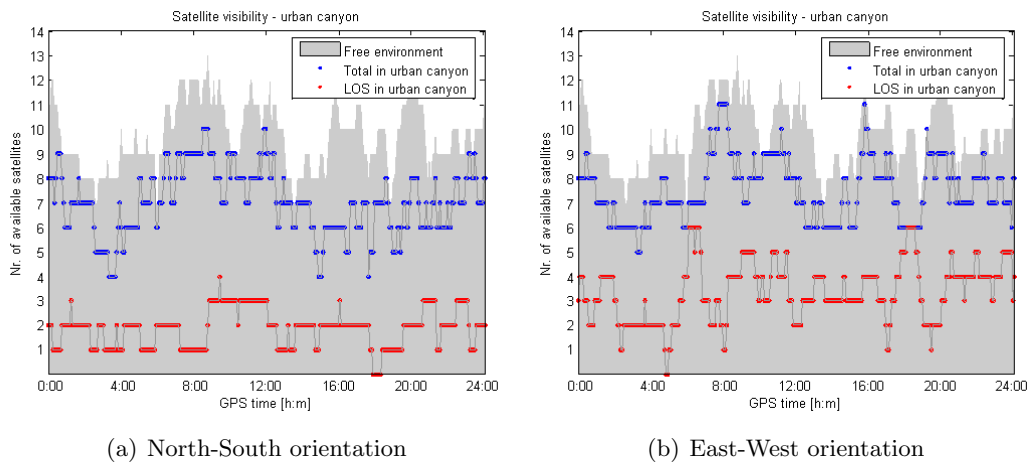
Figure 4.6: *Satellite visibility of the urban canyon simulation in Calgary with different orientation of the canyon*

Figure 4.6(a) represents the N-S oriented canyon, figure 4.6(b) shows the results of an E-W oriented canyon. As expected the available number of LOS satellites is less for the N-S canyon. Here we have an average number of 1.8 LOS satellites, while in the E-W canyon the average number of LOS satellites is 3.3. Similar results can be observed for the total signal reception situation, where the difference between the two canyons is small and not significant. The average signal reception in N-S canyons is from 7 satellites, while for E-W canyons we have an average visibility of 7.5 satellites. In comparison, in a free environment more than 9 satellites are visible. These numbers are valid only for the simulation mentioned above.

A reliable position solution can only be computed if the number of erroneous satellites is smaller than the number of "good" observations. As we can see from figure 4.6 this is not the case for the above simulated situation. It means that in general the position solution cannot be obtained, if we only use measurements from LOS satellites. Additionally the receiver may not be able to distinguish between "good" and erroneous observations because of the lack of "good" observations, which is a problem if the computation algorithm starts to exclude possible outliers. The dis-

cussion shows, that a reliable or high accuracy position solution in an urban canyon cannot be expected using GPS observations only.

The situation changes if the parameters of the canyon change. The simulation results by changing the canyon parameters are not shown but a short summary is given. For the above canyon the ratio between the height of the walls (25 m) and the width of the canyon (18 m) is 1:1.4. Better satellite availability is obtained, if the canyon width is large and the obstacles height is small. For example nearly a free environment case is achieved, if we have ratios of 2:1, which means that the canyon width twice the obstacle height. If the canyon is narrow (for example ratios of 1:2.5), the average satellite visibility can decreases by up to 50% of the visibility in a free environment. As the antenna is simulated in the urban canyon, the number of LOS satellites is very low, and the received signals are mainly reflected signals. For example in urban canyons with ratios of 1:2.5, in average at least half of the measurements are affected by multipath.

Simulations for user positions all over the globe for a 5°-by-5°grid with the above described canyon parameters have been made. The results show a better satellite availability performance in the E-W oriented canyon for user positions on mid latitudes, while for latitudes around the equator the N-S canyon simulations have a better satellite availability. Generally the average number of visible satellites (including direct and indirect signals reaching the antenna) in an urban canyon is 2 to 4 less compared to a free environment, simulated for the above canyon situation.

4.3.2 DOP analysis

The satellite geometry in an urban environment is expectably worse than in a free environment, because some of the satellite signals are blocked by nearby buildings. In the sequel, the DOP factors are compared between free and urban environments. The same simulation scenario is used as for the analysis in section 4.3.1. For the DOP analysis only part of the 24 hour dataset is analyzed, from 10:00 to 15:00 GPS time. This time window has been chosen for visualization purposes and the dataset reflects a typical GPS constellation. Again simulations for a North-South and an East-West oriented canyon are made.

The result for the simulation for the E-W canyon is shown in figure 4.7, while that for the N-S canyon is shown in figure 4.8. In the free environment, both DOP factors are low and thus indicate a good satellite distribution. Due to the obstructions in the urban canyon we have a smaller number of visible satellites and so the DOP factors increase. In the E-W canyon the HDOP is about 1.7 times higher, and the VDOP about 1.3 times higher compared to a free environment. The reason for this difference for the horizontal and the vertical DOP can be attributed to the satellite constellation and the azimuth of the canyon (see figure 4.5). For some periods we can see that the HDOP is higher than the VDOP. During the total simulation, the
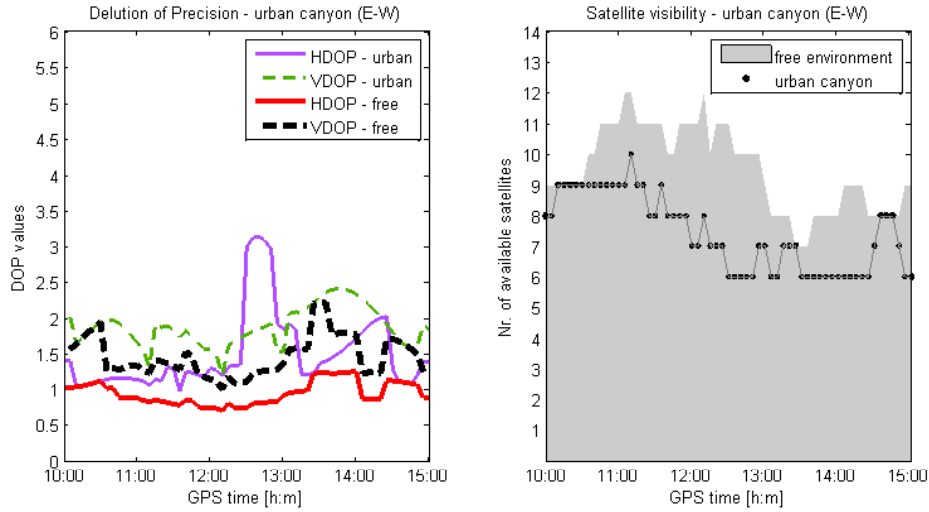
Figure 4.7: *DOPs and satellite visibility for an urban canyon simulation (E-W)*
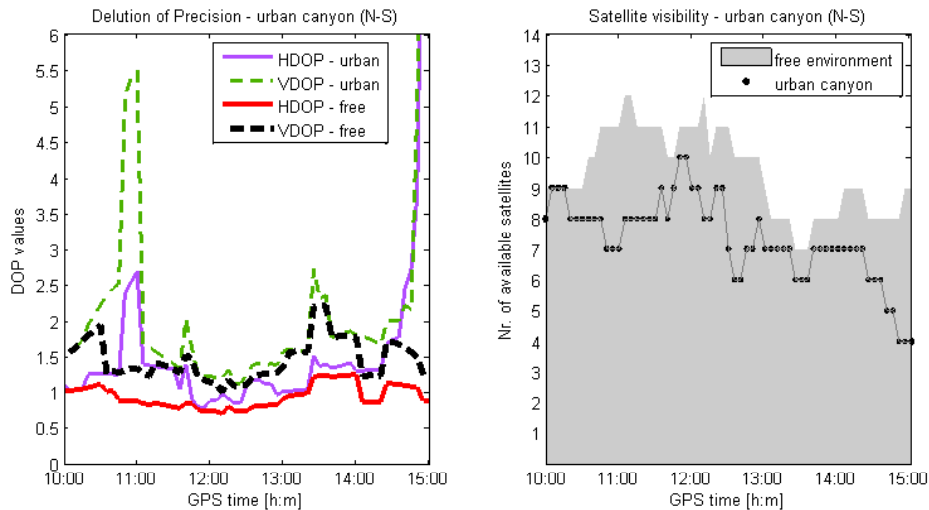
Figure 4.8: *DOPs and satellite visibility for an urban canyon simulation (N-S)*

DOPs are generally lower than 3. The N-S orientation shows two peaks in the time series, where the values are even higher than 6 for some periods. The high DOPs at 15:00 can be attributed to a low satellite visibility of only four satellites. Here the DOP factors for the urban environment are much higher than for the free environment simulation, where for the rest of the period the difference is not significant. Summarized for these scenarios the DOP factors for both HDOP and VDOP are 1.5 times higher than in a free environment.

In table 4.2 the simulation results are summarized. The mean DOP factors for the

total simulation time are shown, but also the worst case epochs for the satellite constellation are pointed out. To obtain the EPA, we can multiply the DOP factors with the standard UERE (see section 2.5). To estimate the position accuracy for the SPS a UERE of 6 m is used. Because this UERE provided by the SPS-PS is a global average over several years, this standard value does not match a typical day-to-day GPS data collection. A more realistic value of 2.2 m is calculated in section 5.2.2 using the average value for a real data collections in Calgary over 24 hours. This result is denoted as realistic SPS (RSPS) and the results are demonstrated in table 4.2 as well.

		DOP factors		UERE · mean(DOP) [m]		
		mean	max		UERE	EPA
SPS free	HDOP	1.0	1.3	2D RMS	6 m	5.7 m
	VDOP	1.5	2.2	v RMS	6 m	8.8 m
SPS UC (E-W)	HDOP	1.5	3.1	2D RMS	6 m	9.0 m
	VDOP	1.9	2.4	v RMS	6 m	11.2 m
SPS UC (N-S)	HDOP	1.6	10.4	2D RMS	6 m	9.8 m
	VDOP	2.2	10.8	v RMS	6 m	13.2 m
RSPS free	HDOP	1.0	1.3	2D RMS	2.2 m	2.1 m
	VDOP	1.5	2.2	v RMS	2.2 m	3.2 m
RSPS UC (E-W)	HDOP	1.5	3.1	2D RMS	2.2 m	3.3 m
	VDOP	1.9	2.4	v RMS	2.2 m	4.1 m
RSPS UC (N-S)	HDOP	1.6	10.4	2D RMS	2.2 m	3.6 m
	VDOP	2.2	10.8	v RMS	2.2 m	4.9 m

Table 4.2: *DOP and positioning error in free and urban canyon environments*

The theoretical results show a surprisingly low EPA. The RSPS results in accuracies better than 4 m for the horizontal position and better than 5 m for the vertical position, as an average for the total simulation time. Since the UERE does not consider multipath effects, this prediction is unlikely the same as the accuracy obtained with real data collections in urban environments. From the simulation of the satellite availability in figure 4.6 we have seen the high numbers of signal affected by multipath. From this it follows that if the position accuracy has to be predicted in urban canyons, the effect caused by multipath has to be evaluated as well.

4.4 Simulation of observation errors

The standard error budget for the contribution of multipath to the UERE is described in section 2.3.1 as ±0.2 m. For urban canyon analysis this error magnitude is not reliable, because multipath is too high.

With the UCM the multipath effect on the pseudoranges can be simulated and dif-

ferent scenarios can be tested. A 24 hour data simulation should provide the reader with an example of the overall signal reception in a canyon environment. The effect of multipath on the pseudoranges is described with a sample dataset of three single satellites. With this small dataset the effect of receiver correlator spacing, the antenna performance, and the effect of the multipath magnitude are discussed in detail and extended for all satellites in view. Simulations with various parameters for the user reception module are made to compare the multipath reception performance for different scenarios. Here worst case scenarios are compared with scenarios where the antenna/receiver performance can partly mitigate multipath effects and the results are shown at the end of this section.

4.4.1 Multipath delay analysis

The multipath delay is one of the parameters which characterize the multipath signal. Due to the constellation of the satellites and the user environment these delays vary from epoch to epoch and from satellite to satellites.

With the next simulation the effect of the total multipath situation is shown for a sample environment and constellation. The data set is the same as in the previous sections: the analysis is simulated over 24 hours (sample interval is 30 seconds) on July 13th 2007 for a location in Calgary. The simulated canyon width is 18 m, the length 100 m, and the height of the walls 25 m.

During the N-S simulation we have an average number of 7 visible satellites. All the received signals from all the satellites can be distinguished between LOS signals and indirect signals, reflected once and twice from the surface. We find an availability of 25% for LOS signals, 40% for signals reflected once, and 35% for signals reflected twice. The number of direct signals is the smallest as more reflected signals are present at the user location. For the E-W simulation the average number of visible satellites is 7.5. Within this simulation we have 39% for LOS signals, 40% for signals reflected once, and 21% for signals reflected twice. Similar results are obtained with simulations for other user positions. If we summarize these results, the general situation is availability between 40% and 50% indirect signals from one reflection, for both urban canyon situations. The percentage of LOS signals varies between 20% and 40%, similar relative frequencies can be observed for signals reflected twice. Generally the occurrence of LOS signals is lower than the occurrence of signals reflected twice in the simulation.

Further we can split the received signals in groups, depending on the path delay. Figure 4.9 shows the histogram of multipath delays for direct and indirect signals, where the bins represent 5 m of multipath delay. In the N-S canyon we can see an accumulation of indirect signals reflected once between 5 m and 15 m. Indirect signals reflected twice have a multipath delay between 15 m and 35 m for this simulation. We can see a similar distribution in the E-W canyon. Just a small amount of signals

(a) North-South orientation   (b) East-West orientation
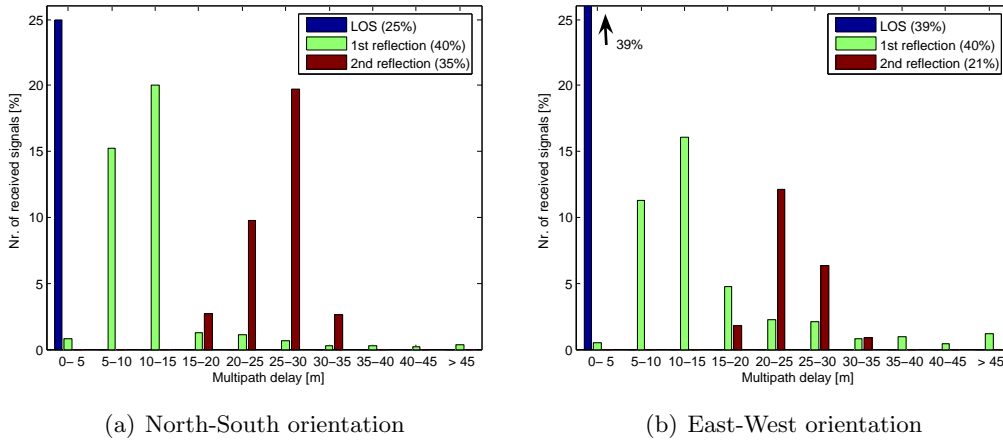
Figure 4.9: *Histogram of multipath delay for direct and indirect signals*

exceeds the path delay of 30 m. Most of the received signals have a path delay between 5 m and 20 m for one reflection, and between 20 m and 30 m for two reflections. The maximum path delay found in this simulation is 94 m (one reflection) and 32 m (two reflections) for the N-S canyon, in the E-W canyon it is 99 m (one reflection) and 32 m (two reflections). For both simulations 95% of all the received signals have multipath delays below 30 m.

If the antenna only receives an indirect signal, this path delay is also the total range error due to multipath. This means that without direct signals, the multipath error can also be several hundred metres, unless the indirect signal is too weak to be received. If the antenna receives LOS signals, the multipath error can be mitigated by the antenna/receiver design. Therefore a situation where the direct signal is received as well, may be better than a situation where only indirect signals can be received by the antenna.

In figure 4.10 the reception scenario is shown for the above described simulation. We can see that the antenna can receive a small amount of multiple signals, which means the LOS and one or more indirect signals are received. For the N-S orientated canyon LOS and indirect signals are received only for 6% of the signals, while in the E-W oriented canyon for 15% LOS and indirect signals are received at the same time by the antenna. If we summarize the results for the two simulations, we can say that the antenna can receive between 20% and 40% LOS signals. Approximately a third of these observations are affected by multipath. Since here we receive both direct and indirect signals, these multipath effects can be mitigated by the antenna/receiver design. The rest of the observations (60% to 80%) are indirect signals, where the range error due to multipath cannot be mitigated.

For a better description of the impact of the receiver design, the antenna gain and the magnitude of reflection on the multipath signal, the observations to three satel-

(a) North-South orientation

(b) East-West orientation
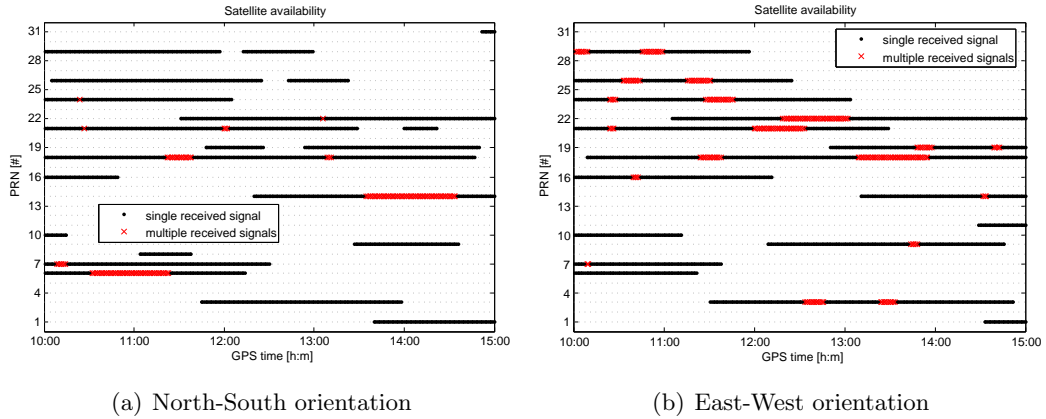
Figure 4.10: *Satellite availability in the urban canyon*

(a) Skyplot
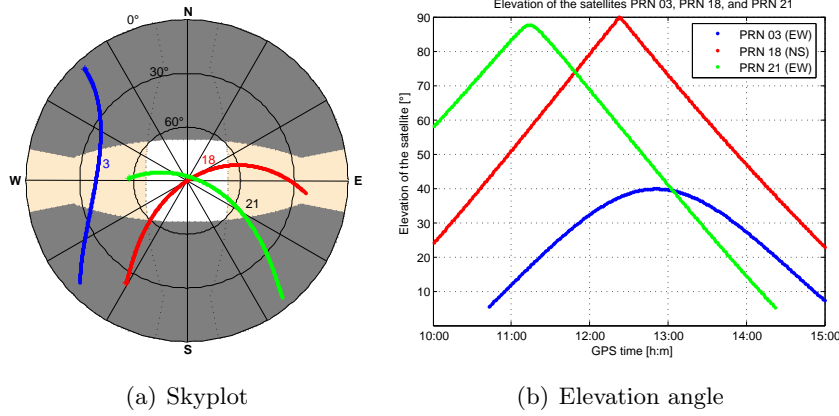
(b) Elevation angle

Figure 4.11: *Skyplot and elevation angles for the satellites PRN 03, PRN 18, and PRN 21*

lites are discussed in detail. The three satellites are PRN 03 and PRN 21 in the E-W oriented canyon, and PRN 18 in the N-S oriented canyon. The different orientations of the urban canyon for the three satellites can also be seen in the skyplot in figure 4.11(a). The bright gray is the LOS obstruction in the N-S canyon (PRN 18), the dark gray is the LOS obstruction in the E-W canyon (PRN 03 and PRN 21). The elevation plot for all the three satellites in figure 4.11 shows that PRN 03 does not exceed an elevation of 40°, while the other two satellites are also visible at the zenith.

The path delays and the possible signal reception scenarios are visualized in figure 4.12. In the figure three specific scenarios are pointed out. In scenario A the antenna receives only LOS signals, which means no multipath errors are affecting the observation. LOS and one or more direct signals are received by the antenna in scenario B. For this case the antenna/receiver performance can mitigate the effect introduced by multipath. The mitigation of such multipath effects using different user reception
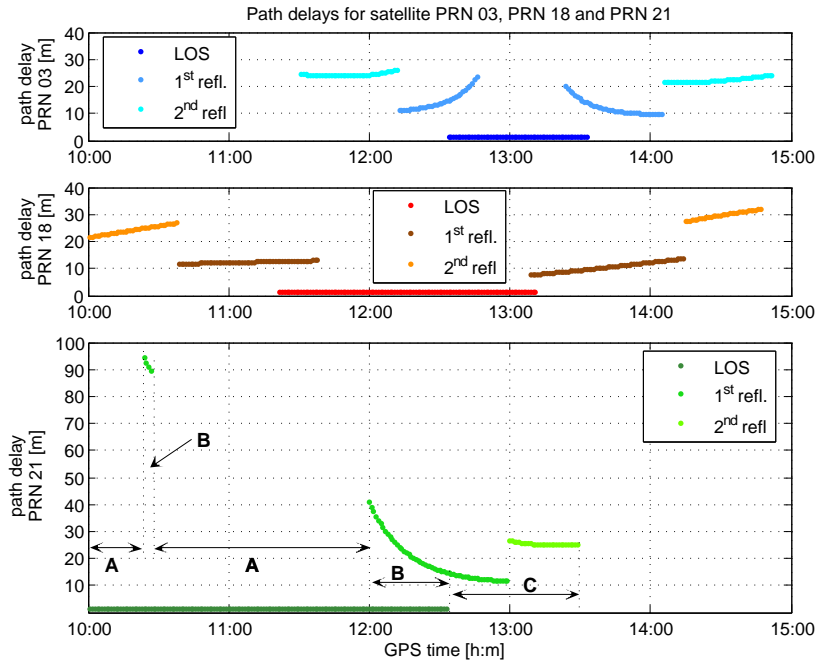
Figure 4.12: *Path delays for PRN 03 (E-W), PRN 18 (N-S), and PRN 21 (E-W). A: only LOS signals, B: LOS and indirect signals, C: only indirect signals*

parameters is explained in the following sections (4.4.2 to 4.4.4). When only indirect signals are received by the antenna (see scenario C), the path delay is also the error in the pseudorange measurement. Another possible scenario, which does not occur in this simulation, is when the antenna can receive two or more indirect signals. Here the total pseudorange error consists of the path delay of the most dominant signal and the signal tracking errors introduced by other indirect signals.

4.4.2 Effect of the correlator spacing

The receiver correlates the incoming signal with an internally generated code by using two correlators, the early and the late correlator (see section 3.5.2). By narrowing the spacing of the two correlators, the tracking algorithm is less affected by multipath, provided that LOS exists. The advantages and disadvantages of the correlator spacing have been summarized in section 4.2.2 and a more detailed description is given in van Dierendonck et al. (1992).

The following simulation will compare the results for two types of DLL designs: the wide correlator with a spacing of 1 chip and the Narrow Correlator™ with a spacing of 0.1 chips. The data have been simulated for the path delays, calculated in section 4.4.1 and visible in figure 4.12, and with a SMR of 3 dB. For the simulation the antenna LC II will be used, which means that left and right hand polarizations have

the same gain. The effect of using a different antenna and different SMRs will be described later in this chapter (see section 4.4.3 and 4.4.4).

Multipath errors can be mitigated when the antenna receives in addition to the direct signal also indirect signals. As described in section 4.2.3 the errors due to multipath can vary between the two extreme values, where the indirect signal arrives IP or OP with respect to the direct signal. Since GPS satellites move, the phase delay is usually non-stationary and fluctuates between these two extreme values. For a static receiver this change might be observable and the maximum range errors due to multipath may appear. If the receiver is moving, the phase change occurs much more rapidly. These rapid fluctuations may not be observable any more and the receiver output will be affected by the average multipath error over a specific time window (Wieser, 2007).

According to this behaviour two different multipath error scenarios are assumed. The worst case scenario uses the absolute maximum of the IP and OP results. The average of IP and OP result represents the case of a moving receiver (even if the receiver is actually stationary in the simulation).
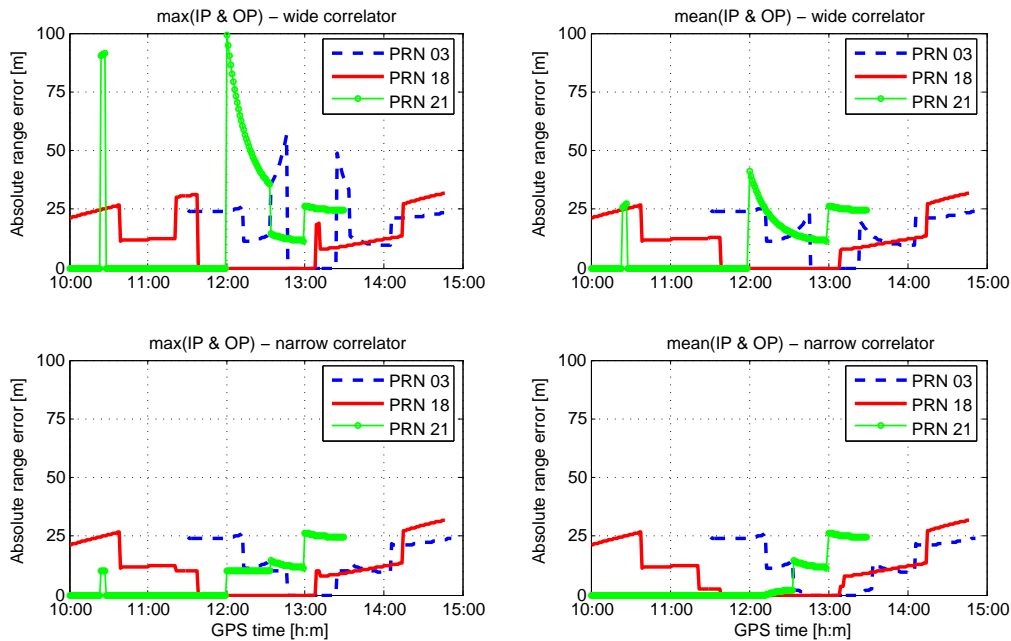
Figure 4.13: *Effect of multipath on the pseudorange with different correlator spacings*

Figure 4.13 shows (i) the different multipath scenarios and (ii) the influence of the correlator spacing on the satellite-to-user ranges. The error effect on the pseudorange is much higher if the correlator spacing is large. An example can be seen with the evaluation of PRN 21 at around 12:00 GPS time. The maximal pseudorange

error with a wide correlator spacing is around 100 m while the error is only 10 m with a narrow correlator spacing for the same time. For this case the multipath error can be reduced by a factor of 10. Also Braasch (1996) mentions the improvements by the same factor for the maximum multipath error using a small correlator spacing. The difference between the two multipath error scenarios can also be seen in figure 4.13. With the wide correlator spacing the maximal multipath effect is approximately double of the effect, if the average values for IP and OP multipath are used. For the Narrow Correlator™, the average multipath effect is even reduced to almost zero. If the range error remains the same in all the four subfigures (for example PRN 18 between 10:00 to 11:00 GPS time), only indirect signals are received and the total path delay is the range error.

To summarize the multipath performance for a given satellite over a certain period, the RMS values are used. The RMS is calculated for maximum and average multipath error scenario separately. The results are visualized in figure 4.14. The worst epoch for the simulation is extracted from the simulation and shown as well in the figure.
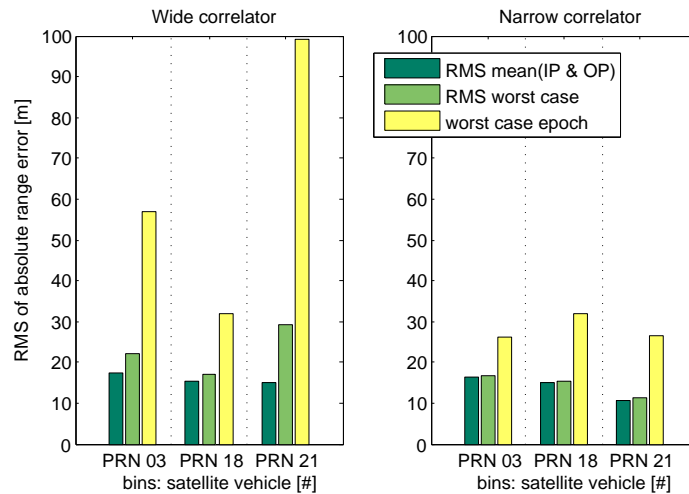
Figure 4.14: *Multipath performance with different correlator spacings for PRN 03, PRN 18, and PRN 21*

As expected, the performance for narrow chip spacing is better. Especially for large path delays the difference between narrow and wide correlator spacing is visible, for example in PRN 21. This behaviour can be explained with the multipath envelope in figure 3.9. From the envelope we can see that the worst wide correlator spacing performance for path delays is around 50 m for OP multipath. PRN 21 has such path delays at some epochs and so the multipath error during this time is very high. The worst epochs for multiple signal reception in the figure 4.14, plotted as yellow bars, show the better performance of the narrow correlator. With the wide

correlator spacing, we have pseudorange errors up to 99 m, while with the narrow correlator the pseudorange error does not exceed 10 m for the same periods (not visible in the figure). The maximum range errors using a Narrow Correlator™ are due to the large path delays if only indirect signals are received.

The difference between maximum and average multipath error scenarios is visible especially for the results using the wide correlator. The two scenarios show differences up to 11 m for PRN 21. These differences are not visible for results with the narrow correlator.

4.4.3   Benefits of antenna gain pattern

Before a satellite signal can be processed by the receiver tracking loop, it has to pass through the antenna. Therefore the antenna can also be designed to mitigate the multipath effects (a more detailed description was given in section 3.4).

For this thesis, only the shape of the antenna gain pattern, excluselively the difference between RHCP and LHCP reception performance, is considered for multipath rejection. Within this work three types of antennas are compared to show the benefit of different designs for antenna gain patterns. The three types of antennas have already been explained within the description of the urban canyon simulation model (see section 4.2.3). A geodetic antenna (gain pattern see figure 3.5) and two low cost (LC) antennas are used. LC I attenuates LHCP signals with respect to RHCP signals, LC II provides the same gain for both polarizations. The data is simulated with a wide correlator spacing, so any improvements in the multipath errors can be exclusively attributed to the antenna gain. We use the same urban canyon scenario as in section 4.4.1, for the reflection of the surface strong multipath (SMR = 3 dB) is considered. The mean RMS for all the results using the three different antennas are compared with a worst case scenario, the maximum error on a single pseudorange for multiple signal reception is also pointed out.

In figure 4.15 the performance of the three antennas are compared. For the geodetic antenna we can assume that the multipath effect of multiple signal reception performance almost vanishes because mean RMS does not show any difference to the worst case RMS. Due to the reflection and the gain pattern the power of the LHCP signal will be reduced to approximately 25 dB. The amplitude of the indirect signal is very small, the indirect signal will not distort the correlation peak significantly. This means the multipath effects are less than 3 m for the simulation (not visible in figure 4.15).

The low cost antenna type I (LC I) does not have such high attenuations for LHCP signals. The gain difference between co- and crosspolarization is 8 dB for signals coming at an elevation of 45°. The lower the gain difference, the stronger the reflected signal. So the worst epoch for multiple signal reception for PRN 21 leads to
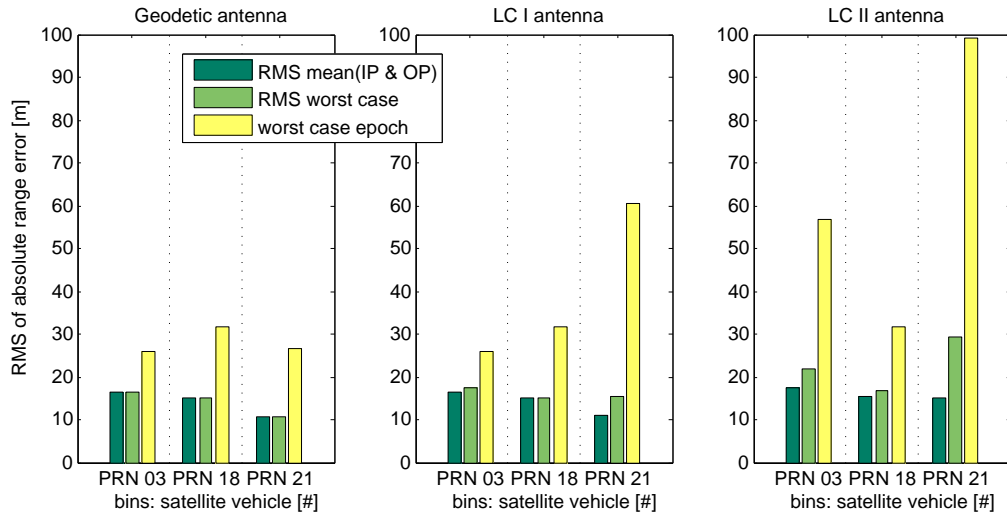
Figure 4.15: *Multipath performance with different antenna gain for PRN 03, PRN 18, and PRN 21*

an RMS value of already 60 m.

If the antenna does not have any attenuation for the reflected LHCP signal, the errors are the highest. Large pseudorange errors due to multipath are possible and the RMS values increases. The highest effects can be seen at PRN 21, where the results are a third worse than when using a LC I antenna.

The NovAtel results show a very good multipath rejection for LHCP reflected signals. It has to be mentioned that, for this simulation, multiple signals are composed of direct signals and LHCP reflected signals. For such cases the multipath effects can be mitigated very well by the antenna, depending on its performance. Other simulations show that it is also possible to have two reflected signals, namely the LHCP signals due to one reflection and the RHCP signals due to two reflections. If the obstacles have good reflection properties, the RHCP signals, which arrive at the antenna later than the LHCP signals, might be the dominant signals. Such scenarios decrease multipath performance within the receiver tracking loops, which always attempt to track the signal at the dominant correlation peaks. For these cases the attenuation of a high attenuation of the LHCP signal may actually be detrimental. However, these cases are rare. The typical attenuation due to reflection described by Jahn et al. (1996) vary between 10 dB and 30 dB, which means that a signal reflected three times is attenuated by 30 dB and so the related tracking errors are not significant.

4.4.4 Effect of the multipath amplitude

Amplitude is one of the three parameters needed to reproduce a multipath signal (see section 3.2.2). The multipath amplitude is the combined effect of the received signal power and the antenna gain pattern. According to Jahn et al. (1996) the average power of near echoes (reflected signals with a small delay corresponding to a maximum of 200 m) in general do not exceeds an attenuation more than 16 dB relative to the average power of the direct signal. Far echoes (signals with path delays longer than 200 m) are in the range of 20 dB to 30 dB attenuation and are not considered here.

The indirect signal distorts the correlation peak of the direct signal. The stronger the multipath signal signal, the higher the pseudorange error. This can also be seen if the multipath envelope for different SMR is plotted. In figure 4.16 the results are shown for a wide and Narrow Correlator™ using different SMRs, from 3 dB (strong multipath) to 20 dB (weak multipath).
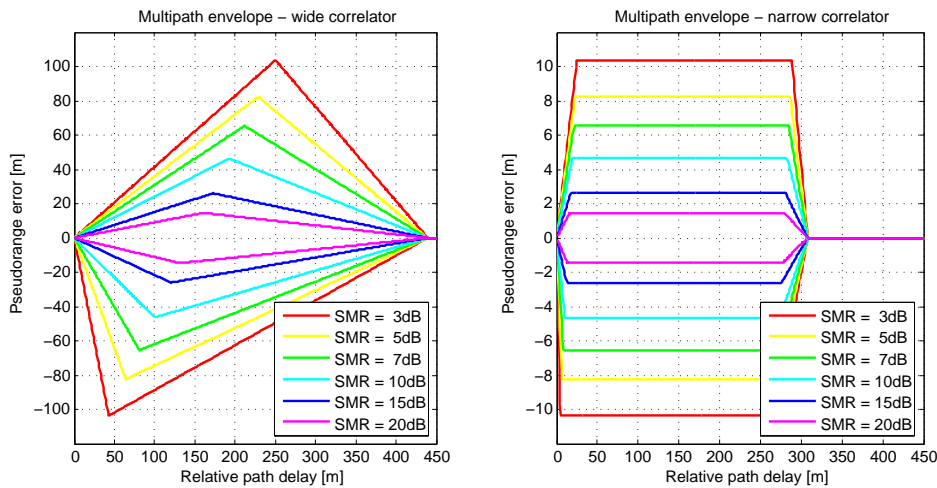
Figure 4.16: *Multipath error envelopes for wide and narrow correlators for different SMR. Note: the scale for the two subfigures is different*

The results demonstrate the effect of the different SMRs. For a strong multipath signal the wide correlator shows pseudorange errors up to ±100 m, while for weak multipath, the effect may not exceed ±20 m. The same, but in order of a magnitude less, is also valid for a narrow correlator chip spacing, where the magnitude of the error changes due to the smaller correlator spacing. Here the effect on the pseudoranges is about ±10 m for strong multipath and less than ±2 m for weak multipath. Further analysis showed, that the error effect due to a lower multipath amplitude decreases exponentially.

The simulation for the three satellites uses three attenuations due to reflection:

strong multipath with $3\,dB$ attenuation, medium multipath ($7\,dB$), and weak multipath with an SMR of $12\,dB$. The amplitude ratios can be compared to reflections on fresh water (strong reflector), medium dry ground, and concrete as a weak reflector (Hannah, 2001). In this simulation we do not consider the antenna gain pattern, and multipath amplitudes result only from the surface reflection. The receiver tracking loop performs with a wide correlator spacing.

The effect of the multipath amplitude for different reflectors is visualized in figure 4.17. Again we can see the larger effect on the pseudoranges with strong multipath. Especially if we look at the worst epochs, we can see that the error is up to three times higher for strong multipath (e.g. PRN 21).
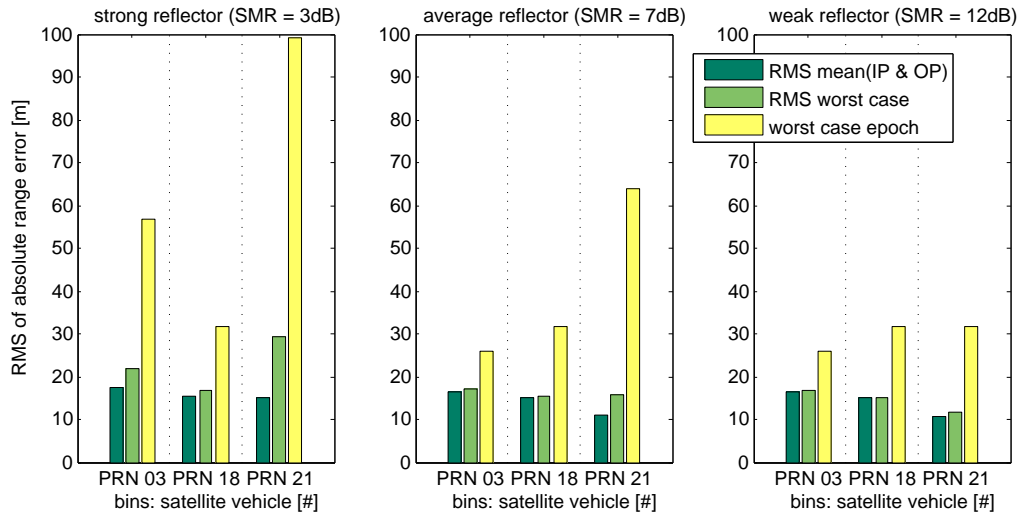
Figure 4.17: *Multipath performance with different multipath amplitudes for PRN 03, PRN 18, and PRN 21*

4.4.5   Total pseudorange error for different scenarios

The previous analyses have shown the effect of the correlator spacing, the multipath amplitude and the antenna gain pattern on single pseudorange measurements. As a conclusion from the previous discussions, all three parameters are combined and tested herein for several combinations. The results are shown for all satellites in view during the simulation time.

Two different antenna/receiver scenarios are computed and compared, a worst case user reception (WCUR) scenario and an average user reception (AUR) scenario. The WCUR scenario uses the following parameters: a correlator spacing of $1\,chip$, a signal power loss due to reflection of $3\,dB$, and no gain difference for RHCP and

LHCP signals. In the AUR case, a simulation with a narrow correlator spacing, power loss due to reflection of 7 dB, and the gain pattern from the antenna LC I are used. The results for all the satellites in view between 10:00 and 15:00 GPS time are visualized for the E-W canyon. The urban canyon parameters are the same as for the previous sections.
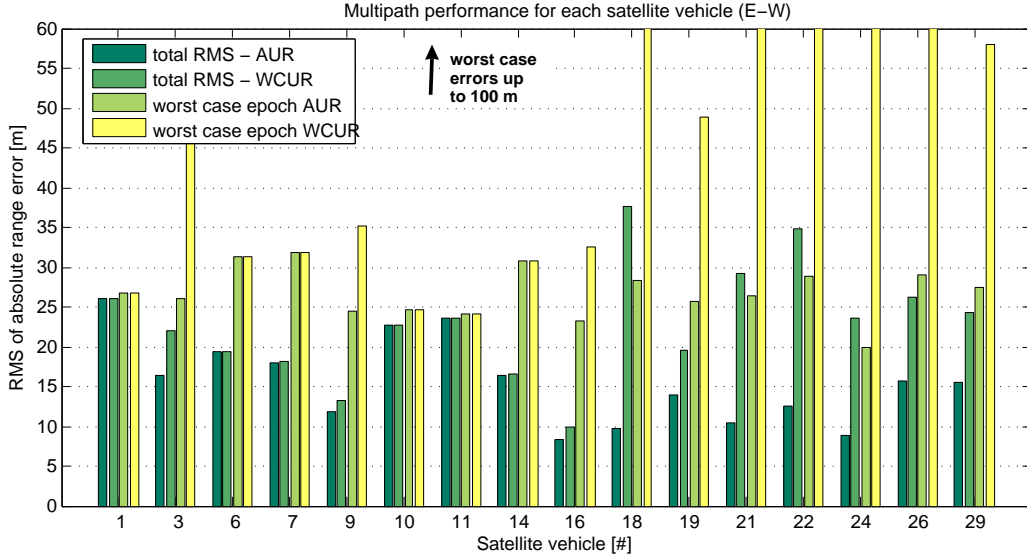
Figure 4.18: *Multipath performance for a worst case and an average scenario*

In figure 4.18 four bars can be seen for each satellite. The dark green bars on the left side show the total RMS performances obtained with the AUR, while the bars beside show the RMS for the WCUR scenario. The other two bars on the right show the worst epochs for AUR and WCUR scenarios, respectively, where delays over 60 m are not displayed in the figure. We can see the improvements due to the antenna/receiver performance. The differences in the total RMS between both scenarios range from less than 1 m up to 28 m (e.g. PRN 18). This difference is even more visible if we compare the worst case epochs for multiple reception, where for some epochs the pseudorange error is over 60 m, obtained with the WCUR scenario.

For the satellites with PRN 1, PRN 6, PRN 10 and PRN 11 total RMS and worst cases compared between AUR and WCUR scenarios are the same. It means that the antenna does not receive multiple signals, speak LOS and indirect signals at the same time (see scenario C in figure 4.12). The total path delay of the indirect signal is the pseudorange error, AUR and WCUR performance are the same. For all the other satellites the antenna receives direct and indirect signals contemporaneously. Here the effect of a second indirect signal can be reduced, seen with the evaluation of the worst case epochs for both scenarios. However, these cases where we have direct and indirect signals reaching the antenna are rare (see section

4.4.1). Most of the time the receiver has a single indirect signal and the multipath effect cannot be reduced for these situations. We also see from figure 4.18 that all the observations are affected by multipath. The minimum RMS range error for this urban canyon simulation is 8 m and 10 m for AUR and WCUR scenario, respectively.

The error performance is evaluated for a N-S canyon as well, but the results are not shown herein. The urban canyon situation is the same as in the E-W canyon, The results shows a similar performance of the total multipath errors for both canyons. In the N-S canyon, the differences between the WCUR and the AUR scenarios are not as high as those in the E-W canyon. As already shown in figure 4.10(a), the number of epochs where the antenna receives direct and indirect signals is very small, which is the reason that AUR and WCUR scenarios are the same. However, the number of indirect signals is higher in the N-S canyon and the path delays are longer, which leads to a similar performance in both canyons.

The analysis shows that large improvements on the multipath performance can be achieved with a good antenna/receiver multipath mitigation performance. The total RMS between AUR and WCUR scenarios are up to 28 m for the simulation in the E-W canyon. The conditions to be able to mitigate multipath effects, is the reception of LOS and indirect signals contemporaneously. If this is not the case, not even the best antenna/receiver performance can decrease the obtained range errors. The occurrence of such situations is very frequently, and therefore the emerging errors are highly affecting the range accuracy for the above simulations.

4.5 Error simulation in the position domain

In this section the errors on the position estimation are evaluated, using the range errors simulated in section 4.4. Additionally to these range errors due to multipath random errors have to be added to the pseudoranges as well. These errors are assumed to be randomly distributed and its standard deviation is simulated as 6 m and 2.2 m, respectively. These values are the same as the assumed UERE in previous sections. Further the results are compared to an evaluation of the EPA, combining UERE and DOP values.

To calculate the user positions, the LS adjustment as described in section 2.2 is used. The variance model which is used to weight the observation is described in Petovello et al. (2005). This model is also used in the software $C^3NAVG^{2™}$ and the variances of the measurements are expressed as a function of the standard pseudorange errors. Typically ionosphere and troposphere effects increase if the satellite elevation decreases, so these errors are a function of the elevation angle, as discussed by Martin (1980).

If the antenna receives direct and indirect signals from the same satellite at the same time, the effect of the indirect signal can be mitigated. The magnitude of mitigation

depends on the antenna/receiver performance. Simulations are made to show the differences between various performances and the results are discussed.

Statistical tests are typically used to detect outliers, and the elimination of those outliers is important to obtain accurate results. In the urban canyon we may have up to 60-80% erroneous observations (see section 4.4.1), which makes it difficult to distinguish between "good" and erroneous observations. In these cases the outlier rejection may not work properly, which means that "wrong" outliers may be excluded. The difference between the position calculation with and without reliability testing is evaluated and discussed in section 4.5.2.

4.5.1 Position calculation without reliability testing

The simulation is based on the results in section 4.4, where the multipath effects on the range have been evaluated. For a first analysis the random errors with a standard deviation of 6 m are added to the pseudoranges. The results for the user position calculation are shown in figure 4.19. Three scenarios to calculate the user position are visualized. The blue dots are the combined results, where both random errors and multipath are applied to the geometric ranges. The other two simulations use only one effect, either multipath or random errors, to simulate the satellite-to-user ranges. For visualization purpose, the results are transformed into a local level system, as described in Hofman-Wellenhof et al. (2001). The RMS values related to the true position in North, East, and Up direction are computed and displayed in a time series, each coordinate separately. The antenna/receiver performance is simulated as AUR, described in section 4.4.5.

If only random errors are added to the ranges, the position solutions have a horizontal RMS of 8 m and a vertical RMS of 12 m. If we compare these results with the results where multipath is the only impact on the ranges, we see that the effect on the position solutions is approximately the same. This show the large impact of the random errors using a standard deviation of 6 m. As we compare the results to a real data collection (described in section 5.2.1), the real data analysis shows a better performance of for the position solution. Also the SPS-PS describes simulation results for an averaged 24-hour navigation solution where the RMS values are 3 m and 5 m for horizontal and vertical positioning. Therefore for further simulations random errors with the standard deviation of 2.2 m will be used.

Figure 4.19 points out that even with such high random errors, multipath is still the dominant effect for the position error. The time series shows RMS values in the horizontal components up to ± 25 m, using multipath errors only. The vertical errors are even higher with a maximum difference to the true position of 42 m. As visible from the figure, the vertical RMS is approximately double of the horizontal RMS, which means the vertical position solution can be estimated less accurate than the horizontal one.
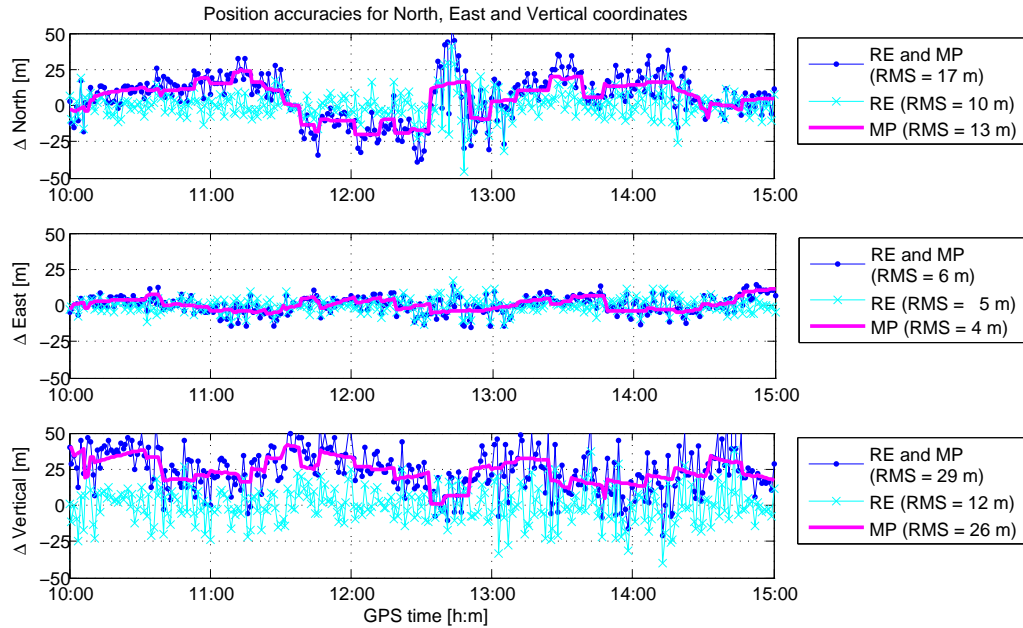
Figure 4.19: *Comparison between position accuracies with random errors (RE) and multipath (MP) in a E-W canyon (AUR scenario, maximal (IP OP))*

To demonstrate the impact of the antenna/receiver performance on the position solution, we can compare the WCUR with an AUR and a favorable user reception (FUR) scenario. The FUR uses a geodetic antenna and a narrow correlator spacing for the tracking loop design. For this scenario the reflection from the surfaces causes an attenuation of 12 dB. WCUR and AUR scenario have been explained in section 4.4.5. For this simulation the standard deviation of 2.2 m has been used for the random errors. The range error is obtained by using the maximum between IP and OP results. The results for the three different simulations are shown in figure 4.20.

In figure 4.20 a very similar performance between the AUR and the FUR scenario can be seen, while the WCUR scenario shows differences of up to 108 m for vertical and 80 m for horizontal position errors. Especially between 12:00 and 14:00 the position error differences between the WCUR and the FUR scenario are large. For a better analysis of these errors, the range errors due to multipath are plotted in figure 4.21.

These range errors are between 0 and 35 m for the AUR and FUR solution, respectively, those for the WCUR solution are in the range of ±100 m. Also the total RMS (calculated for all satellites during all epochs) shows similar values, namely 14.2 m and 14.3 m for the FUR and the AUR scenario, respectively, and a total RMS of 26.0 m for the WCUR scenario. To explain the large differences between FUR/AUR and WCUR scenarios, we have to remember the antenna/receiver properties. For WCUR scenario a wide correlator spacing is used, while for the AUR and the FUR
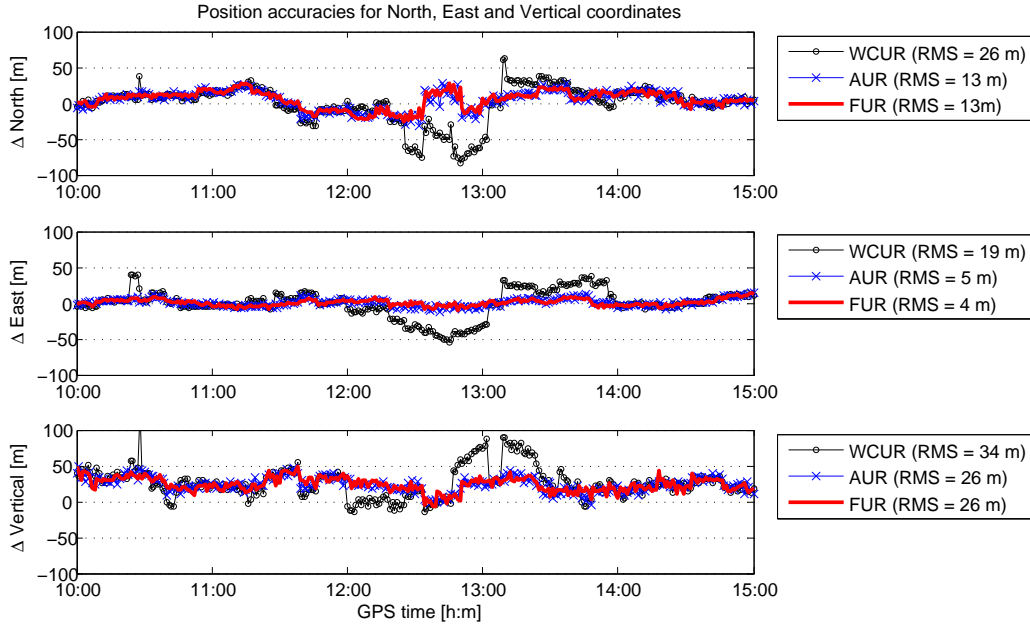
Figure 4.20: *Comparison between WCUR, AUR and FUR scenarios for the antenna/reception performance in a E-W canyon (maximal (IP OP), $\sigma_{RE} = 2.2\,m$)*
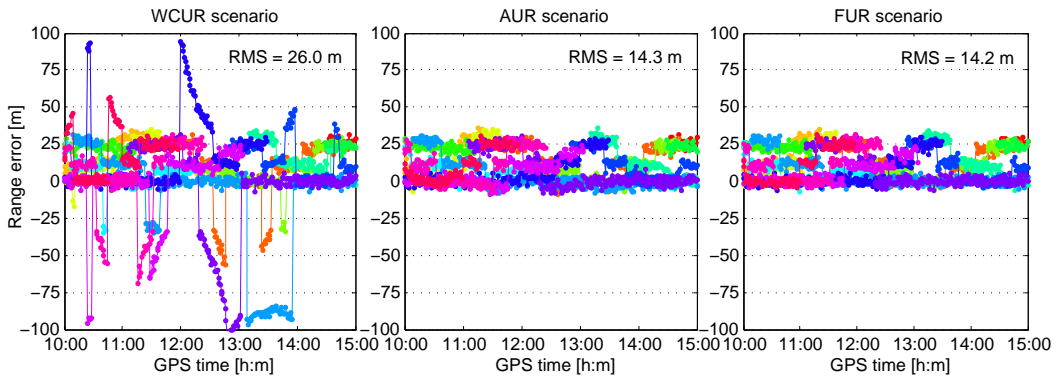
Figure 4.21: *Pseudorange errors of WCUR, AUR and FUR scenarios in a E-W canyon (maximal (IP OP), $\sigma_{RE} = 2.2\,m$)*

scenarios the Narrow Correlator™ is used. As described in section 4.4.2, the maximum multipath error can be reduced by a factor of 10 using a small correlator spacing. This reduced the multipath impact to a maximal range error of 10 m if the SMR is assumed with 3 dB (see figure 4.16). It means that for both scenarios with the Narrow Correlator™ the multipath errors can be reduced significantly, if direct and indirect signals are received by the antenna. Since the percentage of observations, where only the indirect signal reaches the antenna, is about 60-80% (see section 4.4) of total signal reception, the error introduced by these signals, namely only the path delay, is the dominant error for these simulations. Therefore the dif-

ference between AUR and FUR scenario is below a total RMS of 1 m, described in figure 4.21. The mean position accuracy is 10 m and 26 m for horizontal and vertical positioning, respectively, using an AUR or a FUR scenario. In comparison we have accuracy values of 23 m and 34 m for the horizontal and vertical position errors using a WCUR scenario.

Similar results are obtained if the range error due to multipath is not the maximum between IP and OP results but the mean between them (see discussion of static and moving receiver in section 4.4.2). Here the results are the approximately the same as shown in figure 4.20 for AUR and FUR scenarios, but the accuracy slightly changes using a WCUR scenario. We achieve accuracies of 18 m and 33 m for the horizontal and vertical position for WCUR, respectively.

With the last simulation the results for a canyon in the E-W orientation and that in the N-S orientation are compared. The simulation uses an AUR scenario and random errors with a standard deviation of 2.2 m for both canyon simulation.
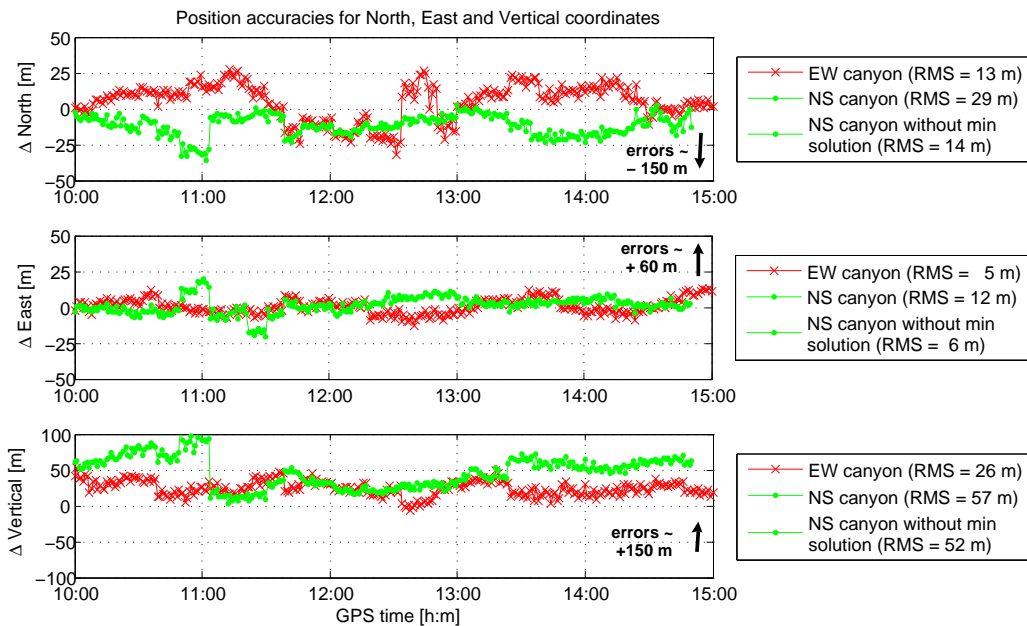
Figure 4.22: *Position solutions for E-W and N-S canyon simulations with an UERE of 2.2 m and AUR (Note: $\Delta Vertical$ is scaled differently)*

In figure 4.22 the results for the N-S canyon are visualized as green dots/lines. The mean RMS values for the total time simulation time are more than twice as high as the values from the simulation in the E-W oriented canyon. This is due to the position solutions for the last five minutes of the simulation. In the plots these results are not visualized, but the position reaches errors of up to ±150 m. Due to the obstructions in the urban canyon the antenna can only receive four satel-

lite signals during this period (see figure 4.8). Two of these four signals two are erroneous, being affected by multipath errors of 25 m and 8 m. The low satellite availability and the high errors in the pseudorange lead to such high errors in the position domain. As discussed in section 4.3.1 a reliable position solution can only be computed if the number of "good" observations is larger than four, which is not given for these last position estimations. If these solutions are not considered as reliable and excluded from the calculation of the RMS values, both canyon simulations have similar performances for the horizontal positions. The vertical positions still show large differences, which can be attributed to the geometry of the satellites and the additional pseudorange errors. The geometry constellation for the urban canyon has been computed in section 4.3.2 and shown in figure 4.8. The satellite availability result around 11:00 GPS time leads to a vertical DOP of 5. Combined with the erroneous pseudoranges, these effects lead to the high errors in the vertical position during that period. Other high errors in the position solution can be seen at around between 13:00 and 15:00 GPS time, where almost all of the satellites are affected by multipath. The number of direct and unaffected signals during these periods varies between 0 and 2.

antenna/rx performance	multipath effects	POS	simulation results - total RMS
WCUR	mean (IP OP)	2D RMS	18.7 m
		v RMS	33.1 m
	max (IP OP)	2D RMS	35.0 m
		v RMS	43.0 m
AUR	mean (IP OP)	2D RMS	9.5 m
		v RMS	25.5 m
	max (IP OP)	2D RMS	9.8 m
		v RMS	25.7 m
BPS	mean (IP OP)	2D RMS	9.4 m
		v RMS	25.5 m
	max (IP OP)	2D RMS	9.5 m
		v RMS	25.5 m

Table 4.3: *Comparison of the antenna/receiver performance and the multipath effects for simulations in the E-W canyon*

In table 4.3 the results for the above discussed position solutions are summarized. for a simulation in an E-W canyon. Here the range errors are obtained only from multipath effects, as the random errors have not been considered. For both scenarios of the antenna/receiver performance, a maximum (maximum between IP and OP) and a mean effect (mean between IP and OP result) caused by multipath are shown. The results show significant improvements in the position domain if the antenna and receiver have better multipath mitigation performances. If the maximum range error due to multipath is used (max (IP OP)), this difference is even higher. We can see

small differences between AUR and FUR results, namely in order of a few dm, but the errors obtained with the WCUR scenario is twice as high as for the other two scenarios. From these results we conclude that the effect of multipath can be much reduced by a high antenna/receiver performance. If these components do not have multipath mitigation techniques, the pseudorange errors increase and the position accuracy decreases.

Orientation	ant./rx perf.	RE + MP effect	POS	results		
				sim.	UERE	EPA
E-W canyon	**WCUR**	RE 2.2 m	2D RMS	35.3 m	6 m	9.0 m
		max (IP OP)	v RMS	43.3 m		11.2 m
	AUR	RE 2.2 m	2D RMS	9.7 m	2.2 m	3.3 m
		mean (IP OP)	v RMS	25.7 m		4.1 m
N-S canyon	**WCUR**	RE 2.2 m	2D RMS	25.8 m	6 m	9.8 m
		max (IP OP)	v RMS	62.0 m		13.2 m
	AUR	RE 2.2 m	2D RMS	22.5 m	2.2 m	3.6 m
		mean (IP OP)	v RMS	57.1 m		4.9 m
N-S canyon no epochs with 4 sat.	**WCUR**	RE 2.2 m	2D RMS	16.3 m	6 m	9.8 m
		max (IP OP)	v RMS	49.5 m		13.2 m
	AUR	RE 2.2 m	2D RMS	11.3 m	2.2 m	3.6 m
		mean (IP OP)	v RMS	52.2 m		4.9 m

Table 4.4: *Comparison for the position solution between simulation results and theoretical results*

In table 4.4 the simulation result RMS values (sim. result) are compared to theoretical results (EPA), where the standard UERE is combined with the DOP factor to form a theoretical estimation for the accuracy of the user position. The computations are of AUR and WCUR scenarios are shown for multipath effects on the pseudorange combined with range errors of 2.2 m. In the N-S canyon the results are also listed without the last epochs, where we have only four visible satellites (N-S canyon no epochs with 4 sat.). All the results show the large impact due to multipath. Again we can see that the accuracy of the position can be improved with multipath mitigation techniques by the antenna and receiver. The vertical solution shows a higher impact due to multipath effects. The results in table 4.4 also show large differences between the simulation results and the EPA values. These theoretical values do not consider multipath effects, which is the dominant effect for the position error in urban canyons. Therefore the accuracy for urban canyon positioning cannot be estimated using standard UERE values and DOP factors. Here a better model of different UERE values may help for a better estimation of the position accuracy in urban canyons.

4.5.2 Position calculation with reliability control

If reliability testing for the GNSS navigation solution is used, possible outliers can be detected and eliminated within a set of observations. The erroneous observations cause errors in the position solutions and therefore these observations should be removed from the dataset. The detection and exclusion of such blunders might be a problem for high multipath environments, like urban canyons. The numbers of erroneous measurements is often higher than the number of unaffected measurements due to high indirect signal propagation. The implemented software to detect and exclude one or more outliers follows the iterative process as discussed in section 2.4. The software rejects one blunder at the time and if more measurements are excluded for the same solution, this has been done sequentially. This sequential exclusion continues until no outliers are found in the observations. If the number of redundant observations is lower than one, the solution cannot be certificated and therefore it is not reliable for the results.

The results for a possible urban canyon scenario is visualized in figure 4.23. The dataset has been simulated for a E-W canyon, the parameters have been described in previous sections (canyon length = 100 m, height = 25 m, and width = 18 m).
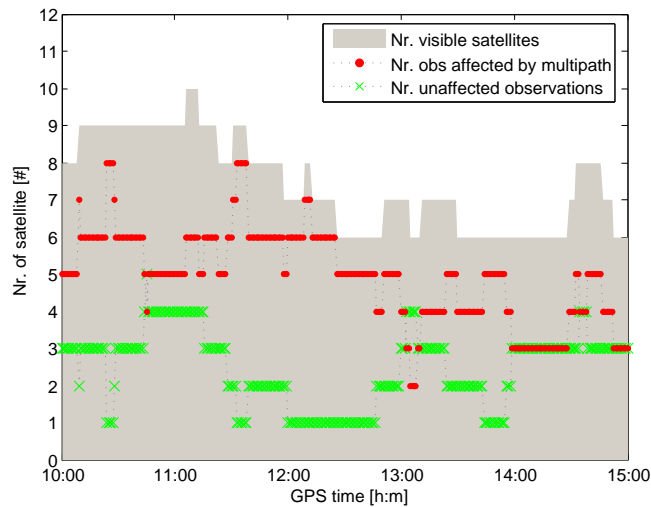
Figure 4.23: *Number of satellites whose observations are affected by multipath in a specific urban canyon*

The green crosses indicate the number of satellites which signals reach the antenna via the direct path. The pseudoranges obtained from these signals are not affected by multipath. The numbers of satellites with erroneous pseudoranges are displayed as red dots and except a short period of time, there are more erroneous observations than ones without errors. For most of the simulation, the number of measurements without multipath errors is less than four.

For later analysis the reliability testing is included for the estimation of the user position. An AUR is used as antenna/receiver design, and the mean between IP and OP is used for the multipath error.Statistical testing identifies potential errors in the data and the observation with the largest normalized residual is rejected from the position solution. The a priori standard deviation is fixed to 2.2 m, which is the same as standard deviation of the random errors which are added to the pseudo-range. After eliminating the erroneous measurements detected with the statistical testing, the solution is considered statistically reliable. This last solution is shown in figure 4.24, compared to the position estimation without error exclusion. If for the computation of the final solution less than five satellites are available or if the global model test failed without detecting any erroneous observations in the local model test, the solution for these epochs is uncontrolled. These epochs are not visualized and not used for the calculation of the RMS values.
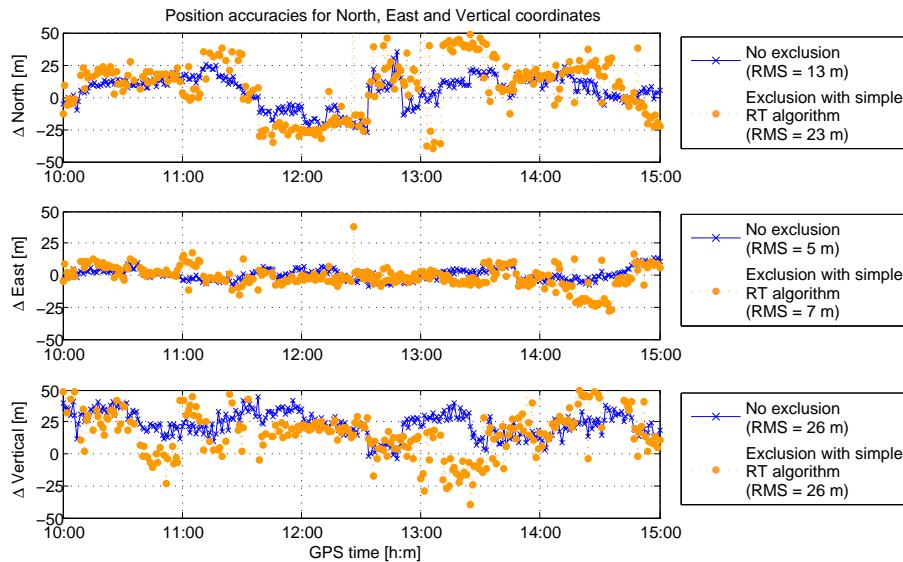
Figure 4.24: *Comparison of the position solution with and without the exclusion of potential errors using a simple reliable testing (RT) algorithm*

Even if the solution may be considered "statistically reliable", the position accuracy is worse than for the solution obtained without any exclusions. The accuracy drops from 10 m to 18 m RMS for horizontal positioning if the estimated erroneous observations are excluded. The time series show high variations, the position can change by 50 m from one epoch to another. Also the minimum and the maximum errors for the position estimation are smaller for the solution without reliability testing, for all three local coordinates.

 The number of visible satellites, the number of exclusions and used observations for the solution are shown in figure 4.25. The number of observations used for the final solution varies between five and eight. With low number of satellites, the geometry will worsen and the accuracy will decrease, which might be one of the reasons of the
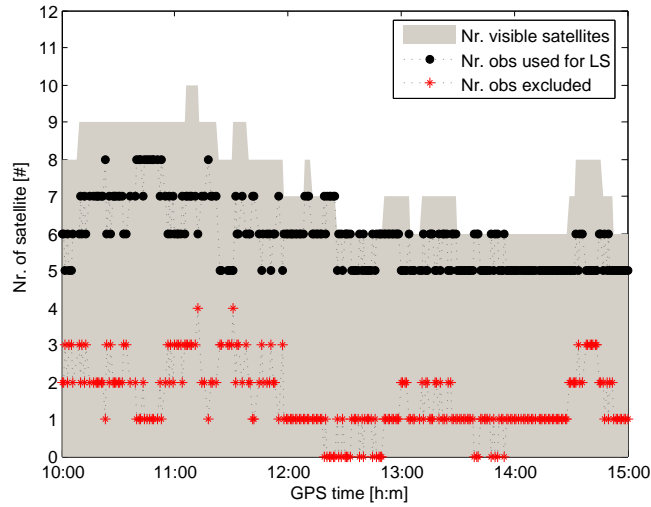
Figure 4.25: *Numbers of visible satellites, number of satellites used for the position estimation and number of satellites excluded due to statistical tests*

large errors in the position domain.

Similar results are obtained if the a priori standard deviation is set higher for the simulation. Although we have a lower number of exclusions, the position solution still shows RMS values of 16 m in the horizontal and 26 m in vertical the direction (the a priori standard deviation is fixed to 6 m). The maximum and minimum errors are reduced compared to the results obtained with a priori standard deviation of 2.2 m, but are still higher as those for the solution without any reliability testing.

For this example, exclusion of observations shows larger errors in the position solutions than the results without reliability testing. The large number of erroneous pseudoranges is a problem for reliability testing. With the LS adjustment, the sum of the squared residuals is minimized. The actual errors caused by multipath are distributed over all the pseudoranges to obtain a best possible solution (see section 2.4). Therefore the distribution of the residuals does not match that of the real errors. As an example the computed pseudorange errors are plotted in figure 4.26 for three satellites, namely PRN 03, PRN 18 and PRN 21. The LS adjustment provides the normalized residuals before elimination of any outliers (a priori standard deviation is fixed to 2.2 m), which are also displayed in the same figure (see axis label on the right).

The comparison shows that, due to the adjustment, the normalized residuals for the three satellites have a different behaviour than the simulated range errors. For example for PRN 03 the residuals are highest if the range errors are small, while the normalized residuals are small if the errors are high (e.g. at the end of the time of simulation: normalized residuals are around zero, while the range errors are around 20 m). Similar results are shown for PRN 18 and PRN 21.Figure 4.26 shows for
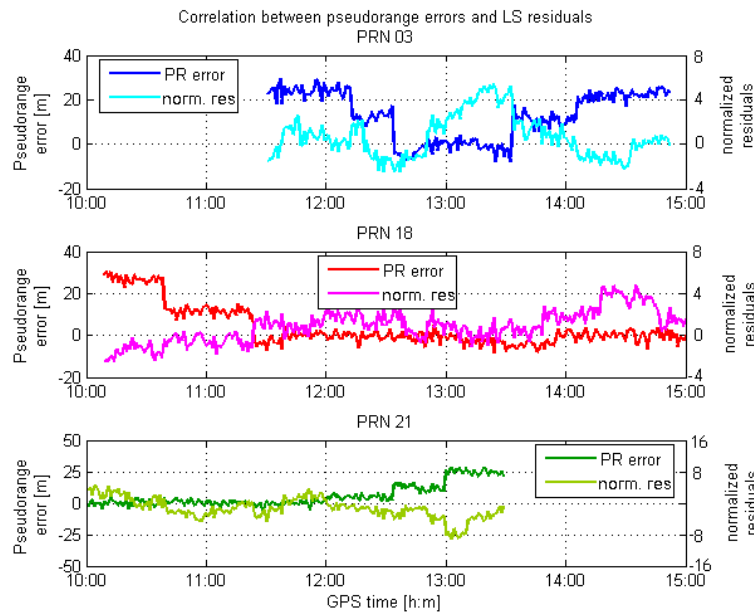
Figure 4.26: *Normalized residuals before elimination of any outliers and pseudorange errors for the satellites PRN 03, PRN 18, and PRN 21*

this example that the residual distribution does not match that of the true range errors. In order to provide the best possible solution, the LS adjustment spread the range of all the errors over all the residuals. Therefore the exclusion of observations might not happen significantly. Ranges with small errors might be excluded, while observations with large errors are still used for the position solution.

This example should not suggest that outliers detection and exclusion should not be made. It should rather point out the difficulty of such detections and exclusions in urban canyons. One has to remember that LS yields optimal and unbiased solutions when the errors have a symmetrical distribution. This is clearly not the case in the presence of multipath in urban canyons. In this case, the errors are large, asymmetrically distributed and evidently non-gaussian. The LS solutions are consequently sub-optimal, may be biased and statistical reliability testing is only partially successful.

Here better variance models may help for a more successful outlier detection and further for a more realistic precision estimation of the results. Wieser et al. (2004) show a way to mitigate this problem by careful selection and mathematical formulation of failure scenarios. A generic model equation for failure identification has been derived, formulating the Kalman filter update as an extended Gauss-Markoff model. Experimental results show relative position accuracies of 1-2 cm for double differenced carrier phase observations, but the results are applicable when processing pseudoranges.

Chapter 5

Field Test and Analysis

5.1 Benefit of real data

Simulations are imitations of the real world, realized by models which represent complex processes. These models are based on simplifications and assumptions. Due to the chosen assumptions, models may not closely represent of real processes.

The model used in this thesis is described as UCM in section 4.2. The assumptions and simplifications for this model are also explained and justified in that section. Field experiments involving real data are helpful to supplement the theoretical results. Data collections are made and the results are compared to those obtained by simulations.

For the data collections two different receivers were used: a NovAtel OEMV2 receiver and a high sensitivity (HS) Antaris ublox receiver. Since the internal properties of the receivers, especially the correlator spacing and the receiver DLL, are not known, an accurate simulation of the receiver design cannot be made. A NovAtel 702-GG Antenna (geodetic antenna with GPS capability) was used. The shape of the gain pattern (see figure 3.5) causes attenuation of LHCP signals, which means that the antenna already mitigates multipath effects.

Three different scenarios were covered during the data collections. A LOS environment collection over 24 hours was made, to show the accuracy of a state-of-the-art GPS solution without signal obstructions. It should give an idea of the accuracy that can be expected for a 24-hour GPS solution. With the collected navigation data, a representative UERE value for a day-to-day data collection is estimated, using the values of the user range accuracy in the navigation file.

A second data collection in an environment with low multipath effects was than made. In the close environment of the antenna, only one large reflector existed and could cause indirect signal propagation. With simulations of the UCM for the selected environment, the pseudoranges affected by multipath from the surface could

be indicated. The results are used to identify possible multipath errors and to show how much these pseudoranges can affect the position estimation. A comparison between simulation and experiment is made and the results are presented.

The third data set was collected in a high multipath environment. Large buildings close to the antenna caused large multipath effects. To map the location and size of the obstructions, the environment was accurately surveyed with a total station. So the user environment can be measured and simulated with the UCM. The simulation results are compared to the real data analysis, possible errors are shown and the accuracy within this high multipath environment is assessed.

5.2   LOS signal environment

The data was collected over a 24-hour period in Calgary. The GPS measurements were made on August 08th and 09th 2007 on the roof of the CCIT (Calgary Center for Innovative Technology) building, located on the campus of the University of Calgary. The antenna was placed on a pillar on the roof with known coordinates. The environment of the data collection is free from any obstructions. We have clear visibility to all the satellites over an elevation mask of 5 °.

The analysis describes mainly two different results: A single point solution should state the position accuracy and the attainable DOP factors for a day-to-day data collection under best possible environment conditions. Additionally, an evaluation of the UERE is made and compared to the theoretical value of 6 m, which is described and defined in the GNSS literature (e.g. Misra and Enge, 2006; Kaplan and Hegarty, 2006). To evaluate the UERE the navigation file for the total data collection has been used. For the position estimation the OEMV2 and the HS ublox receiver show a very similar performance. Therefore only the result for the HS ublox receiver is illustrated.

5.2.1   Attainable position accuracy

The data was analyzed by $C^3NAVG^{2™}$, which was used to calculate the user position using single point positioning with an epoch-by-epoch unconstrained LS adjustment. The solution can be calculated using pseudorange and carrier phase measurements (or only using pseudoranges). If available, ionospheric corrections can be applied and the effect of the troposphere can be mitigated using local temperature, humidity and height data for the specific time of the data collection. The position can only be calculated by post processing. For this experiment, only the pseudoranges were used to estimate the user position. The data is visualized and analyzed for the HS receiver only.

During the 24-hour data collection 27 healthy GPS satellites were visible. The hori-

zontal and vertical DOP factors did not exceed 3.0, and the mean HDOP and VDOP were 1.0 and 1.4, respectively. For the estimation of the static user position, the receiver used over 9 observations on average. The result for the single point position estimation is shown in figure 5.1.
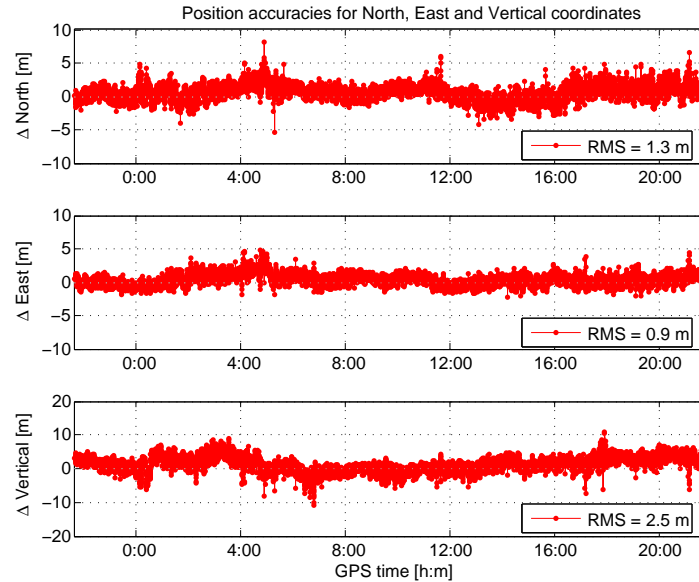
Figure 5.1: *Single point position estimation during a 24-hour data collection with the HS receiver in Calgary (Note: Scale for Δ Vertical is different)*

The HS ublox receiver accuracy is 1.1 m RMS horizontally and 2.5 m RMS vertically. The corresponding maximum errors on the position solution are 8 m and 11 m for the horizontal and the vertical position estimation. As expected, we can see a better accuracy for the horizontal component. For the calculation of the solution, the tropospheric corrections are applied to the pseudoranges.

Estimated values for the position accuracy (denoted as EPA herein) are given by the SPS-PS. The so called "representative SPS SIS position accuracy characteristics" are based on an analysis for a global horizontal and vertical performance. The simulated data in the SPS-PS was averaged for a 24-hour period on June 1st 2000 for locations over the global grid, under a nominal constellation of 24 visible satellites. The SPS SIS UREs of 6 m were used to estimate the pseudorange errors, and resulted in position accuracies of 2.8 m horizontally and 4.7 m vertically.

Since the experiment results in the current LOS environment the solution undergoes local and temporal variations. Therefore standard UERE as a global averaged value does not reflect the day-to-day situation. An example for the possible estimation of the UERE for a specific data collection is shown in the next section.

5.2.2 Evaluation of the UERE

The UERE can be compared to the so-called user range accuracy (URA) in the navigation message with some restrictions. The URA is described by the IDC-200 as a one-sigma estimate of the user range error (URE) for the transmitting satellite. The URE does not include any errors introduced in the user set or the transmission media. In other words, neither atmospheric errors nor receiver noise are used to estimate the URA in the navigation message.

As described in section 2.3.1, the receiver noise is very small compared to the other error sources and can be neglected. The tropospheric delay can be corrected by 80-90% through modeling (see 2.3.1). The actual ionosphere delay can be reduces by about 50% at mid latitudes using the Klobouchar model. This modeled delay does not take fluctuations in the ionospheric effects into account. Actual values will therefore significantly vary from the modeled values as a function of location, progression of the solar cycle and other effects. Another restriction are the effects of additional error sources, for example multipath. As seen in section 4.4 multipath can highly affect the pseudorange and can nor be modeled nor be estimated in real time. Because of these restrictions, the estimation of UERE values using the UREs given in the navigation message is not recommended.However both values are comparable, if the effect of user equipment and propagation errors (speaking tropospheric and ionospheric errors) are known, and no additional errors are affecting the pseudoranges.

The URE is expressed by the URA index (N) as an integer between 0 and 15. While the URE may vary from epoch to epoch, the URA index reported in the navigation messages corresponds to the maximum value of URE anticipated over the fit interval, generally the time for how long the navigation message is valid (2 hours). The relationship of the URA index and the specific URE of the satellite vehicle is described in the ICD 200 (pp. 43) or can be calculated as follows:

$$
\begin{array}{lll}
\text{if} & N \le 6: & \text{URA} = 2^{(1+N/2)}[m] \\
\text{if} & 6 < N \le 15: & \text{URA} = 2^{(N-2)}[m] \\
\text{if} & N = 15: & \text{no accuracy prediction}
\end{array}
\tag{5.1}
$$

For a URA index of 0 and 6, we obtain URE values of 2.0 m and 16.0 m respectively, using equation 5.1. If the URA index is 15, the satellite does not provide any accuracy prediction and the user is advised to use the satellite at his own risk.

To show the performance of the predicted URE values of each individual satellite, the URA indices can be extracted from the navigation message. The indices are extracted form the navigation data over the 24 hour data collection described above. The expected UREs are calculated with equations 5.1 and is visualized in figure 5.2.

Figure 5.2 shows that the URE values from the navigation message are generally smaller than the standard URE of 6 m from the SPS-PS. The URE is usually 2 m,
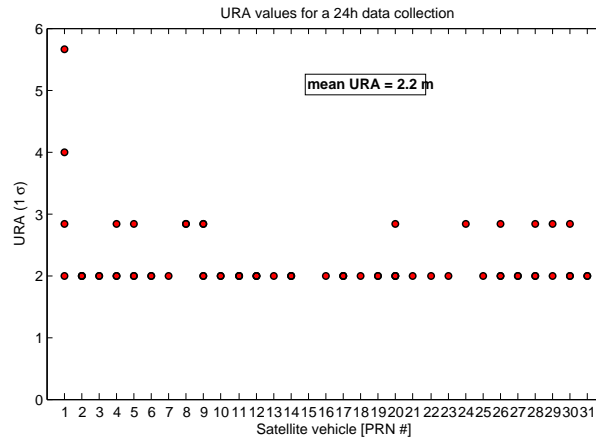
Figure 5.2: *User range accuracy (1σ) according to a 24 hour data collection for all the satellites*

the average performance being 2.2 m for the 24-hour data collection. Since the effect of the ionosphere on the estimated pseudorange is not known, the UERE cannot be estimated. If we assume, that the ionospheric activity has been very weak on the day of data collection (2007 was a year with low ionospheric activity), the average URE can be used as representative UERE value. This is also confirmed by the RMS values for the data collection which are 1.3 m and 2.5 m for horizontal and vertical positioning (see figure 5.1). The URE of 2.2 m has been considered as a representative UERE value for the analyses in section 2.5 and section 4.3.2.

5.3   Low multipath environment

The first scenario is chosen to analyze an environment with low multipath effects. The location has been chosen in a manner that multipath can occur and affect some of the observations. Not all of the observations should be affected, therefore the antenna was placed close to a large building. A favourable location was found in Calgary on the Campus of the UofC. The data was collected at for a very short period, namely 10 minutes. Since we do not know the true position of the antenna during the data collection, we can only analyze the precision of the data set. To be sure that some pseudoranges at the chosen location sites are affected by multipath, a simulation with the UCM was evaluated for the same environment. In figure 5.3 the antenna locations for the data collections are shown in a picture from Google Earth.

The antenna location for the data collection is south of the CCIT building. The perpendicular distance to the wall is 19 m. The building itself is approximately 55 m long, 25 m wide and 22 m high. The surface of the building is made of steel, glass and aluminium and describes a plane surface (see figure 5.3). According to the
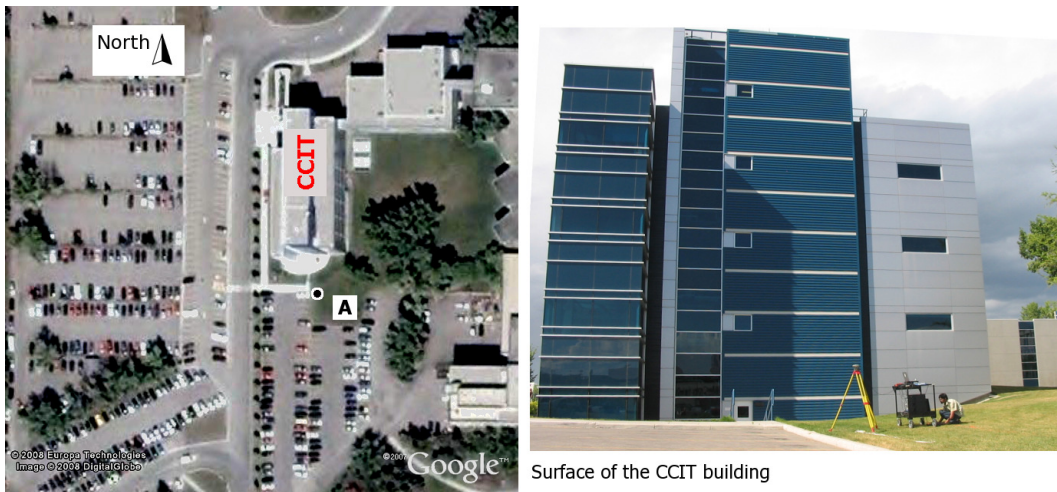
Figure 5.3: *Map for the data collection in picture from Google Earth and picture of the CCIT building*

Rayleigh criterion described in section 3.3.1, the surface of the CCIT building can be considered as smooth. For the data collection the NovAtel 702-GG antenna and a HS ublox and OEMV2 receiver were used. An antenna splitter was use to provide the same signals for both the receivers.

5.3.1 Experimental results

During the data collection we have 8 to 9 visible satellites. As we can see from figure 5.4(a) the satellite PRN 23 has a low elevation and falls below the cut off elevation of 5° for the second period of the data collection, when 8 satellites are available. None of the satellites are obstructed by the building. The navigation data for satellite PRN 28 could not be downloaded from the satellite and it is not used in the solution. The DOP factors are 1.1 and 1.5 for the horizontal and vertical components.

The satellite availability in figure 5.4(b) is shown for the HS ublox receiver in green and for the OEMV2 receiver in black. Both the receivers show very similar performances, a noticeable difference is that the HS ublox receiver can track satellite PRN 23 longer.

The C^3NAVG^{2TM} solutions are shown in the local level system for the north, east and vertical component. The origin of the local level system is the average position solution from both the receivers at the antenna location, obtained with the software. The results are shown in figure 5.5 for the ublox receiver and the OEMV2 receiver.The position estimation shows a smooth behaviour, especially for the OEMV2 receiver. Lower noise for the OEMV2 is expected as this is a high grad geodetic type receiver using Narrow Correlator™ spacing technology.

(a) Skyplot with obstructions

(b) Satellite availability
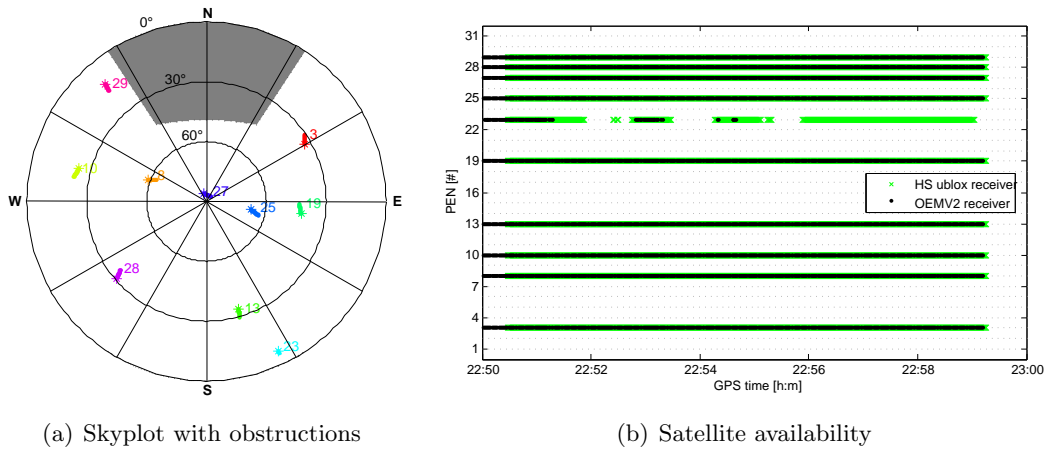
Figure 5.4: *Skyplot and satellite availability for the data collection at CCIT-A*
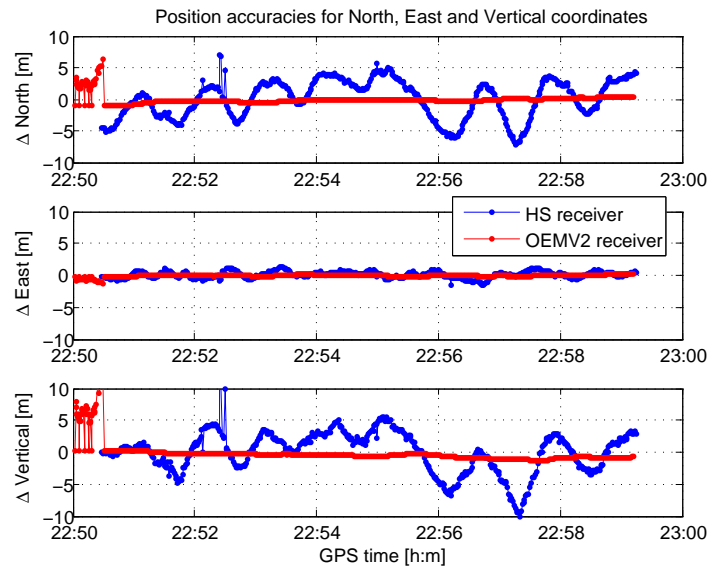
Figure 5.5: *Single point position solution at CCIT-A with two different receivers*

At the beginning of the data collection the position solution vary between $0\,\mathrm{m}$ and $5\,\mathrm{m}$ for the OEMV2 receiver. The reason for these differences is PRN 23. The statistical test in $\mathrm{C^3NAVG^{2\,TM}}$ rejects the observation due to high residuals for some of the epochs, for other epochs no outliers are detected and the pseudorange to PRN 23 is still used to calculate the user position. With the HS ublox receiver we can see similar results. $\mathrm{C^3NAVG^{2\,TM}}$ detects PRN 23 constantly as outlier and the observation is removed from the final position solution. Exceptions can be seen for single epochs, for example around 22:52 in the north and vertical directions, where

the position solution changes immediately if the pseudorange from PRN 23 is not excluded. The position in north and vertical components show variations of $\pm 5\,\text{m}$ from the average solution. The satellite that causes this specific pattern is PRN 13. PRN 13 is affected by multipath, obtained with the simulation in section 5.3.2. The position estimation shows sinusoidal oscillations in the north and vertical components, while the east component is mainly unaffected.

If multipath affects the pseudorange, it also has a visible effect on the C/N_0 values. An indirect signal does not only affect the pseudorange accuracy, but also the measured signal power, which further increases noise. The measured signal power is generally expressed as the ratio of the total signal power to the noise power spectral density (C/N_0). The total power of the carrier is an average of the composite signal, for example a direct and one additional indirect signal. The power of the indirect signal adds constructively or destructively to the direct signal power (see figure 3.8), depending on the relative phase between the direct and indirect signal. As this phase delay varies with time, the measured signal power varies as well. As described in section 4.4.2 the relative phase changes very fast (approx. a few mm/sec for nearby reflectors) and might not be observable, so the phase delay is averaged over a specific time window. Nevertheless the time series for the C/N_0 of a pseudorange affected by multipath undergoes sinusoidal oscillations. The amplitude and the frequency of these oscillations vary, depending on the general impact of the indirect signal (Axelrad, 1994a).

Figure 5.6(a) shows the C/N_0 values for all the satellites. In the UCM simulation satellite PRN 13 is affected by multipath, and the effect should be visible on the C/N_0 values as well. Since we assume that only PRN 13 is affected by multipath (PRN 23 is also affected by multipath, but detected as erroneous and excluded), the error on this observation mainly contributes to the position error. C/N_0 values for PRN 13 and the position solutions in the north component are compared in figure 5.6(b).

As we can see, except for satellite PRN 23, we obtain C/N_0 values mostly above $40\,\text{dB}$. PRN 23 has been excluded from the solution for both receivers. The correlation between C/N_0 for PRN 13 and the north component is clear. For the whole time of the data collection we have similar oscillations for both C/N_0 values and the north component solutions. This correlation confirms the assumption that PRN 13 is affected by multipath. The statistical test cannot detect the observation as erroneous and so it is still used for the solution and contributes the most to the position error.

5.3.2 Simulation results

A simulation for the total dataset has been made to evaluate possible multipath effects on the pseudoranges and to compare the position solution between simulation

(a) C/N$_0$ values for all the satellites

(b) Correltaion between C/N$_0$ PRN 13 and position solution in north direction
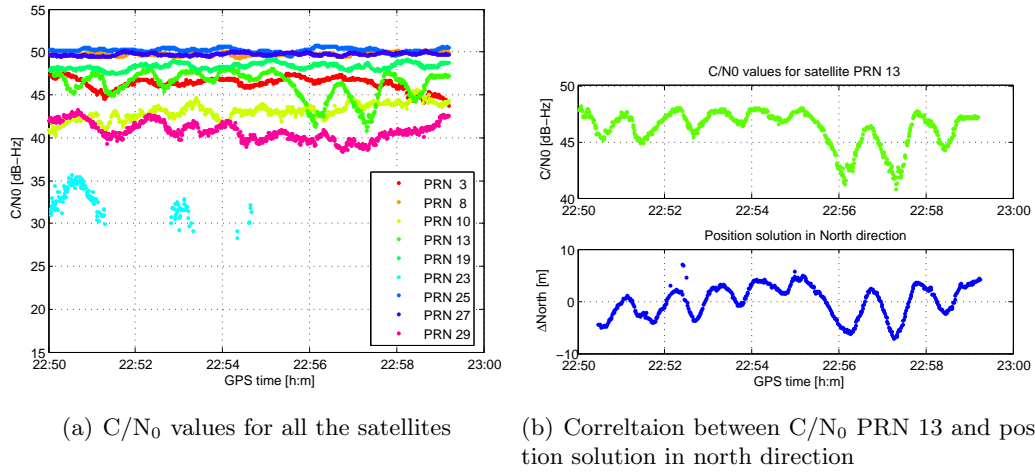
Figure 5.6: *C/N$_0$ values and the correlation to the position solution*

and real data. The reflecting surface can be modelled using the size of the building and its perpendicular distance to the antenna. The satellite availability and the multipath delay are calculated using the UCM and the results are shown in figure 5.7.

(a) Multipath delays

(b) Satellite availability
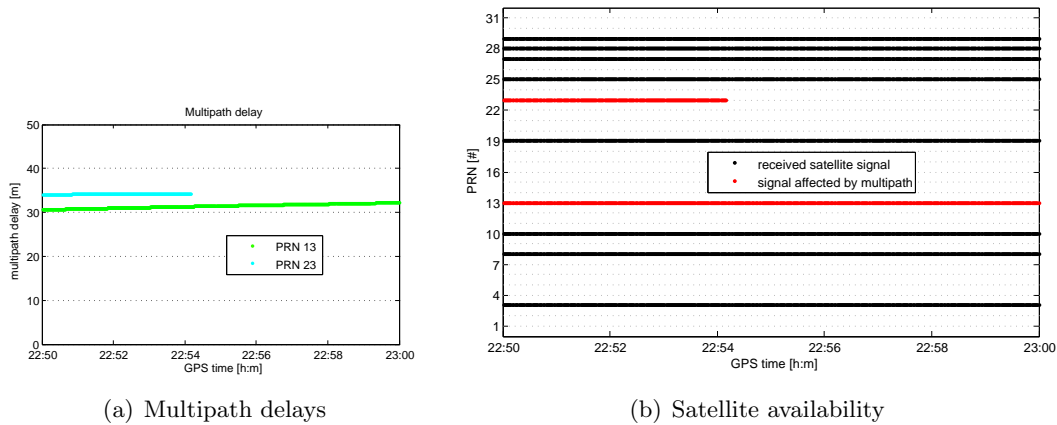
Figure 5.7: *Simulated satellite availability and multipath delays with UCM for period coinciding with real data set at CCIT-A*

The satellite availability in figure 5.7(b) shows similar results as that using real data. PRN 23 disappears after approximately 5 minutes because its elevation is below 5°. All other satellites are visible for the entire time of the simulation. Two satellites are affected by multipath, namely PRN 23 and PRN 13, for the whole time when they were visible. The indirect signals come from the building due to one reflection and the path delay for both satellites is between 30 m and 35 m.

By assuming a specific antenna/receiver design and a signal attenuation due to surface reflection, the user position can be estimated. Two different user reception scenarios are used, namely AUR and WCUR, which were described in section 4.4.5. The AUR scenario uses a narrow correlator spacing, the antenna gain of LC I, and an attenuation of 7 dB. The WCUR scenario has a wide correlator spacing, an LC II antenna, and the attenuation of 3 dB.

To generate comparable results for the experiment, the random errors are not considered for the simulation. The simulation results using the UCM are visualized in figure 5.8, where only the results obtained with AUR scenario are shown. Additionally the EPA from the combined DOP values and an UERE of 2.2 m is calculated and displayed in the figure as well. The simulation results for the WCUR scenario are not shown, but mainly the error during the first part of the data set increased up to variations to the reference position of 80 m in the north component. These high position errors are only visible in the first part of the data simulation where we have two affected measurements.
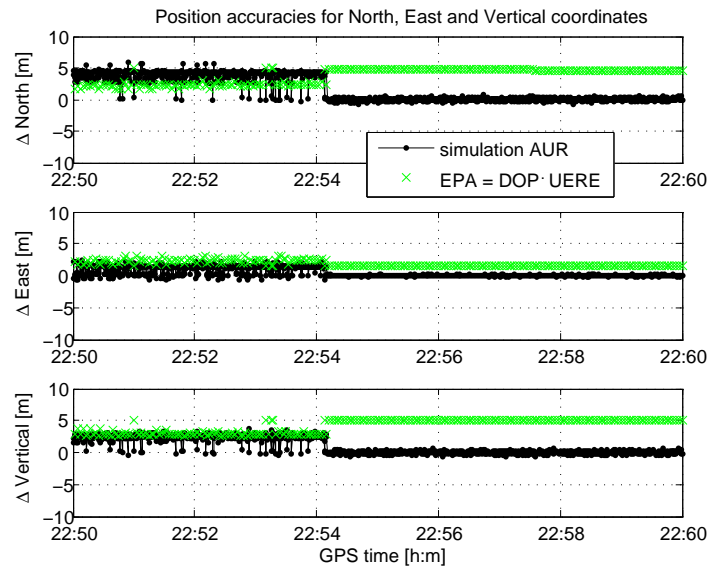
Figure 5.8: *AUR simulation position estimation and comparison to EPA*

The simulation shows errors up to 5 m for the position in north and vertical direction with the AUR scenario at the beginning of the simulation. Two satellites are affected by multipath, namely PRN 13 and PRN 23. Both observations have errors of approximately 5 m, as obtained with the AUR, and the measurements could not be detected as erroneous by statistical testing and therefore not rejected. Similar results are obtained with the OEMV2 receiver, visualized in figure 5.5.

The computation of the EPA shows opposite results. At the beginning of the data

set 9 satellites were visible. As PRN 23 falls below the cut off elevation of 5°, the number of available satellites decreased and so the DOP factor increased, which leads to a larger EPA. Since this computation does not consider multipath effects, the EPA is not a reliable estimation for position accuracies in urban canyons. The low multipath experiment results, simulation results, and EPA values are summarized in table 5.1.

data analysis	description	maximal POS error		average POS error	
experiment	HS ublox rx	2D max	8.8 m	2D std	2.6 m
		v max	22.4 m	v std	9.0 m
	OEMV2 rx	2D max	4.5 m	2D std	1.5 m
		v max	21.5 m	v std	8.6 m
simulation	AUR, no UERE no exclusion	2D max	3.9 m	2D RMS	2.4 m
		v max	3.0 m	v RMS	2.5 m
	WCUR, no UERE no exclusion	2D max	59.8 m	2D RMS	40.6 m
		v max	42.3 m	v RMS	40.9 m
	AUR, no UERE exclusion	2D max	6.0 m	2D RMS	2.0 m
		v max	3.6 m	v RMS	1.7 m
	WCUR, no UERE exclusion	2D max	94.6 m	2D RMS	36.4 m
		v max	50.9 m	v RMS	29.0 m
EPA	DOP·UERE (UERE = 2.2 m)	2D max	5.4 m	2D RMS	4.5 m
		v max	6.0 m	v RMS	4.6 m
	DOP·UERE (UERE = 6 m)	2D max	14.6 m	2D RMS	12.4 m
		v max	16.4 m	v RMS	12.7 m

Table 5.1: *Comparison of the position solution between experiment, simulation, and EPA*

Even if the data set is for low multipath environments, we can have two satellites affected by multipath. The antenna design, the receiver properties, and the power loss due to reflection are factors that can reduce these multipath effects on the estimation of the pseudoranges. This data collection only compares the results between two receivers, but differences on the receiver multipath mitigation performance can already be seen. The analysis of the datasets have also shown that the UCM is capable of predicting multipath effects in a low multipath environment. Since we do not know the receiver properties and the magnitude of the reflected signal for the data collection, the parameters can only be loosely estimated and so the simulation results might not match the experimental results.

The EPA results are also listed in table 5.1. Since the dataset is for 10 minutes only and the true user position is not known, a comparison between experiment, simulation, and EPA is not really helpful. Nevertheless it can be seen that the behaviour of the time series for the position estimation using the EPA does not reflect the behaviour of the results obtained with simulation and from the experiment.

5.4 High multipath environment

After analyzing an environment where multipath effects are relatively small, a data collection in an urban environment was made where much more multipath is expected. The date of the data collection was May 11th 2007. The data was collected for 100 minutes, from 10:00 to 11:40 local time (16:00 to 17:40 GPS time) with 1-second time interval. The user location was in Calgary at the Campus of the UofC. The antenna was placed between the ICT (Information and Communications Technology) and the Earth Science (ES) buildings.


Figure 5.9: *Map for the data collection in picture from Google Earth and surface pictures at site ICT-A*

The picture from Google Earth in figure 5.9 ot the left side represents the location of the user and the buildings around it. In the west and in the east of the antenna (ICT-A) we can see the ICT and ES buildings. These buildings are 37 m and 40 m in hight. South of the antenna we can see another building, which is the walkway between ICT and ES. This walkway has a maximum height of 7 m. On the right side in figure 5.9 we can see the reflecting surfaces from both the ICT (in the middle) and the ES (on the right side) buildings. The ES building is made of glass, steel and metal and the height of irregularities of the surface irregularities do not exceed the critical height calculated with the Rayleigh criterion. The ICT building is made of concrete and its surface is not flat due to the presence of windows. According to the Rayleigh criterion this surface can cause diffuse reflection. However, both reflecting surfaces are simulated as smooth reflectors for the sake of simplicity.

The close user environment, namely the buildings and trees were surveyed with a Total Station. The data from the survey was processed in Matlab and the results are shown in figure 5.10 on a 2D map and as an azimuth-elevation plot, where the obstructions of the buildings can be better seen.

The ES and ICT buildings cause large obstructions at the user position. We have clear visibility toward north, while the ICT building causes obstructions on the east and the ES building causes obstructions on the west side of the antenna. Toward
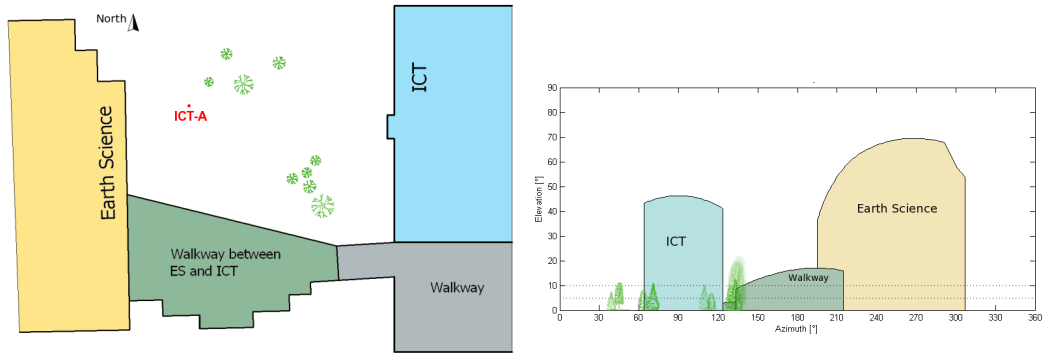
Figure 5.10: *2D Map and azimuth-elevation plot at ICT-A*

south the walkway between the two buildings stops signals from satellites below 16°
elevation.

5.4.1 Experimental results

The satellite geometry during the time of the data simulation is shown as a skyplot
in figure 5.11(a). The obstructions are plotted with a gray background. In figure
5.11(b) the satellite availability is compared between the two receivers.

(a) Skyplot with obstructions

(b) Satellite availability
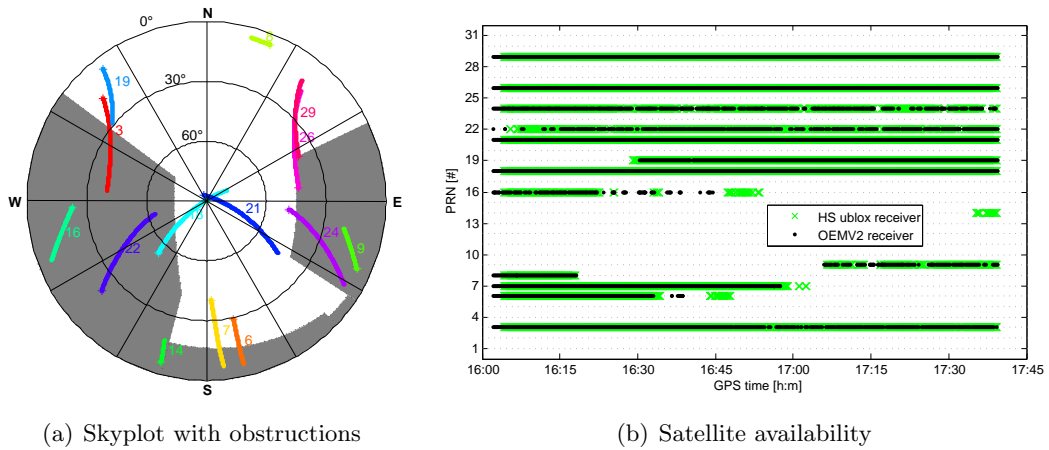
Figure 5.11: *Skyplot and satellite availability for the data collection at ICT-A*

The mean satellite availability is 8 to 9 satellites, depending on the receiver. We
can expect a high number of indirect signals, which can be seen if we compare the
skyplot and the satellite availability plot. For example PRN 22 in the west and
PRN 9 in the east of the antenna are obstructed by the ICT and the ES buildings.
Nevertheless measurements to both satellites can be made, which means the signals
reached the antenna by indirect signal propagation and the receiver was able to es-

timate the pseudoranges.
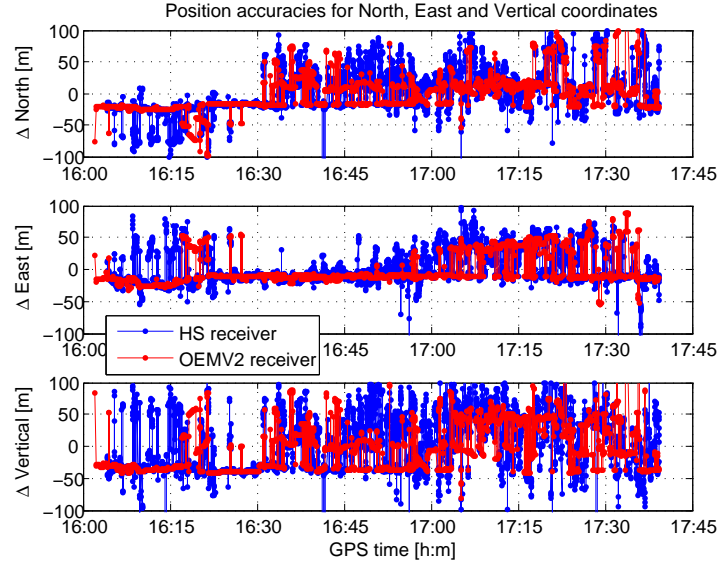
Figure 5.12: *Single point position solution at ICT-A with two different receivers*

The estimated position results are shown in figure 5.12. The position shows errors of $\pm 100\,\mathrm{m}$ an more in north, east and vertical components. The results for this experiments show similar results as obtained from the simulation in section 4.5.2. We know, that outliers may mask each other and therefore it is not possible in this case to detect and exclude all erroneous measurements with statistical testing. The number of visible satellites, the number of used observations for the final position calculation and the number of excluded satellites are shown in figure 5.13. As we can see from the figure we have up to five and six exclusions of observations for the final solution with the OEMV2 and HS receiver, respectively. This high number of exclusions confirms the high number of erroneous measurements.

As discussed in section 5.3.1, the C/N_0 values are closely related to multipath effects. The C/N_0 values for all the satellites and the obstructions from the urban canyon are combined in an azimuth-elevation plot, shown in figure 5.14.

We can see that the C/N_0 values are highest if the satellite is close to the zenith as for PRN 18 and PRN 21. Satellites, which signals are coming from lower elevations, do not have such a high C/N_0. This is caused from (i) the low elevation of the satellite (generally satellites with lower elevation have lower C/N_0 values) and (ii) by multipath, where indirect signals distort the correlation function of the direct signal. Not shown are the time series for the C/N_0 values, which have the characteristic pattern for a signal affected by multipath (see figure 5.6). This analysis shows that signal reception in this experiment is highly affected by multipath.
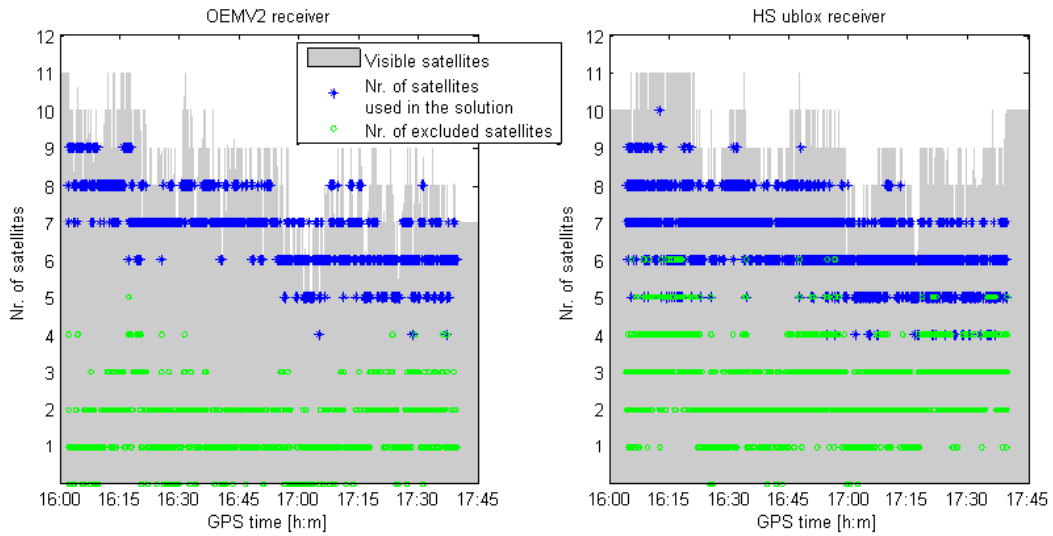
Figure 5.13: *Number of visible satellites, satellites used and excluded for the solution*
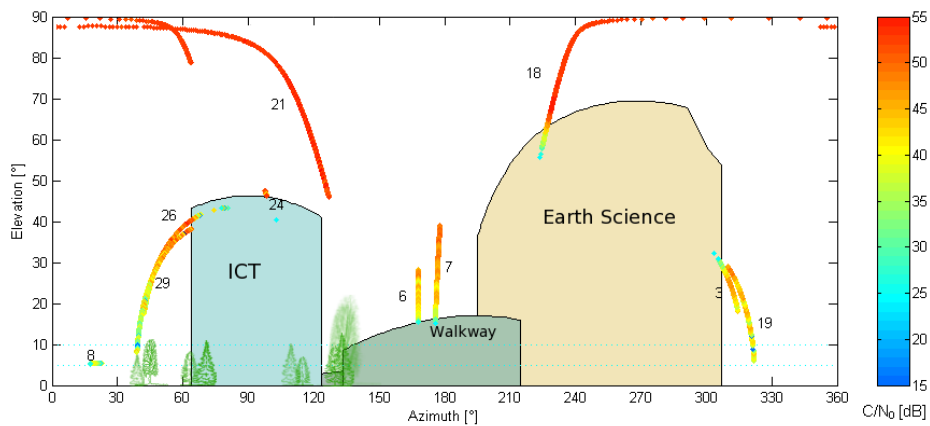
Figure 5.14: C/N_0 *values for the data collection at ICT-A*

As discussed in section 5.3.1 we see again the difficulty of quality assessment in such high degraded environment. With standard procedures of outlier detection and exclusion which are using an iterative rejection of individual observations, it was not possible to detect and exclude all erroneous measurements. Better variance models may help for a more successful outlier detection and further for a more realistic precision estimation of the results (see section 4.5.2).

5.4.2 Simulation results

With the knowledge of the user environment we are able to simulate the experiment
with the UCM. We calculate reflections from the two buildings ICT and ES, where
both of them are simulated as plane surfaces with the same magnitude of reflection.
The path delays are calculated with the UCM, where the reflections up to two reflec-
tions are considered. The results are shown in figure 5.15. The satellite availability
is visualized in figure 5.15(b), separately for observations affected by multipath and
unaffected observations.

(a) Multipath delay due to simulation   (b) Satellite availability with UCM
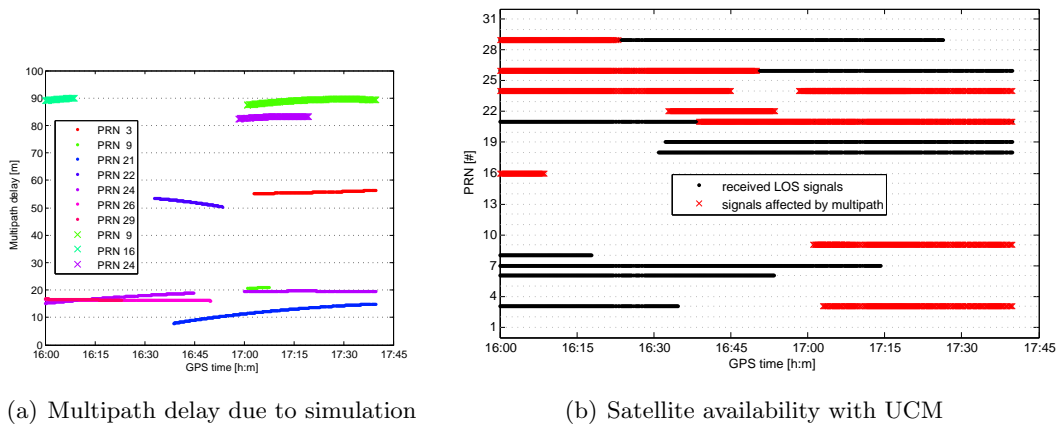
Figure 5.15: *Multipath delays and satellite availability as obtained from the UCM for the
data collection at ICT-A*

The expected multipath delays for the experiment at ICT-A are shown in figure
5.15(a). The pseudoranges from 6 satellites suffer from multipath effects related to
a single reflection from the buildings. The delays range from below 10 m to 60 m.
The crosses in the figure are multipath delays from signals that are reflected twice
from surface of the buildings. Three satellites are affected and the delay varies be-
tween 80 and 90 m. The total signal reception is shown in figure 5.15(b), where
direct and indirect signals are shown separately. As an average, we receive the
signals from 8 satellites during the data collection, with three of them affected by
multipath. During the last part of the data collection the number of signals affected
by multipath is higher than the number of LOS signals.

The calculation of the user position is evaluated for the AUR (average multipath)
and WCUR (worst case) scenario. The simulations pseudoranges are additionally
affected with random errors with a standard deviation of 2.2 m. A statistical test
in the implementation detects possible errors and excludes them from the position
estimation. The final position estimates are shown in figure 5.16.

The solutions vary from ±100 m, depending on the performance of the antenna/receiver
and the magnitude of reflection. As expected the AUR simulation achieves better re-
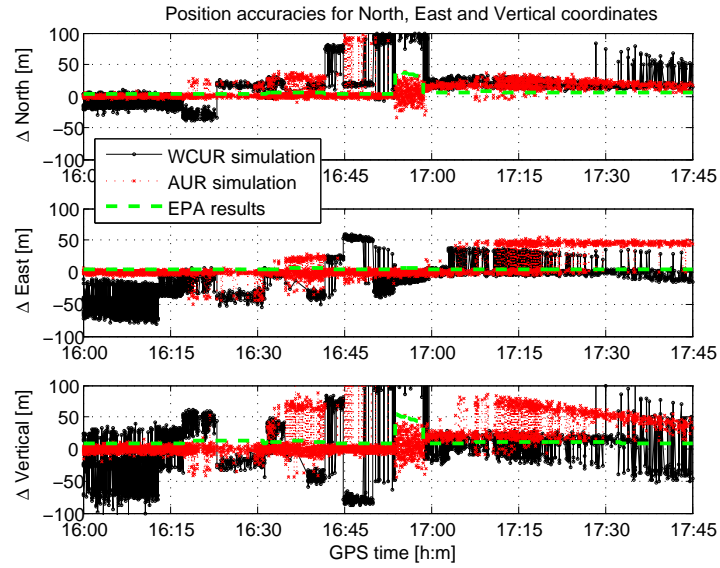
Figure 5.16: *AUR and WCUR simulation results at ICT-A with reliability testing compared to EPA results (UERE = 6 m)*

sults, because the multipath effects are lower. During the first period of the dataset, the solution has errors of 10 m for both horizontal and vertical component, using an AUR scenario. In the WCUR scenario the horizontal and vertical component errors reach -100 m. Similar as with the real data in section 5.4.1, statistical testing could not detect and exclude all outliers due to the high number of erroneous measurements.

data analysis	description	maximal POS error		average POS error	
experiment	HS ublox rx	2D max	568.9 m	2D std	33.2 m
		v max	1139.4 m	v std	58.7 m
	OEMV2 rx	2D max	235.5 m	2D std	27.2 m
		v max	332.1 m	v std	44.1 m
simulation	AUR, RE = 2.2 m exclusion	2D max	307.8 m	2D RMS	16.5 m
		v max	363.4 m	v RMS	28.8 m
	WCUR, RE = 2.2 m exclusion	2D max	307.3 m	2D RMS	39.0 m
		v max	366.0 m	v RMS	61.1 m
EPA	DOP·UERE (UERE = 2.2 m)	2D max	15.1 m	2D RMS	3.2 m
		v max	20.2 m	v RMS	4.6 m
	DOP·UERE (UERE = 6 m)	2D max	41.1 m	2D RMS	8.8 m
		v max	55.0 m	v RMS	12.6 m

Table 5.2: *Comparison of the position solution between experiment, simulation, and EPA*

Figure 5.16 shows the EPA values as well. The EPA for the simulated times does not exceed 16 m in horizontal and 21 m in vertical components, respectively, using an UERE of 2.2 m. These high values are obtained during shortly before 17:00 GPS time, where we only have 5 visible satellites.

All the results for the experiment in a urban canyon with high multipath effects are summarized in table 5.2. The experiment results in this high multipath environment show RMS values of up to 50 m, using a LS adjustment with reliability testing to compute the position. The maximum errors are higher than 100 m, which can be attributed to wrong detection and exclusion of erroneous measurements with statistical testing. Simulations of the different antenna/receiver scenarios with similar statistical testing have been made. Since the surface reflection magnitude and the receiver properties may not match those in the real environment, the result are not directly comparable. However, the simulation results show significant improvements, if an antenna/receiver design with a better multipath mitigation performance is used. Last the EPA results are calculated with UERE values of 6 m and 2.2 m. Compared to the results from the simulation with the UCM and the real data analysis, the EPA values are relatively small. Since the EPA does not consider multipath effects, a comparison of the EPA to real data analysis and its accuracies is not meaningful.

6 Chapter

Conclusion

6.1 Summary

This thesis characterize multipath effects on GNSS, especially GPS, in urban canyons. The degradation of the pseudorange estimates and the position error due to the multipath errors have been discussed in theory, then simulated with an urban canyon model developed for this purpose, and supplemented with actual field data. Additionally these results have been compared to theoretical estimates of position accuracies.

These theoretical estimates (EPAs) used herein are expressed as standard UERE values multiplied with DOP factors. Using a standard value for the UERE of 6 m, analyses showed that the EPA values do not generally exceed 11 m and 14 m (or 4 m and 5 m using an UERE of 2.2 m) for the horizontal and vertical position components, respectively. The standard UERE of 6 m described by the SPS-PS is the one-sigma estimate of the pseudorange errors for global averaged solution. Severe errors such as multipath or strong ionospheric effects (e.g. ionospheric fluctuations) are not accounted for the estimation of the UERE. Actual values will therefore significantly vary from the standard UERE and are not comparable to a actual pseudorange error estimations for a day-to-day data collection. Therefore EPA is a very general quality description for GNSS positioning and cannot describe the attainable accuracy of a specific data collections.

In urban canyons multipath is the major error for GNSS positioning. To mitigate the multipath effect on the pseudoranges, reception of the direct signal, additional to the reception of one or more indirect signals, is required. If the direct signal cannot be received, the multipath error can be several hundred metres, unless the indirect signal is relatively weak. Multipath effects on the pseudoranges can among others be reduced by the antenna design and the receiver tracking loops. Three different antenna designs, the attenuation of LHCP signals is considered as major factors contributing to multipath mitigation at the antenna herein, have been compared. Multipath effects could be reduces from 100 m, using a low-cost antenna with no

attenuation of LHCP signals, to less than 5 m, using a geodetic antenna with high attenuation (of about 25 dB) of LHCP signals. By using a smaller chip spacing in the tracking loops, the multipath effects can be reduced by a factor of 10 for worst case scenarios. The last effect that has been discussed is the magnitude of the indirect signal, a combination of signal attenuation due to antenna and reflection. Since the estimation of the reflection magnitude would have been too complex and extensive for this work, different values are assumed and evaluated. It has been proved that the weaker the reflected signal is, the less error is introduced on the pseudorange.

Using a LS adjustment, the error effect due to multipath has been calculated on the estimated positions. The accuracy estimates for the user position range between a few metres for low multipath environments up to errors above 100 m for high multipath environments. Here the urban canyon scenarios are numerous that a general conclusion on the attainable accuracy cannot be made without specifying the scenario parameters. Too many factors can have an impact on the pseudorange estimation and on the final position solutions. Nevertheless a few conclusions can be made and are summarized below:

- Using better multipath mitigation techniques for the antenna and the receiver, the error on the pseudoranges can be significantly reduced. Also the position estimations using antenna/receiver properties with a better multipath mitigation have shown better accuracies. These improvements depend on many factors and cannot be generalized for a global urban canyon model. Simulations have shown differences between a few metres and more than 100 m, comparing worst case scenarios and best possible solutions.

- In general a higher number of observations leads to better position accuracies. This behaviour can be seen in multipath environments. Here the pseudoranges may be affected by multipath, and increasing the number of observations means also increasing the number of observations which are affected by multipath.

- Statistical testing has been used to detect outliers and to exclude them from the position solutions. In an urban canyon, the number of biased observations might be higher than the number of unbiased observations. In this case, identification of the most significant outliers is not always possible and statistical reliability testing is only partially successful.

- The user model developed herein proved effective to simulate multipath and its effect on observations and position accuracy.

- The simulation results were supplemented by real data results. Here the surface reflection magnitude could only be assumed and the receiver properties were not fully known to create the same conditions for simulation and experimental analysis. Therefore simulation results could only be compared with the real data results in a limited but nevertheless interesting manner.

- Future GPS and Galileo signals can reduce multipath effects, depending on the chipping rate of the BOC modulated signals. Comparison between signals

with an identical chipping rate show a better performance for medium and large multipath delay with the new signal properties.

6.2   Recommendations

The work of this thesis can be seen as an introduction to multipath and its effect in an urban canyons. There are many ways to extend this work for a deeper analysis and the most important once - in my opinion - are mentioned below.

The UCM used for this work uses a basic model of the satellite motion, the user environment, and the user reception. A special interest for further extensions is the environment model which simulates indirect signal propagation using specular reflections from plane and smooth surfaces. This module can be extended by using ray tracing algorithms, which allow better calculations for path delays in more complex environments. Further diffraction and diffuse reflection effects can be implemented and added to the indirect signal propagation model. Carrier phase analysis in the user reception module could help to improve the estimation of the pseudorange error due to multipath. With a better knowledge of the reflection magnitude the power loss due to reflection can be estimated more accurately and so the impact of an indirect signal on the pseudoranges could also be accomplished more precisely.

Since the simulation in this work has been evaluated for GPS only, the task could be extended to other GNSS. The most important system for future implementations would be Galileo, whose performance of the code tracking in presence of multipath signals has been commented herein.

Last the analysis for multipath effects in urban canyons can be extended for (i) more urban canyon situations and (ii) more locations to provide global coverage for a deeper analysis. With this data it might be possible to find connections and correlations for multipath behaviour in urban canyons.

The major limitations that cannot be overcome however will remain the complexity and ruggedness of the reflective surfaces and knowledge of their precise RF characteristics. The approach used herein to complement simulations with field testing in order to attempt "calibration" of the simulations for a specific environment will remain a effective tool to ascertain the validity of the simulations.

Bibliography

Axelrad, P., R.G. Brown (1994), *GPS Navigation Algorithm*, Chapter 9 in Global Positioning System: Theory and Applications, Volume I, ed. B.W. Parkinson, J.J. Spilker Jr., Volume 163, American Institute of Aeronautics and Astronautics, Washington DC, pp. 409-433.

Axelrad, P., C. Comp, and P. MacDoran (1994a), Use of Signal-To-Noise Ratio for Multipath Error Correction in GPS Differential Phase Measurements: Methodology and Experimental Results, in *Proceedings of ION GPS-94*, Salt Lake City, Utah, pp. 655–666. The Institute of Navigation.

Baarda, W., (1968), *A testing procedure for use in geodetic networks*, Netherlands Geodetic Commission, Publication on Geodesy, New Series 2. No. 5, Delft, Netherlands.

Beckmann, P., A. Spizzichino (1963), *The Scattering of Electromagnetic Waves from Rough Surfaces*, Pergamon Press, Oxford.

Braasch, M.S. (1995), *Multipath Effects*, Chapter 14 in Global Positioning System: Theory and Applications, Volume I, ed. B.W. Parkinson, J.J. Spilker Jr., Volume 163, American Institute of Aeronautics and Astronautics, Washington DC, pp. 574-586.

Cannon, M.E., G. Lachapelle (2006), *Satellite Positioning*, ENGO 465 Course Notes, Department of Geomatics Engineering, University of Calgary, Canada.

Caspary, W.F. (2000), *Concepts of Network and Deformation Analysis*, Third corrected impression, Monograph 11, School of Geomatic Engineering (formerly Surveying), The University of New South Wales, Sydney.

Collin, R.E. (1985), *Antenna and Radio Wave Propagation*, McGraw-Hill Book Company, Toronto, Canada.

van Dierendonck, A.J., P.C. Fenton, and T. Ford. (1992), Theory and Performance of Narrow Correlator Spacing in a GPS Receiver, in *Journal of the Institute of Navigation*, Vol. 39, No. 3.

van Dierendonck, A.J. (1995), *GPS Receivers*, Chapter 8 in Global Positioning System: Theory and Applications, Volume I, ed. B.W. Parkinson, J.J. Spilker Jr., Volume 163, American Institute of Aeronautics and Astronautics, Washington DC, pp. 329-408.

Griffiths, D.J. (1999), *Introduction to Electrodynamics*, 3rd edition, Prentice-Hall Inc., New Jersey.

Hagerman, L.L. (1973), *Effects of Multipath on Coherent and Noncoherent PRN Ranging Receiver*, Aerospace Corporation Report No. TOR-0073(3020-03)-3.

Hannah, B.M. (2001), *Modelling and Simulation of GPS Multipath Propagation*, PhD. Thesis, The Cooperative Research Centre for Satellite Systems, Queensland University of Technology, Canada.

Hofman-Wellenhof, B., H. Lichtegger and J. Collins (2001), *GPS - Theory and Practice*, Fifth revised edition, Springer, Wien.

International GNSS service (2008), *The international GNSS Service (IGS)*, www.igscb.jpl.nasa.gov,
last accessed: March 2008.

ICD-200 (2004), Interface Specification IS-GPS-200, Revision D, Navstar GPS Space Segment/Navigation User Interface, Navstar GPS Joint Program Office.

Irsigler, M., G.W. Hain, B. Eissfeller (2004), Multipath Performance for Future GNSS Signals, in *Proceedings of ION National Technical Meeting 2004*, January 26-28, 2004, San Diego, California, pp. 225-238. The Institute of Navigation.

Jahn, A., H. Bischl, and G. Heiss (1996), Channel Characterization for Spread Spectrum Satellite Communications, in *Proceedings of IEEE 4th International Symposium on Spread Spectrum Techniques and Applications (ISSSTA 1996)*, Mainz, Germany, September 1996.

Kaplan, E.D., C.J. Hegarty (2006), *Understanding GPS: Principles and Applications*, Second Edition, Artech House, Boston.

Klobuchar, J.A. (1987), Ionospheric Time-Delay Algorithm for Single-Frequency GPS Users, *IEEE Transactions on Aereospace and Electronic Systems*, Vol. AES-23, No. 3, pp.325-331.

Klobuchar, J.A. (1996), *Ionospheric Effects on GPS*, Chapter 12 in Global Positioning System: Theory and Applications, Volume I, ed. B.W. Parkinson, J.J. Spilker Jr., Volume 163, American Institute of Aeronautics and Astronautics, Washington DC, pp. 485-515.

Kraus, J.D., K.R. Carver (1973), *Electromagnetics*, Second Edition, McGraw-Hill Book Company.

Kuusniemi, H. (2005), *User-Level Reliability and Quality Monitoring in Satellite-Based Personal Navigation*, PhD. Thesis, published as Publication 544, Tampere University of Technology, Finnland.

Leick, A. (2004), *GPS Satellite Surveying*, 3rd edition, John Wiley and Sons Inc., Hoboken, New Jersey.

Martin, E.H. (1990), GPS User Equipment Error Models in *Global Positioning System Papers*, Vol. 1, Institute of Navigation, Washington DC, pp. 109-118.

Misra, P., P. Enge (2006), *Global Positioning System: Signals, Measurements, and Performance*, Second Edition, Ganga-Jamuna Press, Massachusetts.

Parkinson, B.W. (1994), *GPS Error Analysis*, Chapter 11 in Global Positioning System: Theory and Applications, Volume I, ed. B.W. Parkinson, J.J. Spilker Jr., Volume 163, American Institute of Aeronautics and Astronautics, Washington DC, pp. 469-483.

Petovello, M.G., M.E. Cannon and G. Lachapelle (2005), C^3NAVG^{2TM} *Operating Manual*, Version 4, Department of Geomatics Engineering, University of Calgary, Canada.

Ray, J.K. (2000), *Mitigation of GPS Code and Carriere Phase Multipath Effects using a Multi-Antenna system*, PhD. Thesis, published as Report No. 20136, Department of Geomatics Engineering, University of Calgary, Canada.

Ray, J.K. (2007), *Advanced GNSS Receiver Technology*, ENGO 638 Course Notes, Department of Geomatics Engineering, University of Calgary, Canada.

Ryan, S.M. (2002), *Augmentation of DGPS for Marine Navigation*, PhD. Thesis, published as Report No. 20164, Department of Geomatics Engineering, University of Calgary, Canada.

Spilker, J.J., (1994), *GPS Navigation Data*, Chapter 4 in Global Positioning System: Theory and Applications, Volume I, ed. B. W. Parkinson and J. J. Spilker Jr., Volume 163, American Institute of Aeronautics and Astronautics, Washington DC, pp. 121-175.

Spilker, J.J., (1994a), *Tropospheric Effects on GPS*, Chapter 13 in Global Positioning System: Theory and Applications, Volume I, ed. B. W. Parkinson and J. J. Spilker Jr., Volume 163, American Institute of Aeronautics and Astronautics, Washington DC, pp. 517-546.

Taylor, J., E. Barnes, (2005), GPS Current Signal-in-Space Navigation Performance, in *Proceedings of ION GNSS 2005*, January 24-26, 2005, San Diego, California, pp. 385-393. The Institute of Navigation.

Tiberius, C.J.M., (1998), Quality Control in Positioning, in *The Hydrographic Journal*, Issue: 199810, London, pp. 3-8.

U.S. Coast Guard Navigation Center (2002), GPS Almanac Information
www.navcen.uscg.gov/gps/almanacs.htm
last accessed: December 2007.

SPS-PS (2001), *Global Positioning System Standard Positioning Service Performance Standard*, U.S. Department of Defense, www.navcen.uscg.gov/gps/geninfo/2001SPSPerformanceStandardFINAL.pdf.

Warren, F.L. (1983), Terrain effects and Multipath propagation, Chapter 6 in *Propagation Effects on Satellite Systems at Frequencies below 10 GHz, A Handbook for Satellite System Design*, 1st edition, NASA Reference Publication 1108, Jet Propulsion Laboratory, California Institute of Technology, pp. 6-1−6-30.

Weiss, J.P. (2007), *Modeling and Characterization of Multipath in Global Navigation Satellite System Ranging Signals*, PhD. Thesis, Department of Aerospace Engineering Sciences, University of Colorado, Boulder.

Wieser, A. (2002), *Robust and fuzzy techniques for parameter estimation and quality assessment in GPS*, Shaker Verlag, Engineering Geodesy – TU Graz.

Wieser, A., M.G. Petovello, G. Lachapelle (2004), Failure Scenarios to be Considered with Kinematic High Precision Relative GNSS Positioning, in *Proceedings of ION International Technical Meeting 2004*, September 21-24, 2004, Long Beach, California, pp. 1448–1459. The Institute of Navigation.

Wieser, A. (2007), *GPS based velocity estimation and its application to an odometer*, Shaker Verlag, Engineering Geodesy – TU Graz.